NASA Technical Memorandum 4015

Wall Interference Tests of a CAST 10-2/DOA 2 Airfoil in an Adaptive-Wall Test Section

Raymond E. Mineck
Langley Research Center
Hampton, Virginia

National Aeronautics
and Space Administration

**Scientific and Technical
Information Division**

1987

Summary

A wind-tunnel investigation of a CAST 10-2/DOA 2 airfoil model has been conducted in the adaptive-wall test section of the Langley 0.3-Meter Transonic Cryogenic Tunnel (0.3-m TCT) and in the National Aeronautical Establishment (NAE) High Reynolds Number Two-Dimensional Test Facility. The primary goal of the test was to assess two different wall-interference correction techniques: adaptive test-section walls and classical analytical corrections. The 0.3-m TCT adaptive-wall test section has four solid walls with flexible top and bottom walls. The ratio of the test-section height to the model chord is 1.4. Tests were conducted over a Mach number range from 0.3 to 0.8 and over a chord Reynolds number range from 6×10^6 to 70×10^6. The angle of attack was varied from about $-2°$ up to stall (except when wall positioning hardware limited wall adaptation). The same model has previously been tested in the NAE High Reynolds Number Two-Dimensional Facility over the same Mach number range and over a chord Reynolds number range from 10×10^6 to 20×10^6.

The airfoil aerodynamic characteristics from the tests in the 0.3-m TCT have been corrected for wall interference by the movement of the adaptive walls. No additional corrections for any residual interference have been applied to the data, to allow comparison with the classically corrected data from the conventional NAE tunnel. The data are presented graphically in this report as integrated force-and-moment coefficients and chordwise pressure distributions. These data, as well as the spanwise distributions of pressure coefficient and drag coefficient and the test-section top and bottom wall pressure distributions and wall vertical displacements, are presented in tabular form in a supplement to this report. The results are presented without analysis.

Introduction

The presence of wind-tunnel walls often compromises the ability of wind tunnels to simulate the "free air" conditions encountered in flight. In the past, corrections have been applied to wind-tunnel results to account for the presence of the walls. These corrections are relatively simple for tests of unpowered models in closed test sections at low subsonic speeds. However, the corrections become more complex and difficult to apply for ventilated test sections at high subsonic speeds because of difficulties with mathematically modeling and experimentally measuring the flow field at the wall. The high-speed digital computer has facilitated the development of sophisticated wall correction techniques for ventilated test sections at high subsonic speeds. These techniques often depend on extensive measurements taken at or near the test-section boundaries. Several examples of these techniques are presented in reference 1. The high-speed digital computer has also facilitated the development of adaptive-wall test sections which have the potential of removing the wall interference at its source. Therefore, free-air results can be approached using a post-test wall correction technique, a real-time adaptive-wall test-section technique, or some combination thereof. The technique chosen to correct the data should be validated.

The National Aeronautical Establishment (NAE) of Canada and the National Aeronautics and Space Administration (NASA) have a cooperative agreement to develop and validate methods for correcting and/or eliminating wall interference in transonic two-dimensional wind-tunnel testing. The NAE uses a post-test wall correction technique for airfoil data from its High Reynolds Number Two-Dimensional Test Facility, whereas NASA uses a real-time adaptive-wall test-section technique for airfoil data from the Langley 0.3-M Transonic Cryogenic Tunnel (0.3-m TCT). Both organizations wanted to validate wall interference correction methods for data obtained at high Reynolds number. To do this, one model was tested in both wind tunnels. The corrected results could then be compared to assess each correction technique.

Under the agreement, the NAE designed and fabricated a CAST 10-2/DOA 2 airfoil model with a 9-in. chord. This airfoil profile was chosen because its aerodynamic characteristics are sensitive to changes in Mach number and Reynolds number. The airfoil model was then tested in the NAE facility. This facility, described in reference 2, has a 60-in. by 15-in. test section with perforated top and bottom walls. The ratio of the tunnel height to the model chord was 6.67 for this experiment. Typically, for other facilities, this ratio is in the range of 3.5 to 4.5. As a result of this large ratio, the magnitude of the top and bottom wall interference for the NAE facility was expected to be moderate. The results from the NAE tests, presented in reference 3, were corrected for top and bottom wall interference after the test using the method of reference 4.

The same model was subsequently tested in the Langley 0.3-m TCT with the two-dimensional, adaptive-wall test section. Details of the tunnel may be found in reference 5. The 13-in. by 13-in. test section has four solid walls with flexible top and bottom walls. The relatively small ratio of test-section height to chord of 1.44 would provide a good test of the adaptive-wall technique. Tests were conducted at Mach numbers from 0.3 to 0.8 and chord Reynolds

numbers from 6×10^6 to 70×10^6. The angle of attack was varied from about $-2°$ to either model stall or until an adaptive-wall positioning system hardware limit was reached.

This report presents the results obtained on the model in the 0.3-m TCT. The results have been corrected for top and bottom wall interference by the movement of the adaptive walls using the method of reference 6. No additional corrections have been applied to the data to remove any residual interference.

The run schedule for the tests in the 0.3-m TCT is presented in a "Supplement to NASA TM-4015." Also presented in the supplement are the tabulated airfoil pressure distributions, the integrated force-and-moment coefficients, and the wall boundary conditions. The supplement is available upon request, and a request form is included at the back of this paper.

Symbols

AOA	angle of attack
BLC	boundary-layer control
C_p	local pressure coefficient
c	model chord, in.
c_d	section drag coefficient, measured on tunnel centerline
c_m	section pitching-moment coefficient, resolved about 0.25c
c_n	section normal-force coefficient
M_∞	free-stream Mach number
R_c	free-stream Reynolds number based on model chord
x	chordwise position, measured aft from leading edge, in.
y	spanwise position, measured to right from model centerline, in.
z	vertical position, measured up from model chord plane, in.
α	geometric angle of attack, deg

Wind Tunnel and Model

Wind Tunnel

The tests were conducted in the 13-in. by 13-in. two-dimensional adaptive-wall test section of the 0.3-m TCT. A sketch of the tunnel is presented in figure 1, and a photograph of the upper leg of the tunnel circuit is presented in figure 2. The 0.3-m TCT is a fan-driven, cryogenic pressure tunnel which uses gaseous nitrogen as a test medium. It is capable of operating at stagnation temperatures from just above the boiling point of liquid nitrogen, approximately 80 K, to 327 K and at stagnation pressures from 1.2 atmospheres to 6.0 atmospheres. The fan speed is variable so that the empty-test-section Mach number can be varied continuously from about 0.20 to 0.95. This combination of test conditions provides a test envelope of chord Reynolds numbers up to about 100×10^6 based on a model chord of 12 in. Additional details of the tunnel may be found in reference 5.

Figure 3 is a sketch of the adaptive-wall test section with the test-section plenum wall removed, and figure 4 is a photograph of the test section. The test section is 13 in. by 13 in. in cross section at the entrance. All four walls are solid. The sidewalls are rigid, whereas the top and bottom walls are flexible and movable. The flexible walls are 71.7 in. long. The rear 15.9-in. portion diverges 4.1° to form a transition between the test section and the high-speed diffuser. The test section is therefore considered to be 55.8 in. long. The flexible walls are anchored at the upstream end. The shape of each wall is determined by 21 independent jacks. The jack locations relative to the center of the turntable are presented in table 1. The jack at −1.75 in. upstream of the turntable on the bottom wall was inoperative during this test. The connection between this jack and the flexible wall was removed. With the connection removed, the wall displacement could not be determined. The wall was free to "float" to a position determined by the jack just upstream and the jack just downstream of the inoperative jack. Each wall positioning jack is driven by a stepping motor located outside the test-section plenum. The jacks have a design displacement range of 3 in. up and 1 in. down. However, the available displacement for each jack varies because of limits on allowable wall stress due to curvature. Pressure orifices are located at each jack position on the wall centerline and 1.0 in. upstream of the wall anchor point.

The model mounting system is designed for two-dimensional models. The model is supported between two turntables centered 30.7 in. downstream of the test-section entrance. Models with chords up to 13 in. can be tested over an angle of attack range of 40°. The turntables are driven by an electric stepping motor, which is connected through a yoke to the perimeter of both turntables. This arrangement drives both turntables to eliminate possible model twisting. The angular position of the turntables and, therefore, the geometric angle of attack of the model

is measured using a digital shaft encoder geared to the left turntable.

A vertical traversing mechanism may be installed at 12.5 in., 17.5 in., or 22.5 in. downstream of the center of the turntables. The maximum traverse limits are from 3 in. below the centerline to 5 in. above the centerline. The traversing mechanism is driven by a stepping motor mounted externally to the tunnel. The vertical position of the traversing mechanism is measured by a digital shaft encoder geared to the stepping motor. The traversing mechanism normally supports a wake rake with three static- and six total-pressure probes as shown in figure 5. This arrangement allows the total-pressure variation in the model wake to be determined at six spanwise locations. As shown in figure 6, the wake rake is located at the center station, 17.5 in. downstream of the center of the turntable, for this investigation. This location was 1.2 chords downstream of the model trailing edge.

Model

The model used in this test had a 9.002-in. chord and a CAST 10-2/DOA 2 airfoil section which is nominally 12 percent thick. The model was constructed from 18 percent nickel maraging steel in two parts: the airfoil body and the cover plate over the channel for the pressure orifice tubes. After installation of the pressure tubes, the cover plate was bonded to the main body. The design and measured model ordinates are presented in table 2, and a sketch of the airfoil shape is presented in figure 7. The measured profile differs from the design by less than 0.001 in., therefore, an accurate representation of the desired airfoil contour is produced. The model had a 15-in. span to fit the NAE test section. Since the 0.3-m TCT test section was 13 in. wide, the outer 1 in. on each end of the model extended into the model mounting blocks. (See fig. 8.) With this arrangement, the model centerline and the test-section centerline coincided. The model chord was on the test-section centerline at 0° angle of attack. The model rotated about the 44-percent-chord position.

The model was equipped with 80 pressure orifices: 45 in a chordwise row on the upper surface, 23 in a chordwise row on the lower surface, 6 in a spanwise row on the upper surface at the 90-percent-chord station, and 6 in a spanwise row on the lower surface at the 90-percent-chord station. A sketch of the orifice layout is presented in figure 7, and a list of the orifice locations is presented in table 3. The orifices in the chordwise rows were staggered about the model centerline to minimize interference on the neighboring orifices. The orifices from the leading edge back to the 22-percent-chord location were 0.010 in. in diameter. Smaller orifices were used over the forward portion of the airfoil to reduce any orifice size effects where the pressure gradients could be large. All other orifices were 0.014 in. in diameter.

Wall Adaptation Technique

Wind tunnels with adaptive walls attempt to eliminate the wall-induced interference at its source. This is accomplished by modifying the flow field near the test-section boundaries such that the flow field in the vicinity of the model duplicates free-air conditions. To do this, the flow field is split into two regions: a "real" flow field inside a control surface at or near the test-section walls and an "imaginary" flow field extending from the control surface to infinity. The wind tunnel simulates the real flow field where there are compressibility and viscous effects. Computational fluid dynamics techniques are used to simulate the imaginary flow field. Potential flow methods can be used in the imaginary region if it is assumed to be irrotational.

The adaptive-wall concept requires that the real flow field match the imaginary flow field at the control surface. This requirement is satisfied if two independent parameters are matched. For the adaptive-wall test section at the 0.3-m TCT, the control surface coincides with the effective wall position defined by the wall position minus the wall boundary-layer displacement thickness. The two independent parameters matched at the control surface are the flow direction and the flow velocity (magnitude). The flow direction is determined by the slope of the effective wall shape, and the flow velocity is determined from the wall static pressure.

To begin the iterative wall adaptation process, the wall static pressures are measured for the initial wall locations to determine the real flow field parameters on the control surface. This initial wall shape is then used as a solid boundary in a potential flow solver to determine the control-surface parameters for the imaginary external flow field. Thus, the flow direction (wall shape) for the two flow fields is identical at the control surface. The measured real flow-field velocity on the control surface is compared with the computed imaginary flow-field velocity. The mismatch in these two velocities is used to determine a corrected wall position which is the input for the next wall adaptation cycle. Five convergence criteria, which are listed in table 4, are examined for each iteration. If all these are satisfied, the desired wall shape has been obtained and the wall adaptation process is complete; otherwise, the procedure is repeated. Specific details of the method are given in reference 6.

Test Instrumentation and Procedures

Test Instrumentation

A detailed discussion of the instrumentation and procedures for the calibration and control of the 0.3-m TCT can be found in reference 7. For two-dimensional airfoil tests, the 0.3-m TCT is equipped to obtain static-pressure measurements on the airfoil model surface, total-pressure measurements in the model wake, and static-pressure measurements on the test-section sidewalls, top wall, and bottom wall. Except for the wall pressures, all measurements use individual pressure transducers.

Tunnel test conditions. The tunnel test conditions were determined by three primary measurements: the total pressure, the static pressure, and the total temperature. The total pressure and static pressure were measured by individual quartz differential pressure transducers referenced to a vacuum. The transducer has a range of ±100 psi and an accuracy of ±0.006 psi plus ±0.012 percent of the pressure reading. The stagnation temperature was measured by a platinum resistance thermometer. The analog output from each of these devices was converted to digital form by individual digital voltmeters for display and recording.

Airfoil model pressures. The pressures on the airfoil model are measured by individual transducers connected by tubing to each orifice on the model. The transducers are a commercially available, high-precision, variable-capacitance type. The maximum range of these differential transducers is ±100 psi with an accuracy of ±0.25 percent of the reading from −25 percent to +100 percent of full scale. They are located outside the tunnel and its high-pressure, cryogenic environment, but as close as possible to the test section to minimize the tubing length and reduce the response time. To provide increased accuracy, the transducers are mounted on thermostatically controlled heater bases to maintain a constant temperature and on "shock" mounts to reduce possible vibration effects. The electrical signals from the transducers are processed by individual signal conditioners located in the tunnel control room. The signal conditioners are autoranging and have seven ranges available. As a result of the autoranging capability, the analog output to the data acquisition system is kept at a high level, even though the pressure transducer may be operating at the low end of its range.

Wall pressures. The top and bottom flexible wall pressures are measured using a scanivalve system capable of operating ten 48-port scanivalves. Because of the large changes in the pressure in the tunnel over its operational range, the same variable-capacitance-type pressure transducers and autoranging signal conditioners described previously are used with the scanivalve instead of the more typical strain-gage transducer.

Wake pressures. The total-pressure loss in the model wake is measured with the momentum rake described previously. The pressure in each of the six total-pressure tubes is measured with the same type of pressure transducer described previously. The static pressures in the model wake are measured on the right sidewall at eight vertical positions at the tunnel station opposite the momentum rake. The static-pressure probes on the rake were not used because they have not provided reliable data in the past. Individual pressure transducers of the same capacitance type described previously, but with a maximum range of ±20 psi, are used for the wake pressures.

Procedures

Figure 9 shows the test program (R_c versus M_∞) used in this investigation. These test conditions were chosen to match those from the first series of tests in the NAE tunnel presented in reference 3 and from tests of a different CAST 10-2/DOA 2 airfoil model in the 8-in. by 24-in. two-dimensional, slotted test section of the 0.3-m TCT presented in reference 8. The very high Reynolds number test conditions were added to explore the test envelope for airfoil tests conducted in the adaptive-wall test section. The primary goal of the tests was to assess test-section wall-interference correction techniques for an adaptive-wall tunnel and a classical passive wall tunnel, and not airfoil performance. Thus, the experiments were designed primarily to investigate wall-interference effects. Previous tests of a CAST 10-2/DOA 2 airfoil section in the ONERA/CERT T2 adaptive-wall tunnel indicated that the shock location differs significantly for fixed and free transition at a chord Reynolds number of 13×10^6 (ref. 9). Thus, for Reynolds numbers of 13×10^6 or less, tunnel turbulence levels would be expected to influence the shock location. Since the primary purpose of these tests was to evaluate two wall-interference correction techniques utilizing two different tunnels, the effect of tunnel turbulence on transition and shock location had to be removed from the experiments. Therefore, the tests were conducted with transition strips placed on both surfaces of the model at the 5-percent-chord location. The grit size was determined using the method of reference 10 for a Reynolds number of 10×10^6. Carborundum grit no. 320 with an average grit size of 0.0011 in. from the same container used for the NAE tests was used

for this test. The transition strip was nominally 0.1 in. wide.

The following procedure was used to set the test conditions. The tunnel total pressure and temperature and the fan speed were set for the desired Mach number and Reynolds number, and the model turntable was adjusted to the desired angle of attack. The desired angle is the NAE corrected angle of attack biased by -0.3° to account for a model installation misalignment. When the test conditions become stable, the wall adaptation process described previously begins. After the wall adaptation process is complete, the flexible wall position and static pressures associated with the adapted walls are recorded on the data tape. Twenty samples of the airfoil static pressures, the test conditions, the momentum rake total pressures, and the wake static pressures are then recorded over a period of 1 sec. Since there were individual transducers for each orifice on the model, each sample consisted of simultaneous static-pressure readings from all orifices on the model. The wake rake was moved to the next vertical location and another 20 samples were recorded. All data were obtained at 50 locations of the model wake rake.

Data Reduction

Because the tunnel operating envelope includes high pressures and low temperatures, real-gas effects are included in the data reduction for the tunnel test conditions using the thermodynamic properties of nitrogen gas calculated from the Beattie-Bridgeman equation of state. This equation of state has been shown in reference 11 to give essentially the same thermodynamic properties and flow calculation results in the temperature-pressure regime of the 0.3-m TCT as those given by the more complicated Jacobsen equation of state. Detailed discussions of real-gas effects when testing in cryogenic nitrogen are contained in references 12 and 13.

Section normal-force and pitching-moment coefficients are calculated using the trapezoidal method of numerical integration of the local surface pressure coefficient measured at each orifice. Only those data from the first rake position are used in the normal-force and pitching-moment integration. The section drag coefficient is calculated from the wake survey pressures by first computing an incremental or point drag coefficient by the method of reference 14 for each rake tube pressure at each rake location. These point drag coefficients are then numerically integrated across the model wake, again using the trapezoidal method. A threshold value of 0.0002 was used to determine the limits of integration of the point drag coefficient. This value was chosen based on previous test experience in this tunnel and accounts for the noise in the wake pressure measurements. The results of this integration are total drag coefficients at each of the six momentum rake tube locations.

The pressure data for each of the six total-pressure tubes was examined to insure that the wake survey covered the entire wake and to determine when two-dimensional flow was not present across the model. Examination of the wake surveys indicated that some were inadequate, especially when a strong shock was present on the model. For these surveys, a linear least-squares curve was fitted to the variation of incremental drag coefficient with wake position, and the incremental drag coefficient was extrapolated out to the point where it was 0.0002. The area under the extrapolated region was added to the drag coefficient for that tube. This correction was limited to changes in the drag coefficient of 0.0005. If the correction was larger, too much of the wake was considered to be missed and the drag data was voided. The examination of the data from each rake total-pressure tube showed that the data from the tube 1 in. from the sidewall was not consistent with the data from the other five total-pressure tubes. It is suspected that this tube was immersed in the combined sidewall boundary layer and model wake. Therefore, this tube was not included in the final data reduction or analysis. Examination of the spanwise distributions of section drag coefficient showed that as the normal-force coefficient increased above a certain level, the section drag began to vary across the span; this variance indicated that two-dimensional flow was beginning to break down. This level decreased with increasing Mach number. The results of the examination are presented in figure 10. The lower left region of the figure indicates two-dimensional flow occurred across the five remaining tubes. The sparsely hatched region indicates where two-dimensional flow was measured across at least 50 percent of the model span. The densely hatched region indicates where two-dimensional flow is not likely. Caution should be exercised when using data not in the envelope for two-dimensional flow conditions. All drag data presented in this report are for the tube on the tunnel centerline. Drag measurements for the other tubes are included in a supplement to this report.

The airfoil aerodynamic characteristics have been corrected by the appropriate movement of the flexible (adaptive) walls. No classical corrections for any residual wall-interference effects have been applied to the basic experimental data.

Presentation of Results

The results from this investigation are intended for use in validating wall-interference correction and elimination techniques. The airfoil data, the wall pressure distributions, and the wall displacements are needed for the validation. A tabular listing of these data is available in a supplement to this report. The airfoil data are presented graphically herein only to show the data trends. The results are presented as follows:

Concluding Remarks

A wind-tunnel investigation of a CAST 10-2/DOA 2 airfoil model has been conducted in the two-dimensional adaptive-wall test section of the Langley 0.3-Meter Transonic Cryogenic Tunnel. This investigation was designed to gather data to support a cooperative agreement to evaluate two wall-interference correction techniques using the same model in two different wind tunnels. The operating envelope of the adaptive-wall test section was also explored. The results were corrected for top and bottom wall interference by the appropriate movement of the flexible (adaptive) walls. No classical corrections for any residual wall interference have been applied to the data. The results are presented without analysis.

NASA Langley Research Center
Hampton, Virginia 23665-5225

October 15, 1987

References

1. Mokry, M.; Chan, Y. Y.; and Jones, D. J.: *Two-Dimensional Wind Tunnel Wall Interference.* AGARD-AG-281, Nov. 1983.
2. Ohman, L. H.; Brown, D.; Bowker, A. J.; and Ellis, F. A.: *Recent Improvements to the NAE 5 Ft × 5 Ft Wind Tunnel.* Aeronautical Note NAE-AN-31 (NRC No. 24882), Natl. Aeronautical Establishment (Ottawa, Canada), Aug. 1985. (Available from DTIC as AD A162 034.)
3. Chan, Y. Y.: *Wind Tunnel Investigation of CAST-10-2/DOA-2 12% Supercritical Airfoil Model.* LTR-HA-5x5/0162, National Aeronautical Establishment, National Research Council Canada, May 1986.
4. Mokry, M.; and Ohman, L. H.: Application of Fast Fourier Transform to Two-Dimensional Wind Tunnel Wall Interference. *J. Aircr.*, vol. 17, no. 6, June 1980, pp. 402–408.
5. Ray, Edward J.; Ladson, Charles L.; Adcock, Jerry B.; Lawing, Pierce L.; and Hall, Robert M.: *Review of Design and Operational Characteristics of the 0.3-Meter Transonic Cryogenic Tunnel.* NASA TM-80123, 1979.
6. Judd, M.; Wolf, S. W. D.; and Goodyer, M. J.: *Analytical Work in Support of the Design and Operation of Two Dimensional Self Streamlining Test Sections.* NASA CR-145019, 1976.
7. Ladson, Charles L.; and Kilgore, Robert A.: *Instrumentation for Calibration and Control of a Continuous-Flow Cryogenic Tunnel.* NASA TM-81825, 1980.
8. Dress, David A.; Johnson, Charles B.; McGuire, Peggy D.; Stanewsky, Egon; and Ray, Edward J.: *High Reynolds Number Tests of the CAST 10-2/DOA 2 Airfoil in the Langley 0.3-Meter Transonic Cryogenic Tunnel—Phase I.* NASA TM-84620, 1983.
9. Seraudie, Alain; Blanchard, Alain; and Breil, Jean-Francoise: *Rapport d'Essais du Profil CAST 10, en Transition Déclenchée, Effectués dans la Soufflerie Transsonique Cryogénique T2 en Présence de Parios Auto-Adaptables.* R.T. 0A 63/1685 AND, ONERA, CERT (Toulouse, France), Aug. 1985.
10. Braslow, Albert L.; and Knox, Eugene C.: *Simplified Method for Determination of Critical Height of Distributed Roughness Particles for Boundary-Layer Transition at Mach Numbers From 0 to 5.* NACA TN 4363, 1958.
11. Hall, Robert M.; and Adcock, Jerry B.: *Simulation of Ideal-Gas Flow by Nitrogen and Other Selected Gases at Cryogenic Temperatures.* NASA TP-1901, 1981.
12. Adcock, Jerry B.: *Real-Gas Effects Associated With One-Dimensional Transonic Flow of Cryogenic Nitrogen.* NASA TN D-8274, 1976.
13. Adcock, Jerry B.; and Johnson, Charles B.: *A Theoretical Analysis of Simulated Transonic Boundary Layers in Cryogenic-Nitrogen Wind Tunnels.* NASA TP-1631, 1980.
14. Baals, Donald D.; and Mourhess, Mary J.: *Numerical Evaluation of the Wake-Survey Equations for Subsonic Flow Including the Effect of Energy Addition.* NACA WR L-5, 1945. (Formerly NACA ARR L5H27.)

Table 1. Flexible Wall Positioning Jack Stations
[Jack station locations are referenced to center of turnable]

Jack	Station, in.	Notes
	−31.25	Test-section entrance pressure orifice
	−30.25	Anchor point
1	−26.00	First test-section jack
2	−20.25	
3	−15.25	
4	−11.25	
5	−8.25	
6	−6.25	
7	−4.75	
8	−3.25	
9	−1.75	Lower-wall jack at this station not operational
10	−.25	
11	1.25	
12	2.75	
13	4.75	
14	6.75	
15	8.75	
16	11.75	
17	15.75	
18	20.75	Last test-section jack
19	25.75	Start of transition section
20	30.75	
21	36.75	

Table 2. Airfoil Model Ordinates

(a) Upper surface

x/c	z/c design	z/c measured
0.0000	0.0034	0.0034
.0003	.0062	.0063
.0015	.0094	.0093
.0033	.0124	.0123
.0063	.0159	.0158
.0140	.0217	.0217
.0195	.0250	.0251
.0247	.0279	.0279
.0356	.0331	.0332
.0470	.0376	.0377
.0654	.0432	.0433
.0846	.0478	.0478
.1179	.0536	.0536
.1519	.0580	.0580
.2139	.0633	.0633
.2764	.0665	.0665
.3321	.0681	.0681
.3949	.0689	.0689
.4576	.0686	.0685
.5132	.0673	.0672
.5757	.0645	.0644
.6376	.0601	.0600
.6925	.0542	.0541
.7539	.0453	.0452
.8152	.0338	.0337
.8763	.0203	.0202
.9172	.0106	.0105
.9511	.0024	.0024
.9782	−.0042	−.0042
1.0000	−.0095	−.0095

(b) Lower surface

x/c	z/c design	z/c measured
0.0000	0.0034	0.0034
.0004	.0004	.0004
.0014	−.0021	−.0021
.0031	−.0043	−.0043
.0061	−.0066	−.0065
.0096	−.0081	−.0081
.0153	−.0099	−.0099
.0273	−.0127	−.0128
.0339	−.0141	−.0142
.0470	−.0169	−.0169
.0673	−.0205	−.0206
.0874	−.0238	−.0238
.1148	−.0277	−.0277
.1562	−.0328	−.0329
.2741	−.0446	−.0447
.3366	−.0492	−.0492
.3919	−.0520	−.0520
.4539	−.0532	−.0532
.5161	−.0520	−.0520
.5714	−.0489	−.0488
.6340	−.0436	−.0436
.6967	−.0373	−.0374
.7525	−.0316	−.0317
.8149	−.0255	−.0257
.8775	−.0204	−.0206
.9189	−.0177	−.0178
.9468	−.0162	−.0164
.9743	−.0151	−.0152
1.0000	−.0145	−.0146

Table 3. Pressure Orifice Ordinates

(a) Chordwise row, upper surface

Orifice	x/c	z/c	y/c
1	0.000	0.000	0.000
2	.001	.006	−.033
3	.006	.012	.033
4	.012	.017	−.016
5	.021	.023	.017
6	.030	.028	−.033
7	.041	.033	.033
8	.051	.037	−.017
9	.062	.040	.017
10	.074	.043	−.033
11	.086	.046	.033
12	.101	.049	−.017
13	.121	.053	.017
14	.146	.056	−.033
15	.172	.059	.033
16	.198	.062	−.033
17	.224	.064	.033
18	.249	.066	−.033
19	.275	.067	.033
20	.301	.069	−.033
21	.327	.070	.033
22	.355	.071	−.033
23	.381	.071	.033
24	.406	.072	−.033
25	.432	.072	.033
26	.459	.072	−.033
27	.485	.072	.033
28	.511	.072	−.033
29	.536	.071	.033
30	.562	.070	−.033
31	.582	.070	.033
32	.602	.069	−.033
33	.622	.067	.033
34	.642	.066	−.033
35	.662	.064	.033
36	.682	.062	−.033
37	.701	.060	.033
38	.720	.058	−.033
40	.764	.052	.033
42	.808	.044	−.033
44	.849	.036	.033
46	.892	.027	−.033
48	.936	.017	.033
50	.979	.007	−.033
51	1.000	.002	.000

(b) Chordwise row, lower surface

Orifice	x/c	z/c	y/c
52	0.004	−0.008	−0.025
53	.010	−.012	.042
54	.019	−.014	−.042
55	.028	−.016	.025
56	.039	−.018	−.025
57	.054	−.021	.042
58	.080	−.025	−.042
59	.119	−.030	.033
60	.179	−.036	−.033
61	.252	−.042	.033
62	.324	−.047	−.033
63	.397	−.049	.033
64	.469	−.049	−.033
65	.511	−.048	.033
66	.552	−.045	−.033
67	.592	−.042	.033
68	.633	−.037	−.033
70	.713	−.028	.033
72	.794	−.019	−.033
74	.856	−.012	.033
76	.897	−.009	−.003
78	.939	−.006	.033
80	.980	−.003	−.033

(c) Spanwise row, upper surface

Orifice	x/c	z/c	y/c
39	0.900	0.025	−0.171
41	.900	.025	−.337
43	.900	.025	−.504
45	.900	.025	.171
47	900	.025	.337
49	.900	.025	.504

(d) Spanwise row, lower surface

Orifice	x/c	z/c	y/c
69	0.900	−0.008	0.163
71	.900	−.008	.330
73	.900	−.008	.486
75	.900	−.008	−.163
77	.900	−.008	−.330
79	.900	−.008	−.496

Table 4. Adaptive-Wall Method Convergence Criteria

Average C_p error, top wall	<0.01
Average C_p error, bottom wall	<0.01
Induced angle of attack, deg.	<0.015
Induced camber	<0.07
Average C_p error along model chord	<0.007

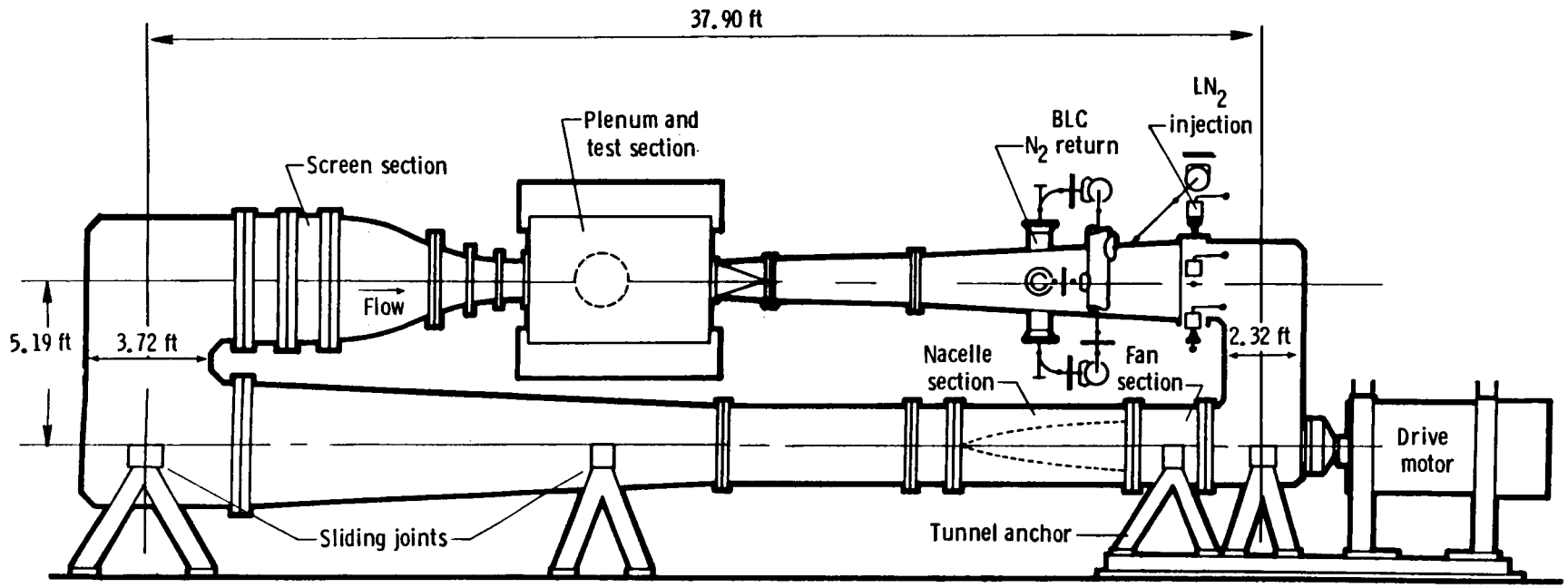

Figure 1. Sketch of Langley 0.3-Meter Transonic Cryogenic Tunnel with 13-in. by 13-in. two-dimensional adaptive-wall test section.

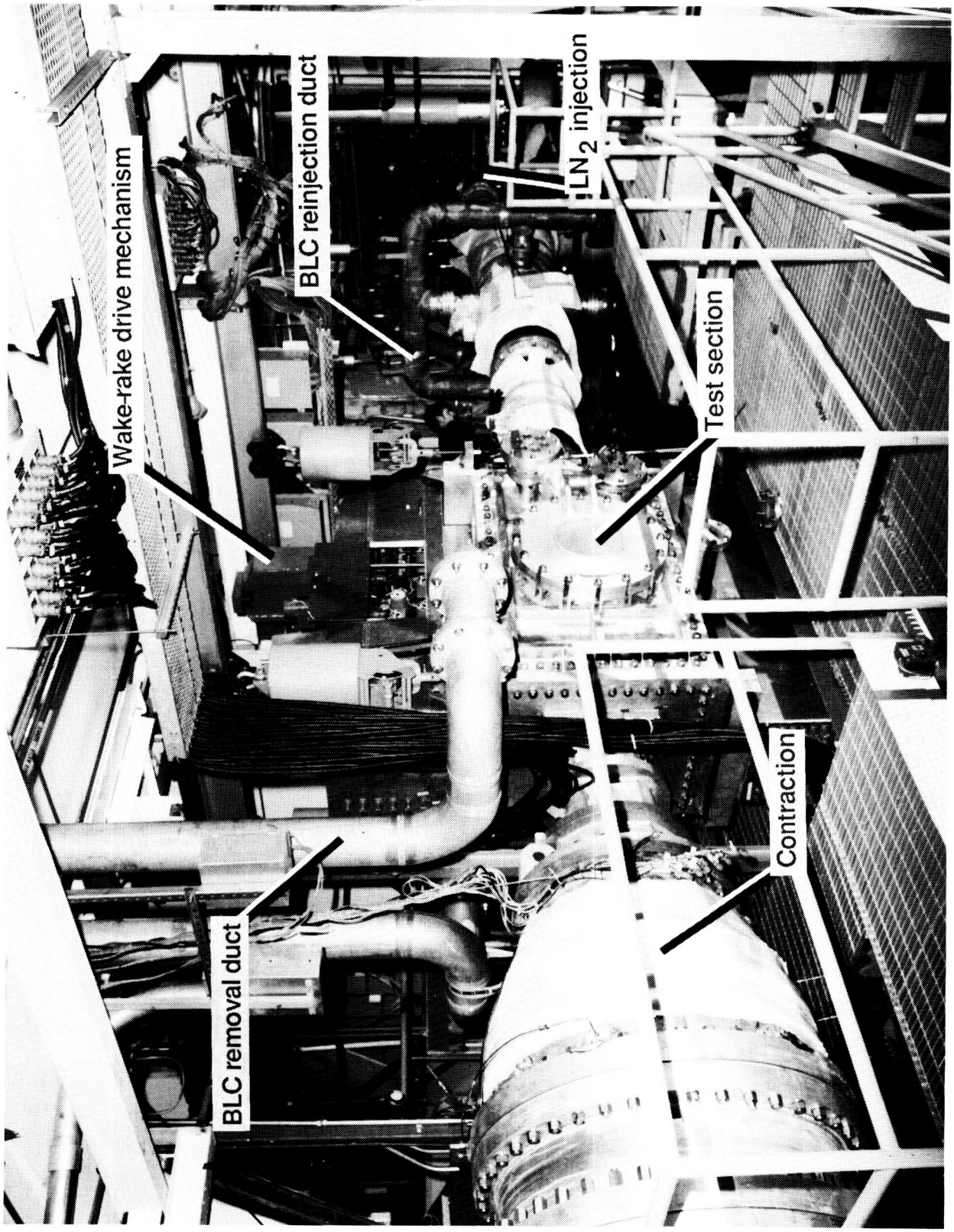

L-85-9893

Figure 2. Upper leg of Langley 0.3-Meter Transonic Cryogenic Tunnel with 13-in. by 13-in. adaptive-wall test section.

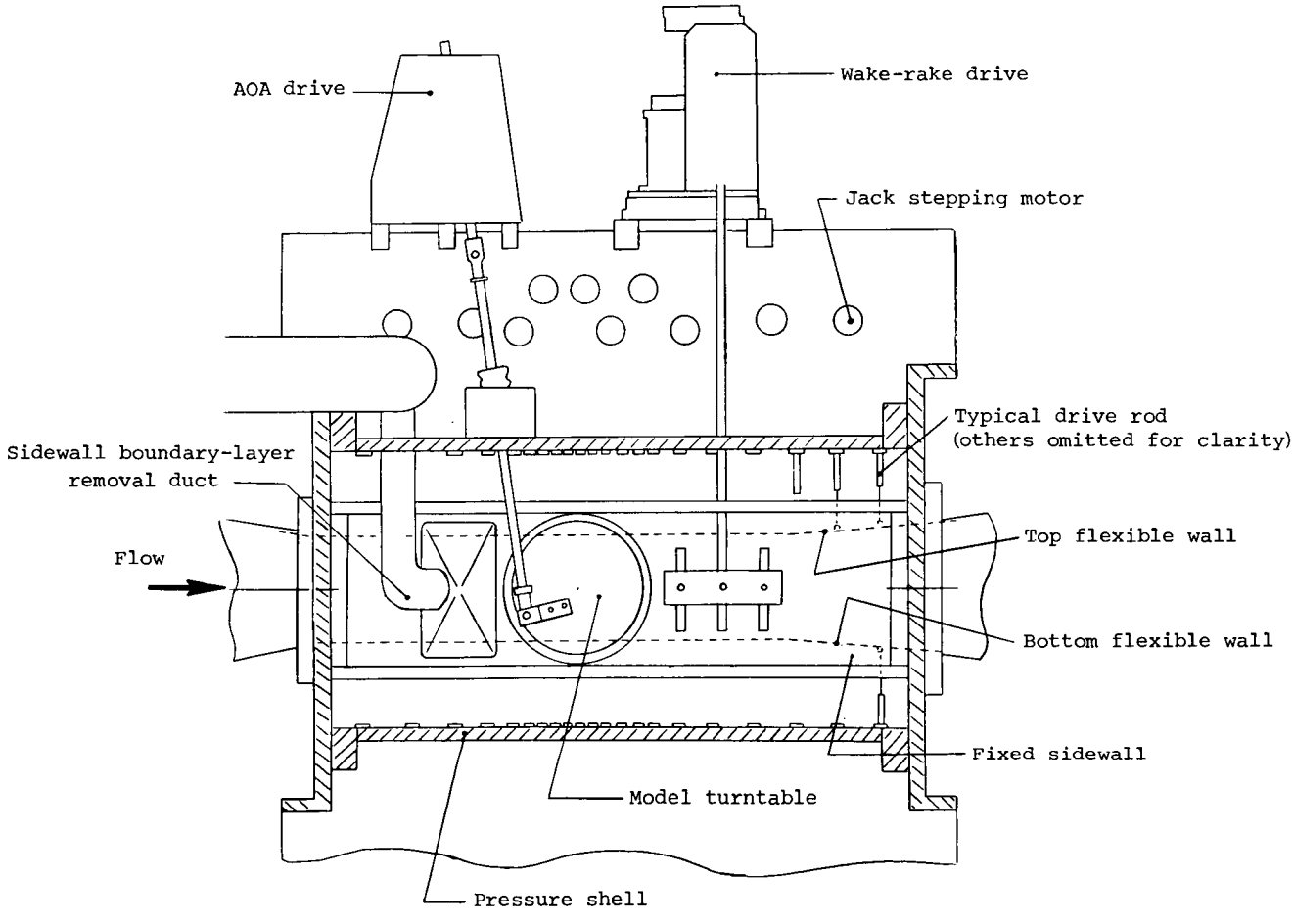

Figure 3. Sketch of 13-in. by 13-in. adaptive-wall test section (plenum wall removed).

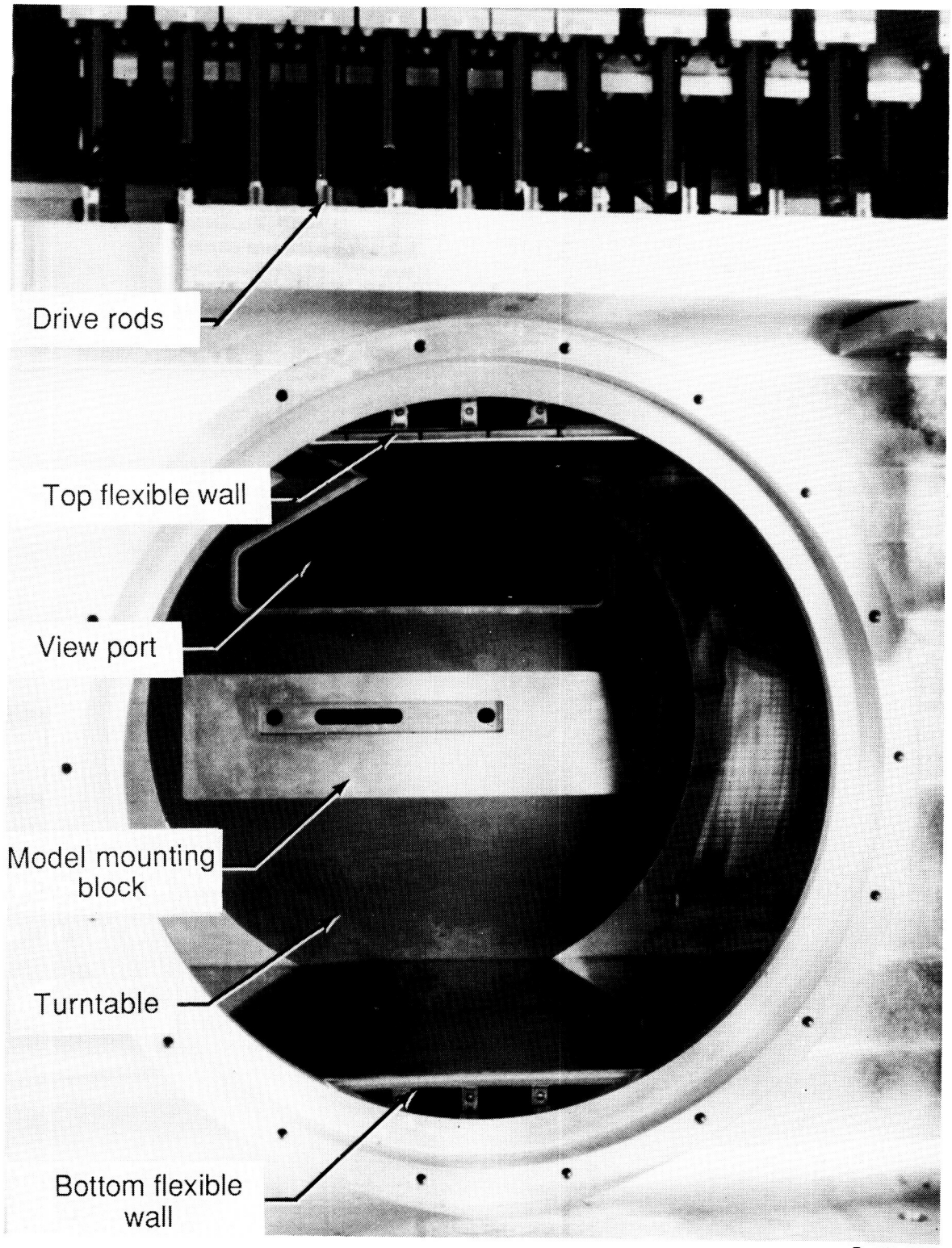

L-87-659

Figure 4. Model mounting system of 13-in. by 13-in. adaptive-wall test section.

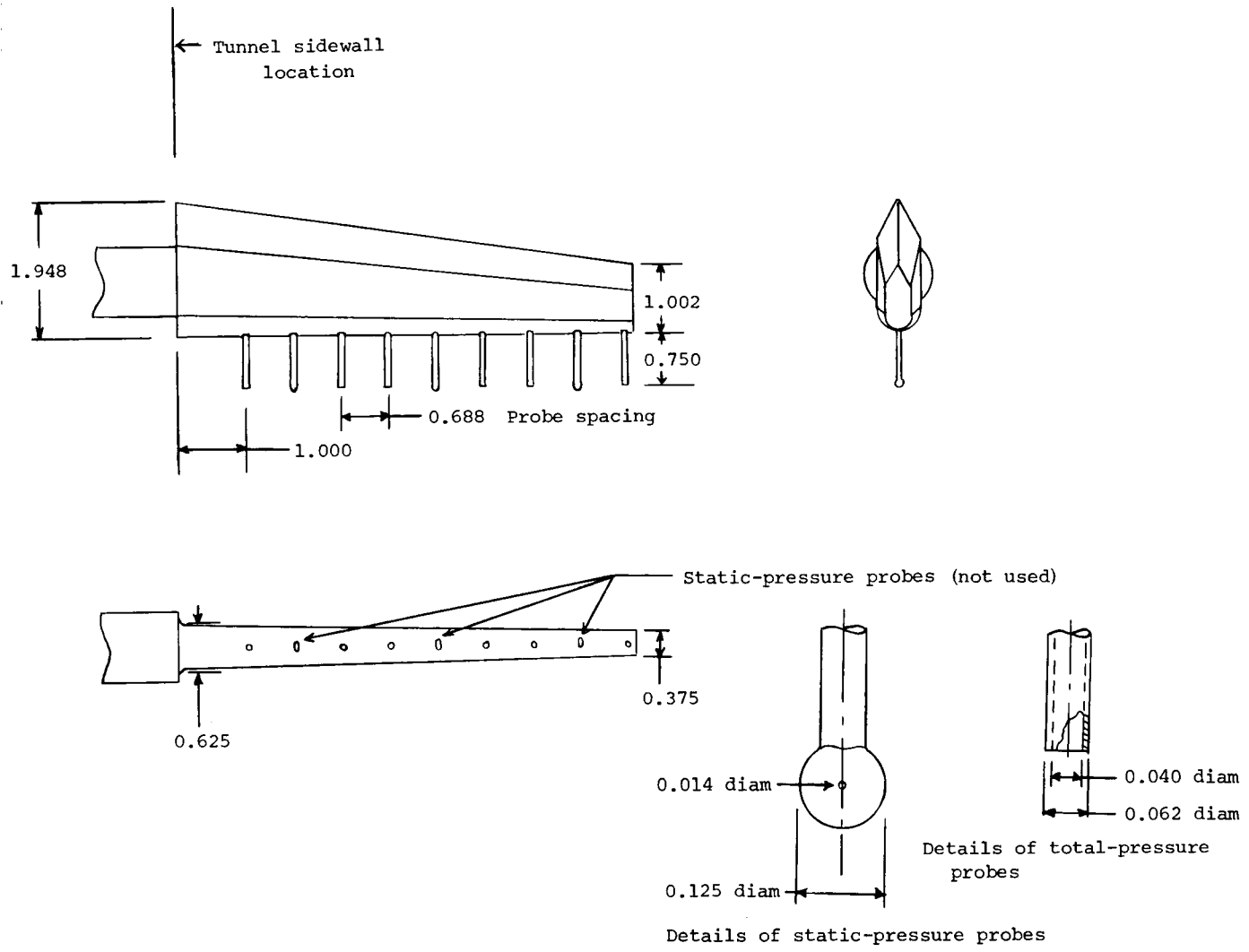

Figure 5. Sketch of wake survey probe. All dimensions in inches.

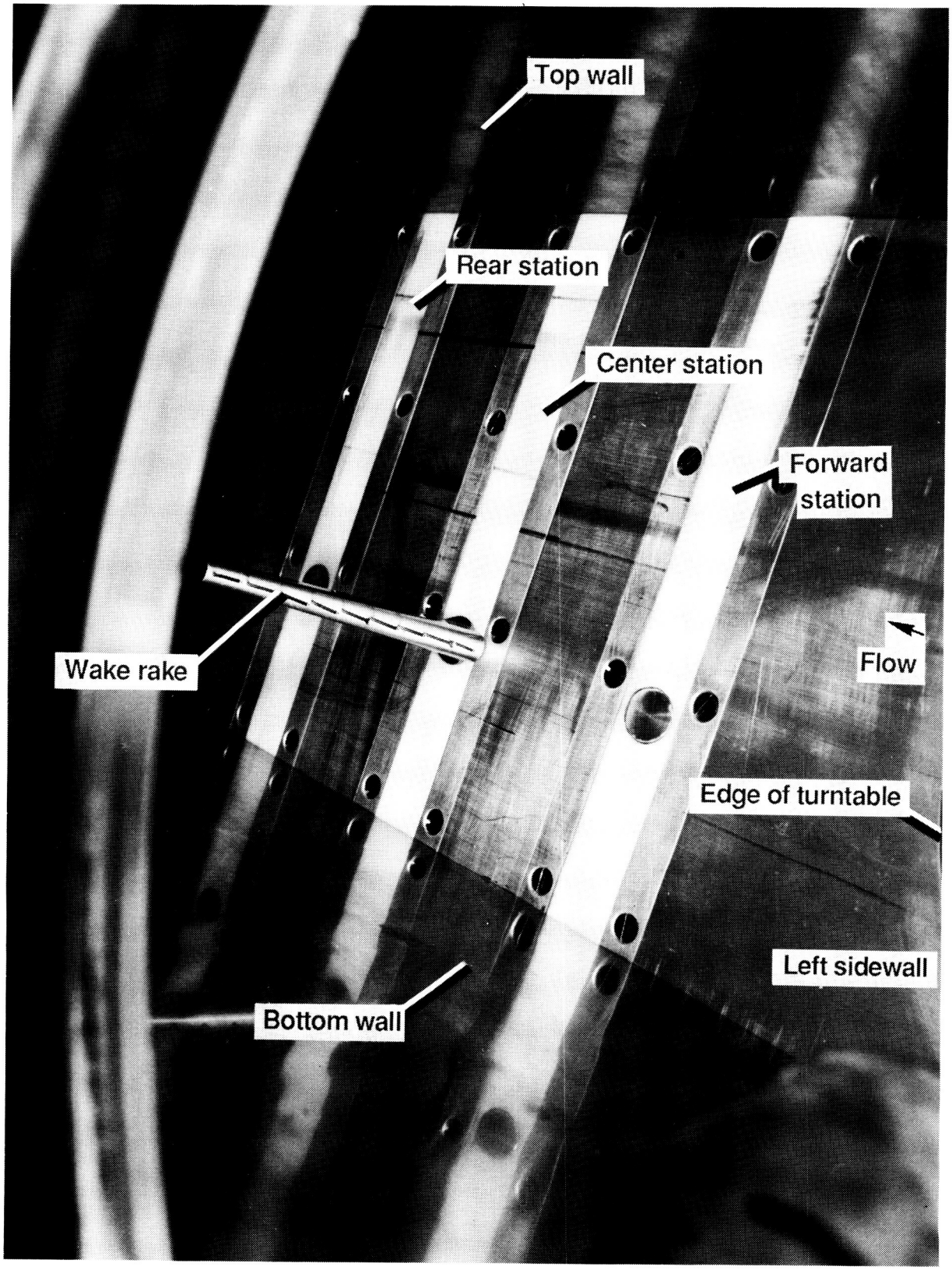

L-86-7617

Figure 6. Wake survey probe mounted in center survey station.

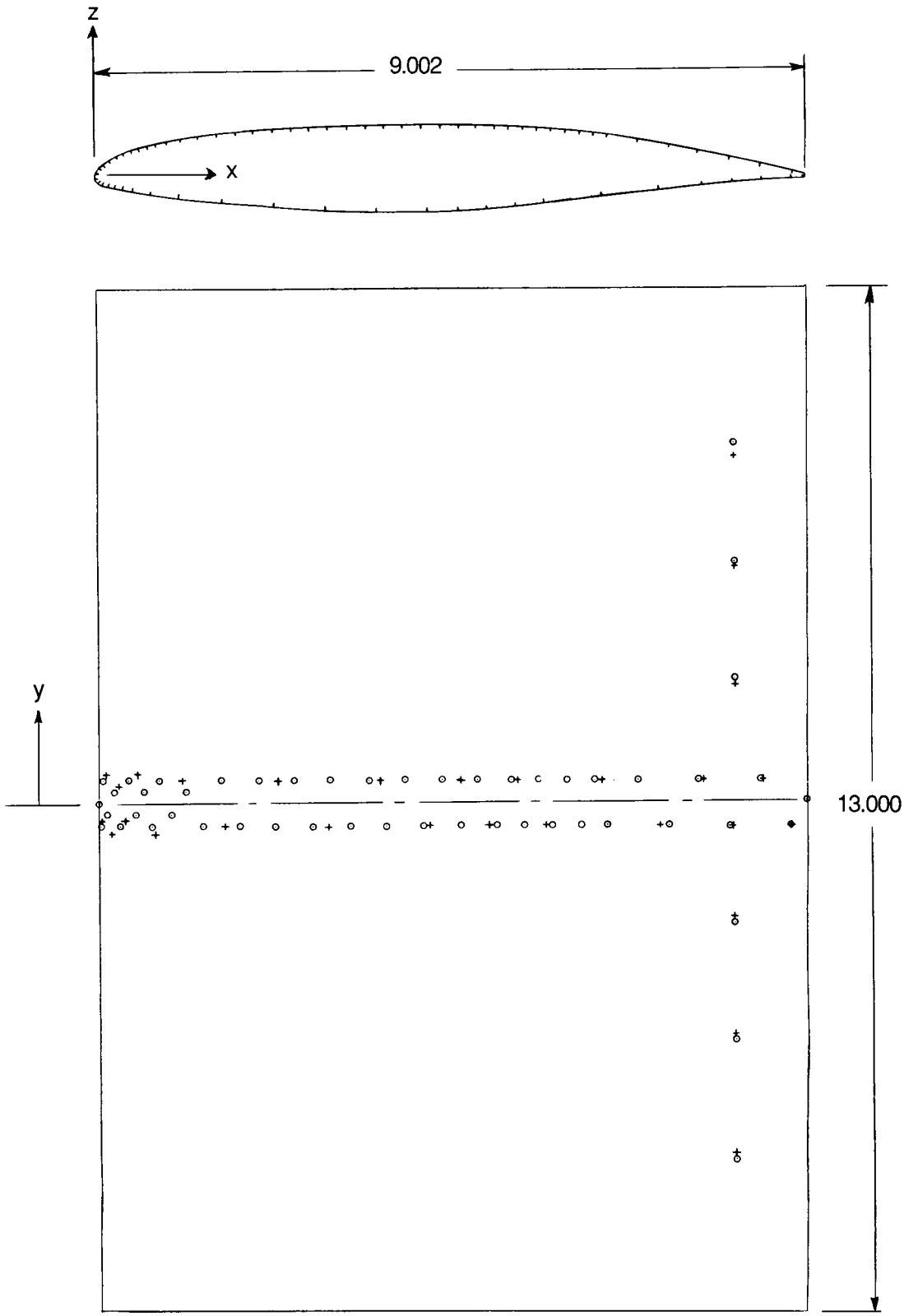

Figure 7. Layout of pressure orifice locations. All dimensions in inches. Open symbols denote upper surface; "+" denotes lower surface.

L-86-9833

Figure 8. CAST 10-2/DOA 2 airfoil model and turntable mounting blocks.

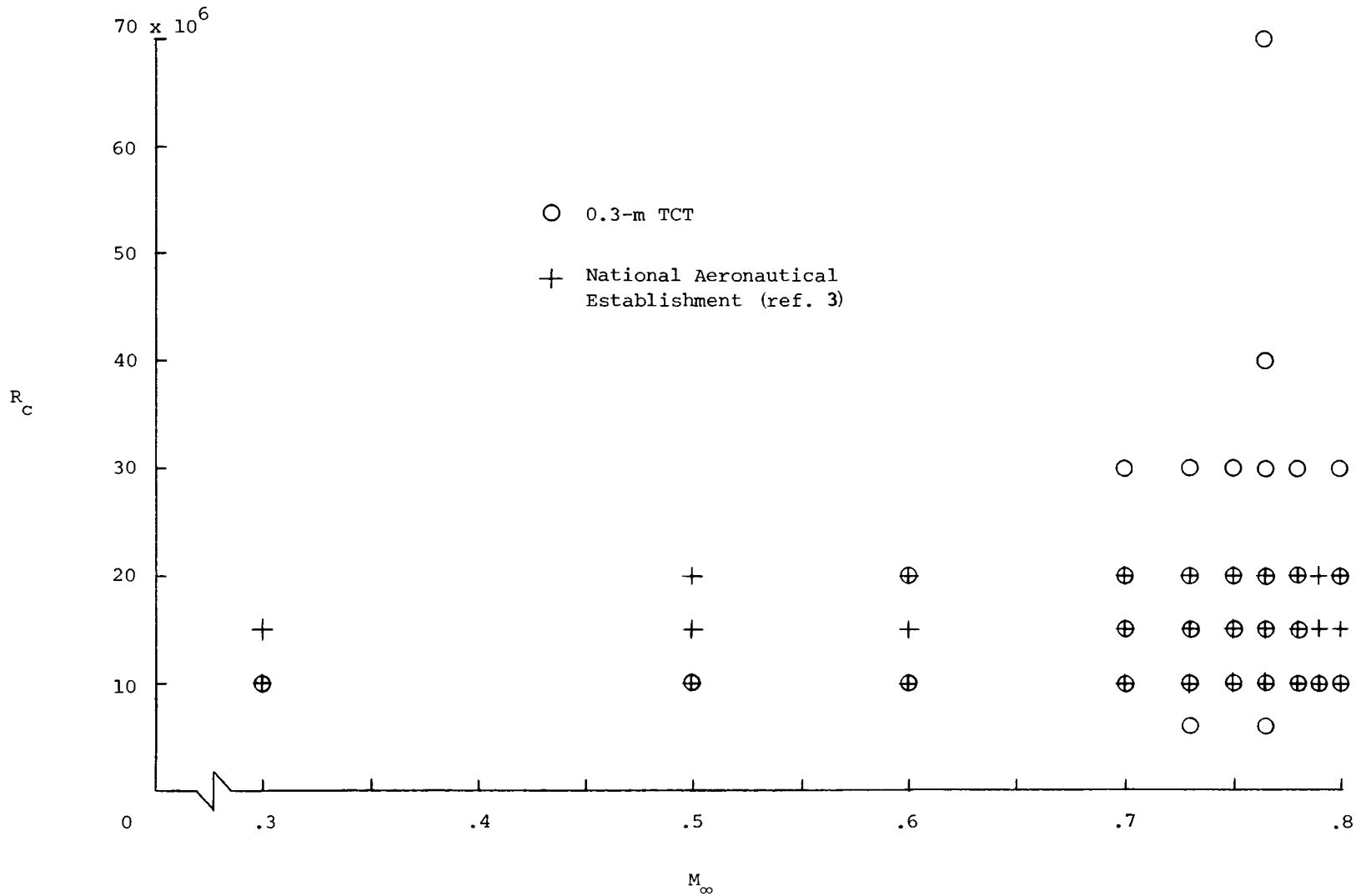

Figure 9. Matrix of test conditions used.

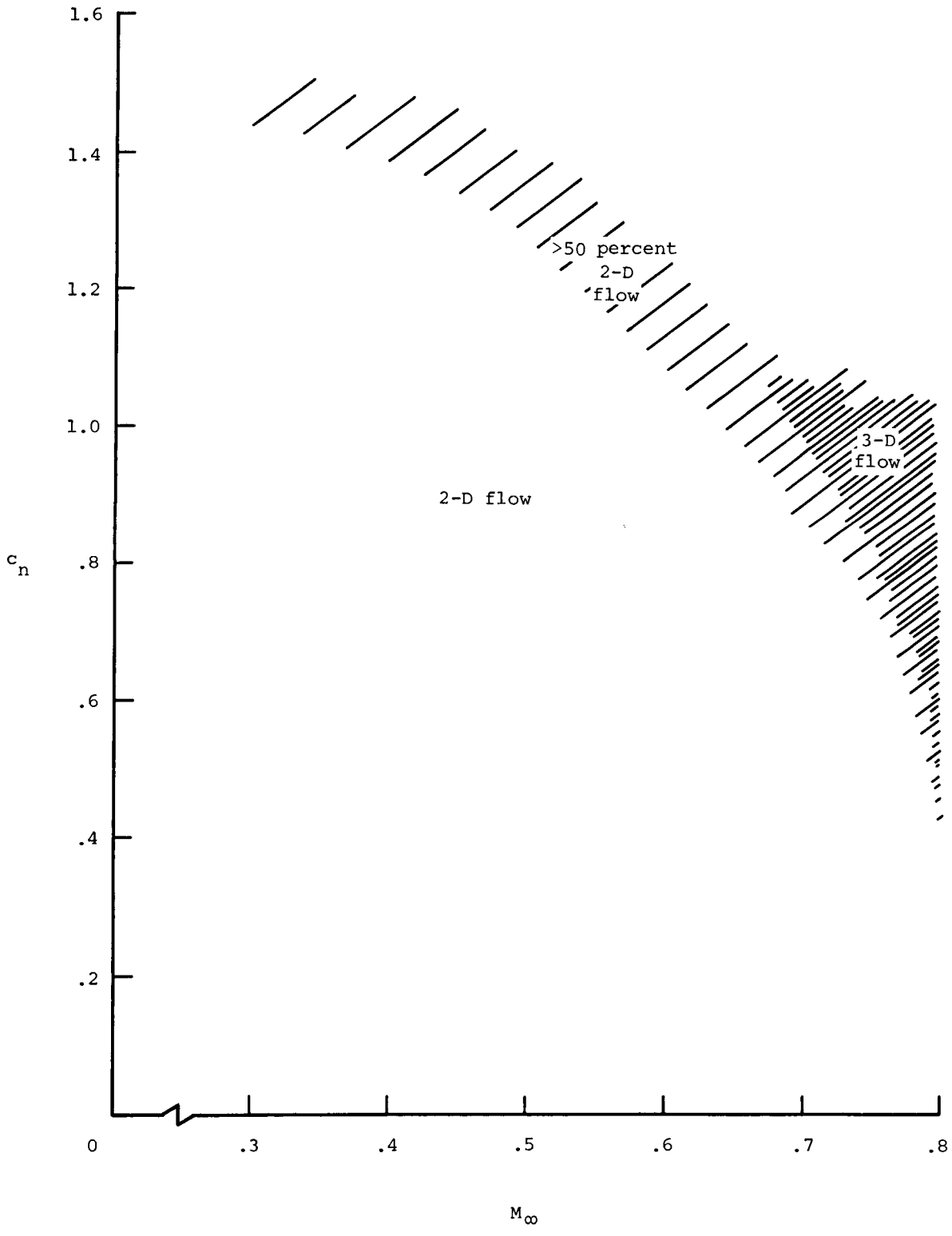

Figure 10. Matrix of test conditions for two-dimensional flow over model.

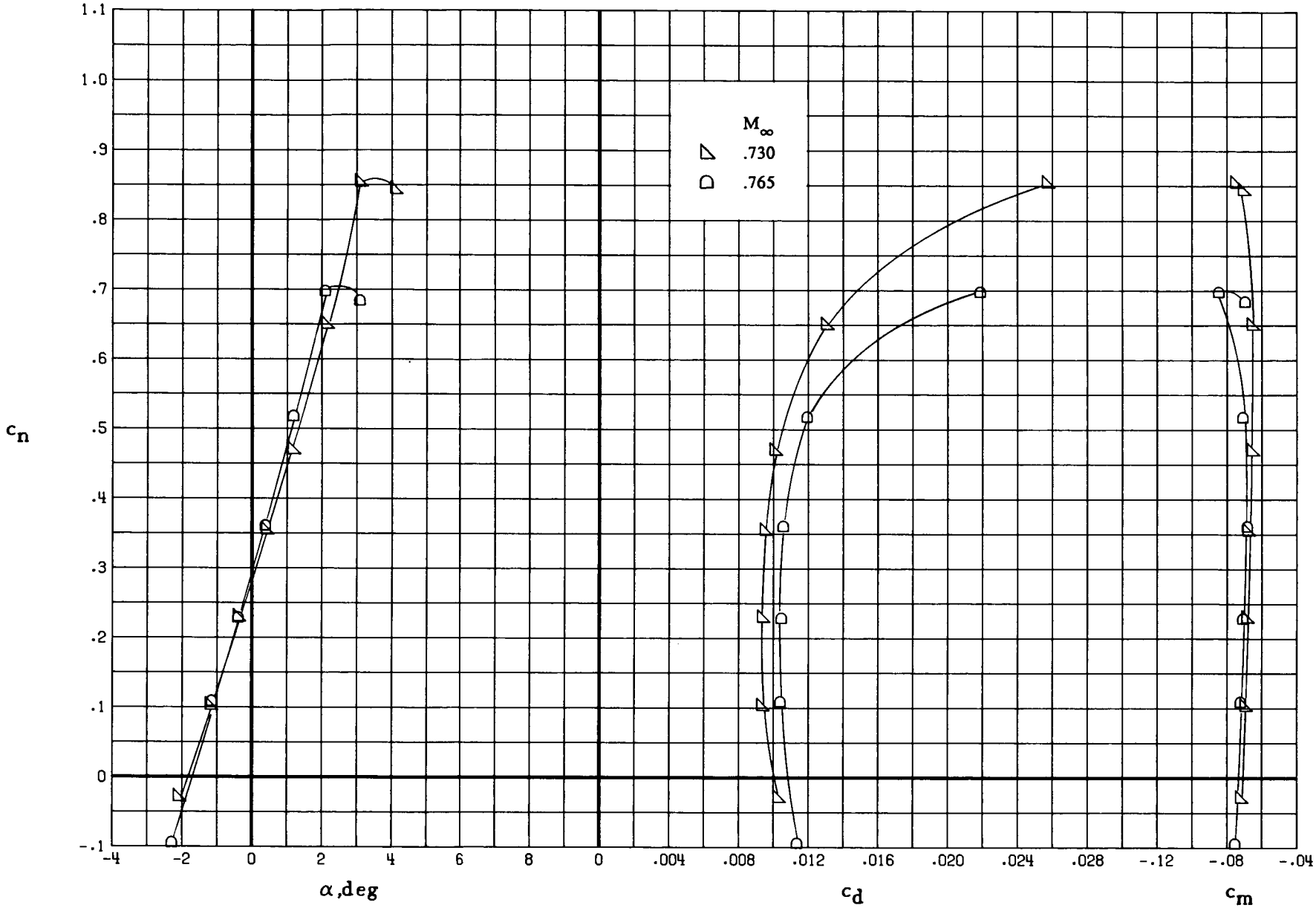

(a) $R_c = 6 \times 10^6$.

Figure 11. Effects of M_∞ on integrated force-and-moment coefficients.

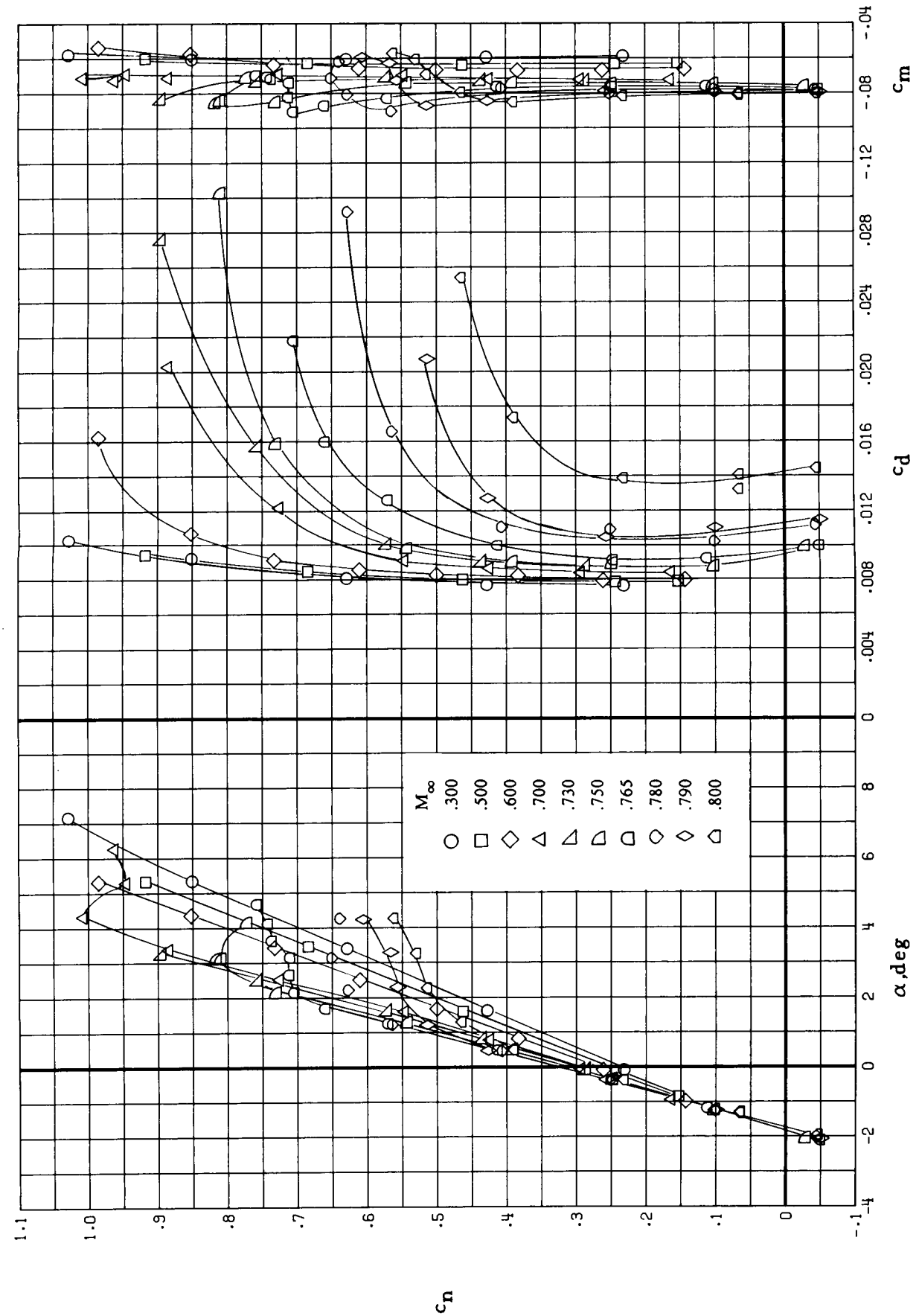

(b) $R_c = 10 \times 10^6$.

Figure 11. Continued.

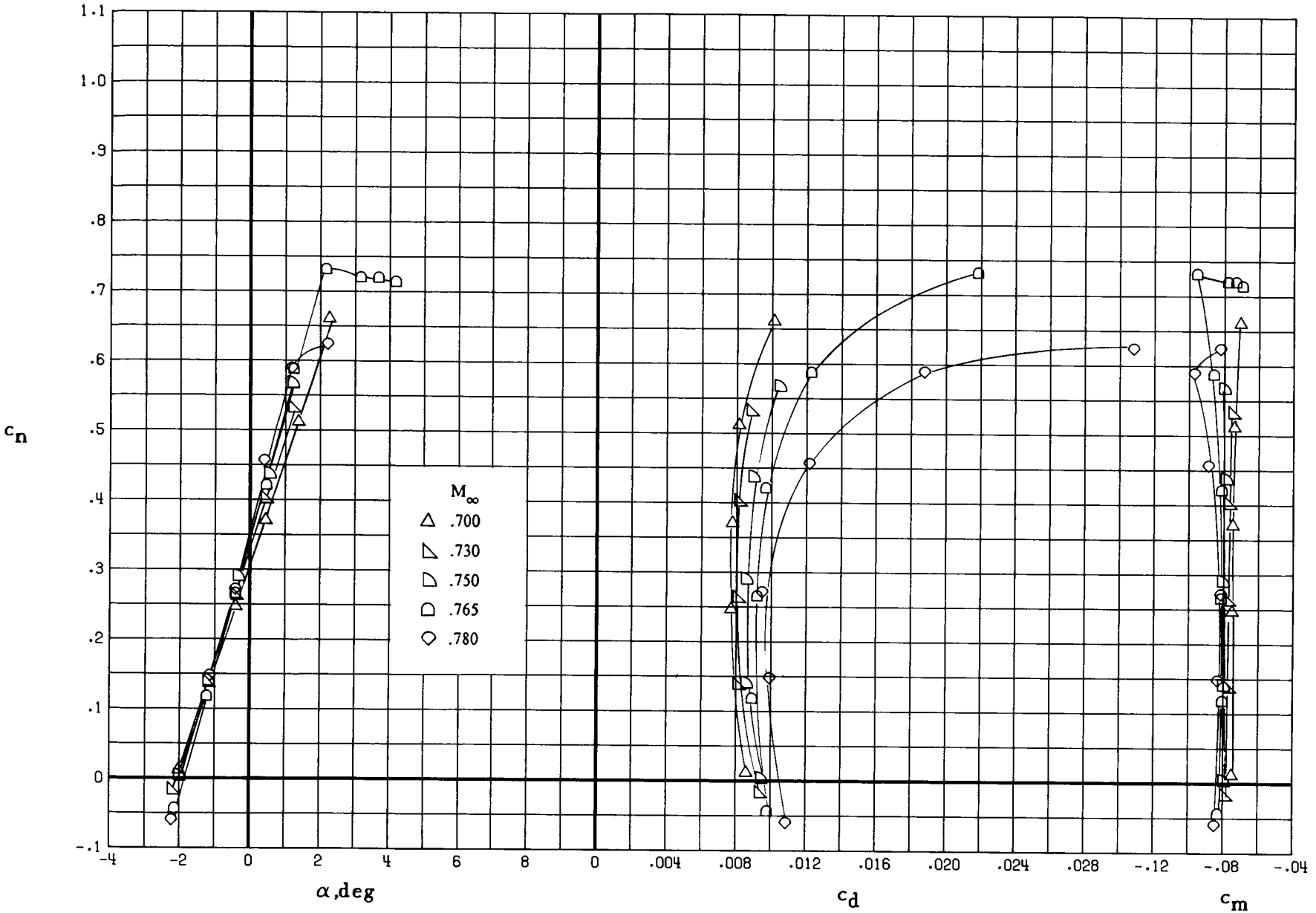

(c) $R_c = 15 \times 10^6$.

Figure 11. Continued.

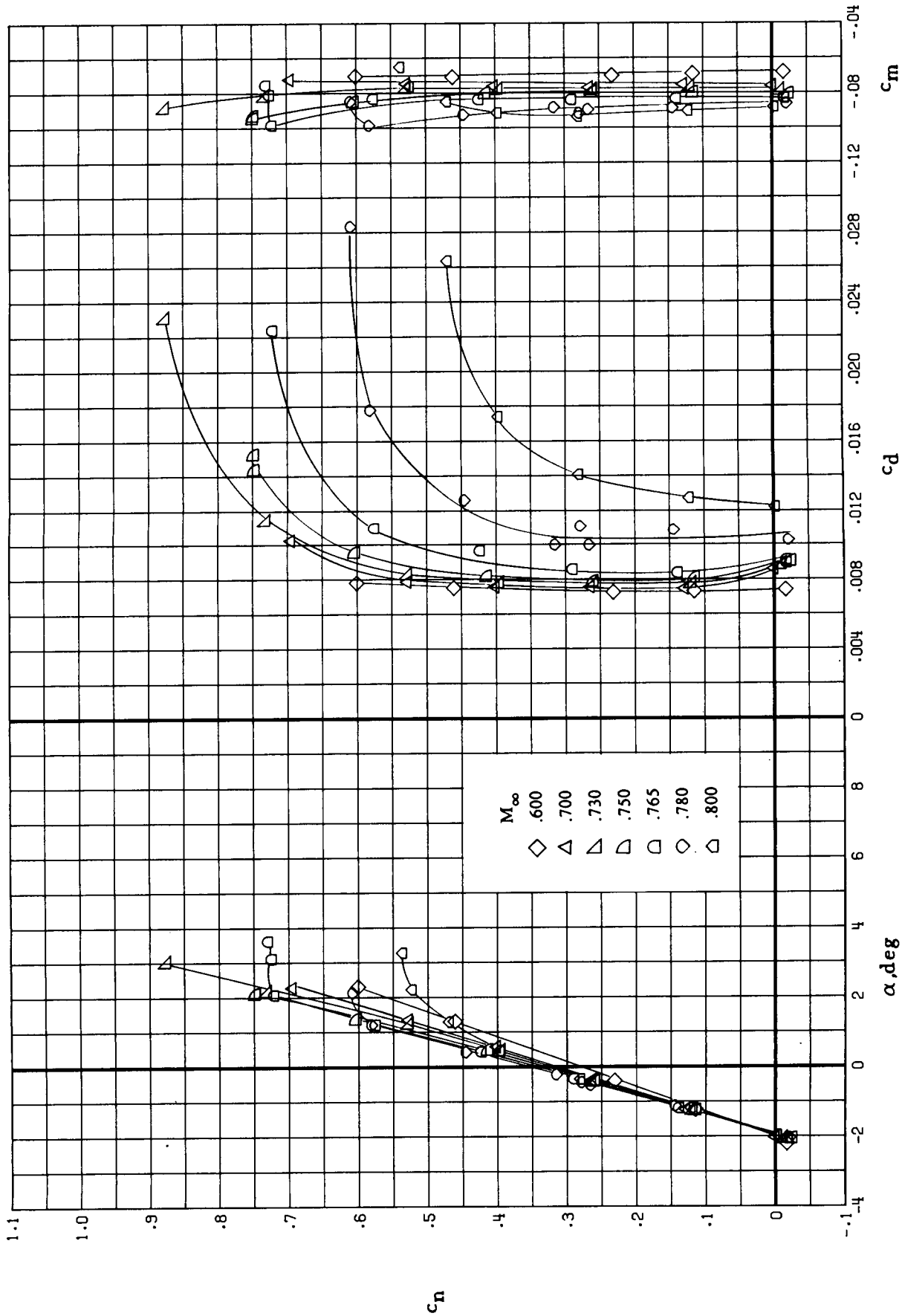

(d) $R_c = 20 \times 10^6$.

Figure 11. Continued.

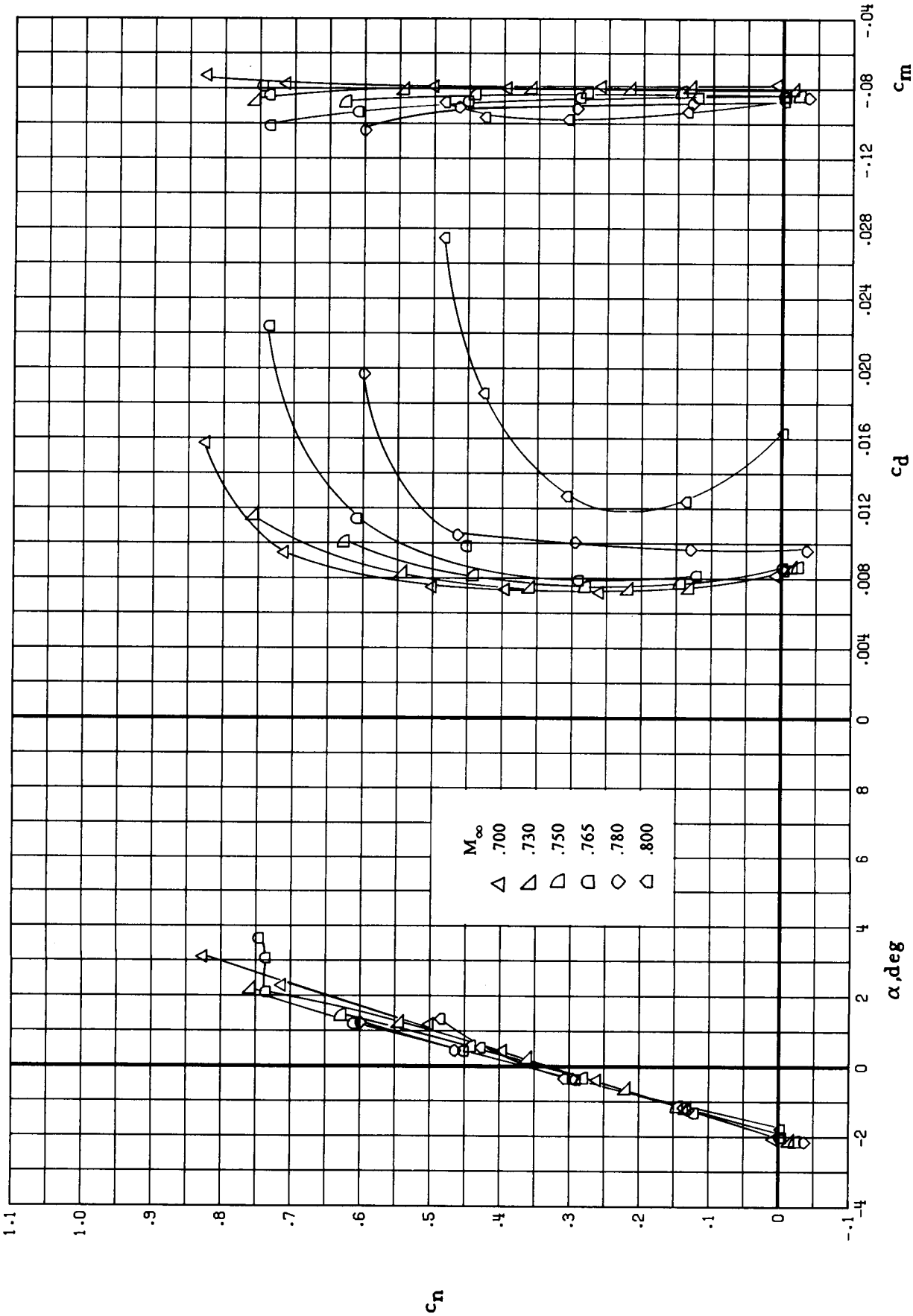

(e) $R_c = 30 \times 10^6$.

Figure 11. Concluded.

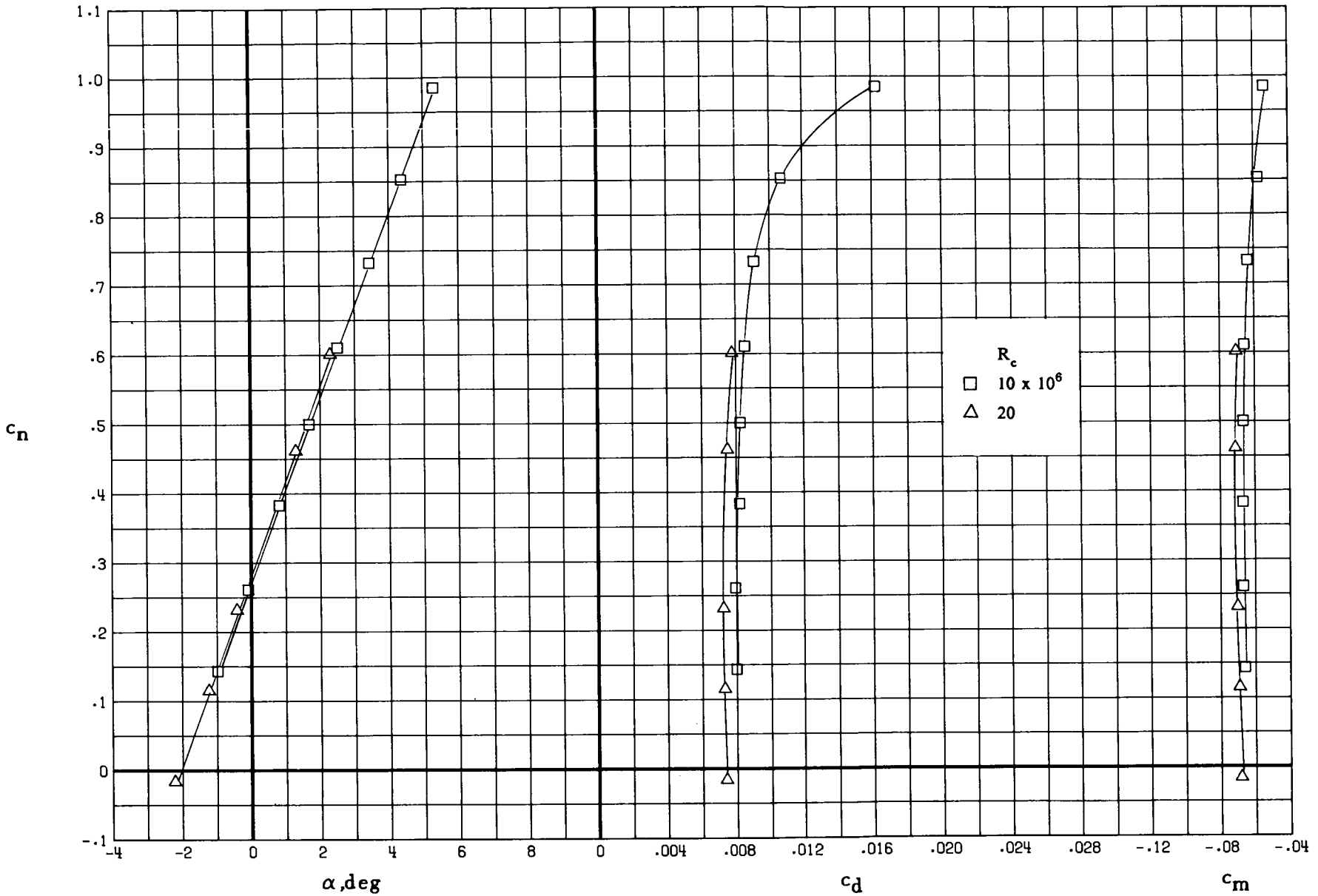

(a) $M_\infty = 0.60$.

Figure 12. Effect of chord Reynolds number on integrated force-and-moment coefficients.

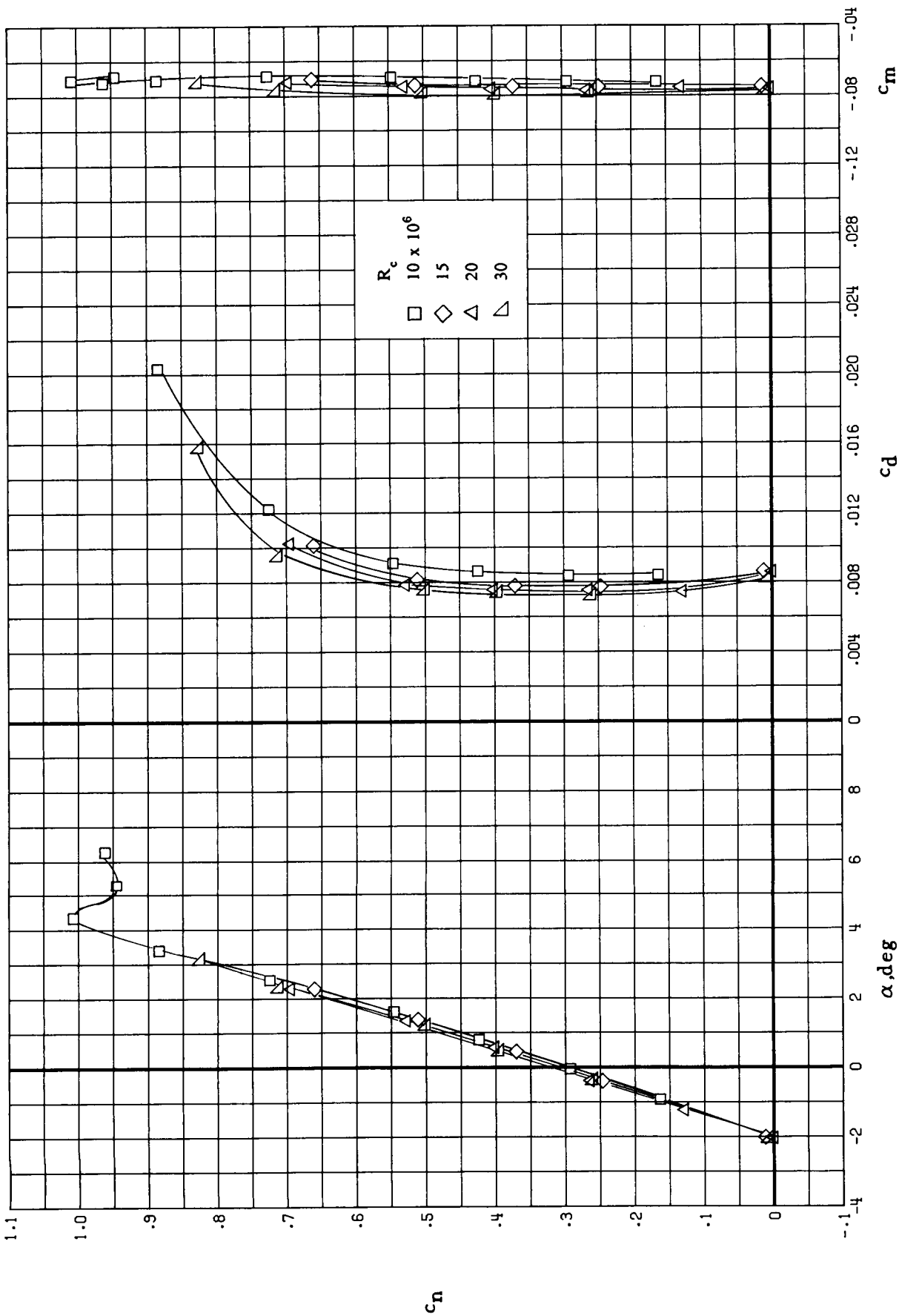

(b) $M_\infty = 0.70$.

Figure 12. Continued.

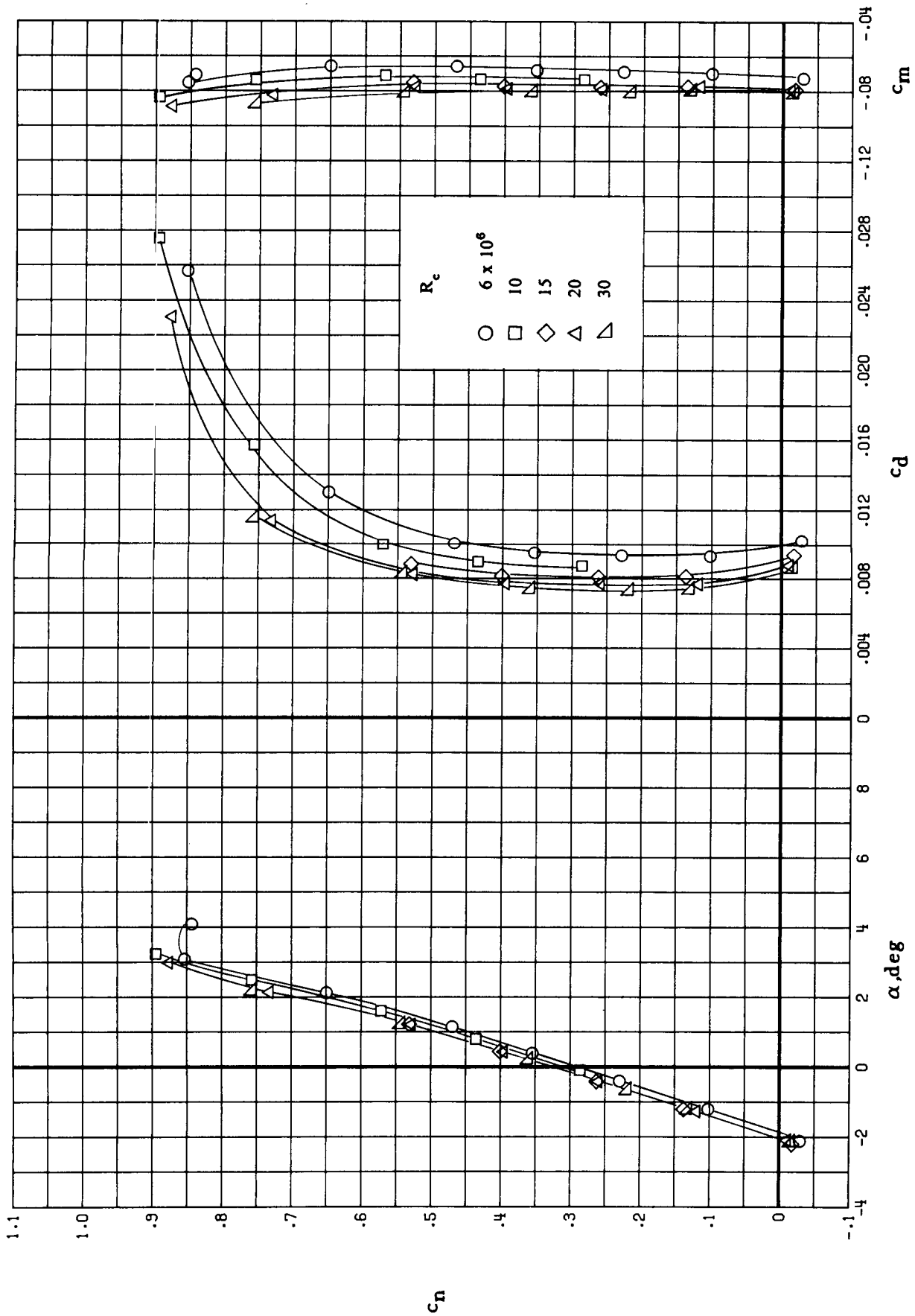

(c) $M_\infty = 0.73$.

Figure 12. Continued.

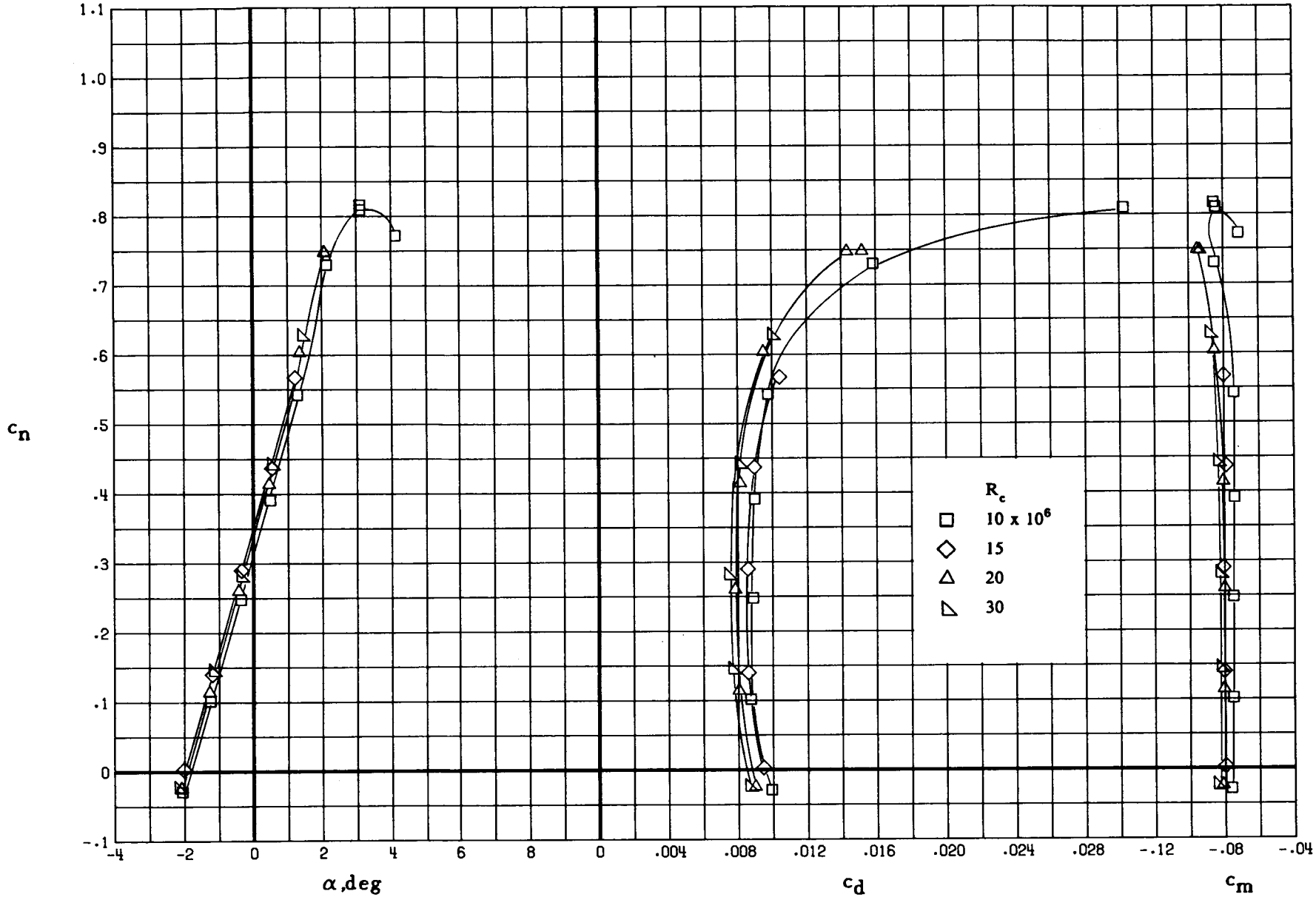

(d) $M_\infty = 0.75$.

Figure 12. Continued.

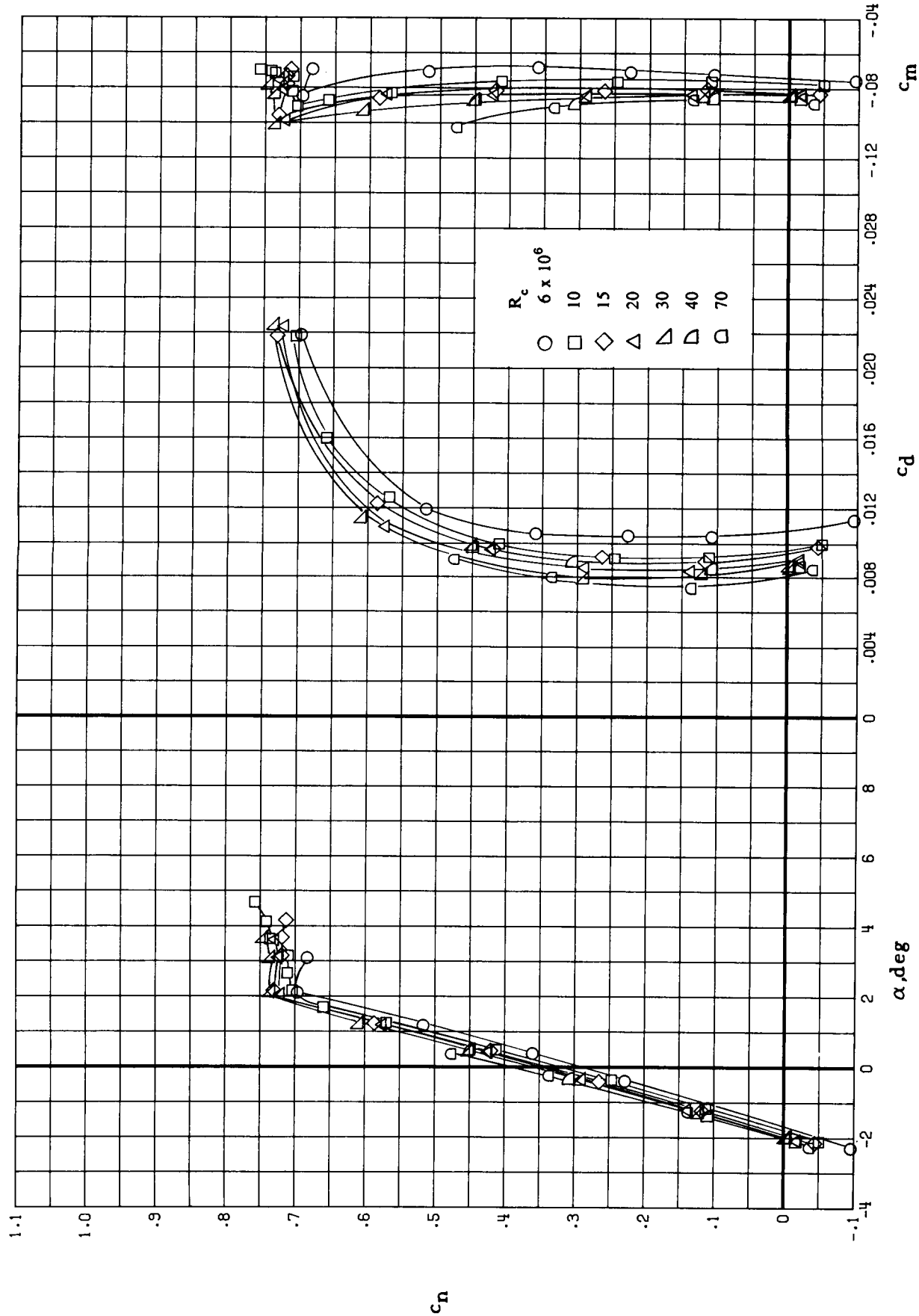

(e) $M_\infty = 0.765$.

Figure 12. Continued.

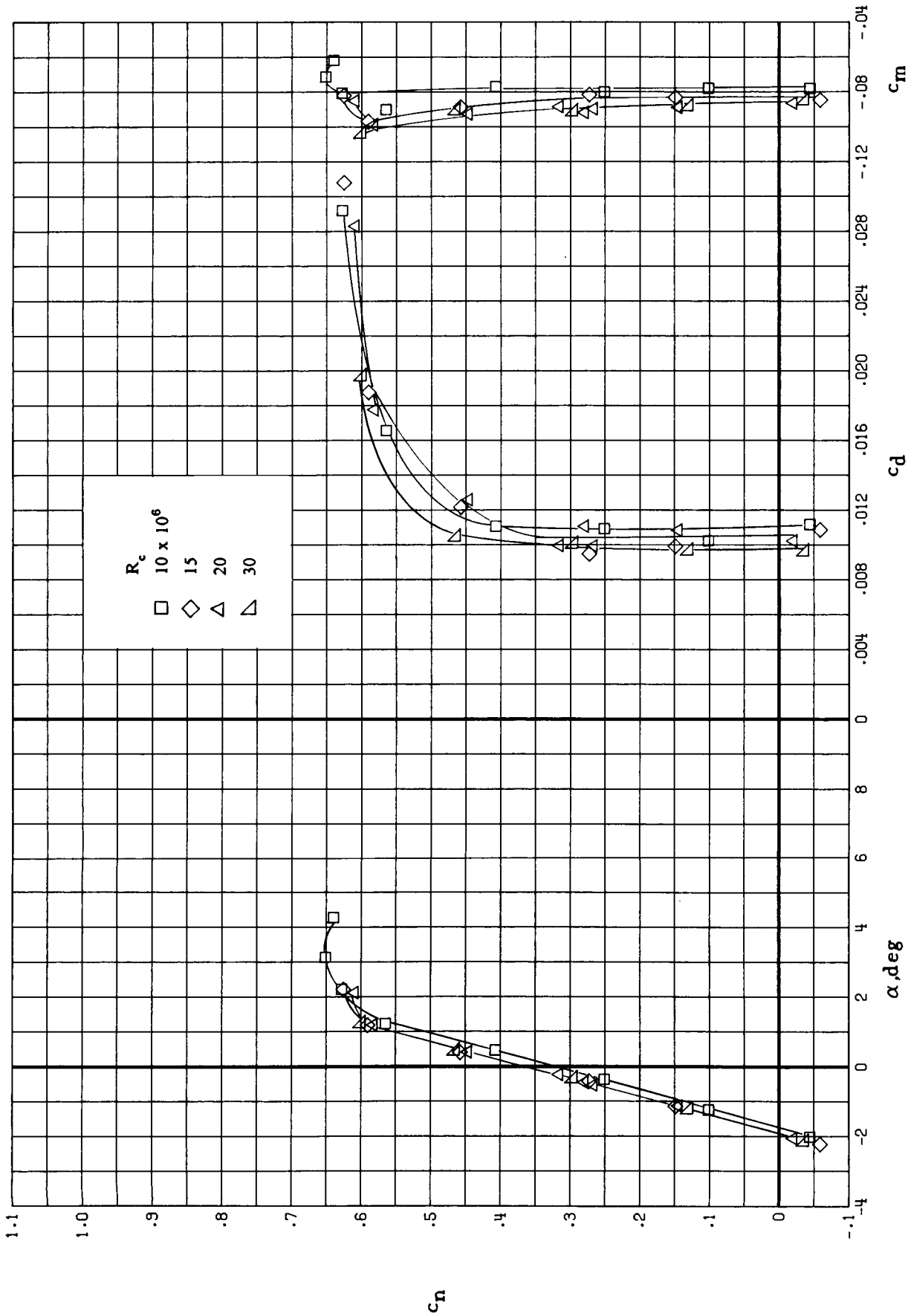

(f) $M_\infty = 0.78$.

Figure 12. Continued.

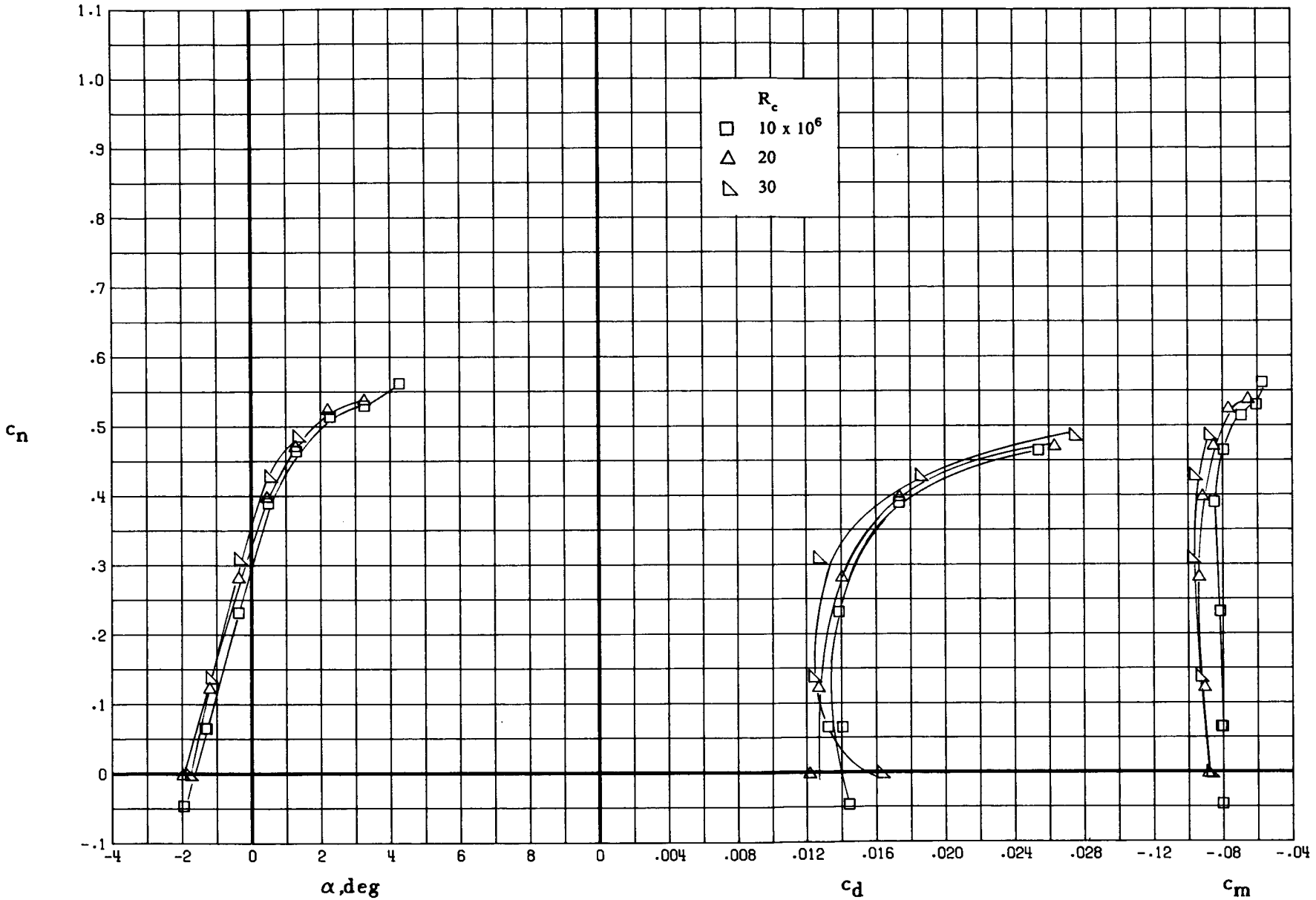

(g) $M_\infty = 0.80$.

Figure 12. Concluded.

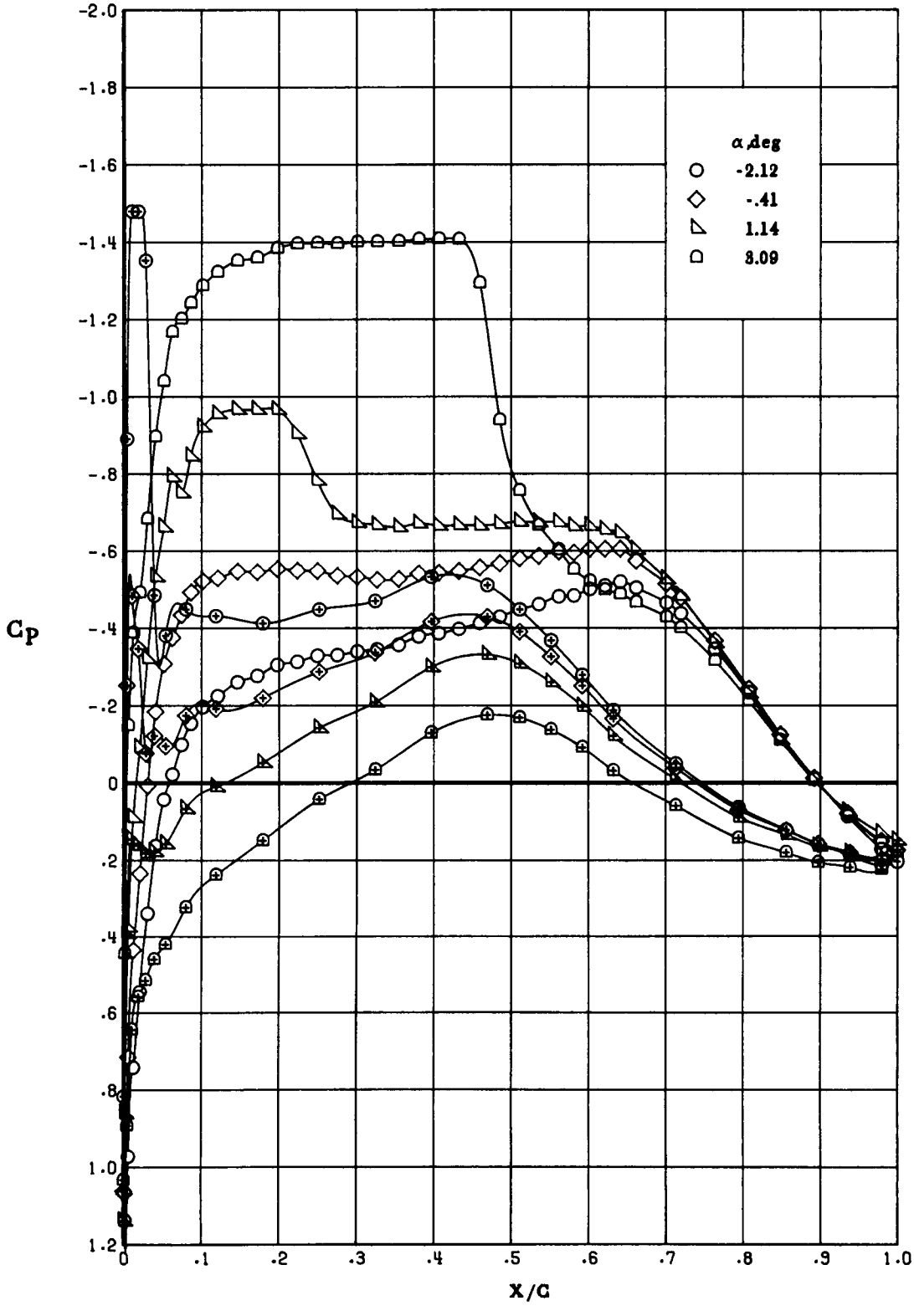

(a) $M_\infty = 0.73$.

Figure 13. Effect of α on chordwise pressure distribution at $R_c = 6 \times 10^6$. Open symbols denote upper surface; "+" within symbols denotes lower surface.

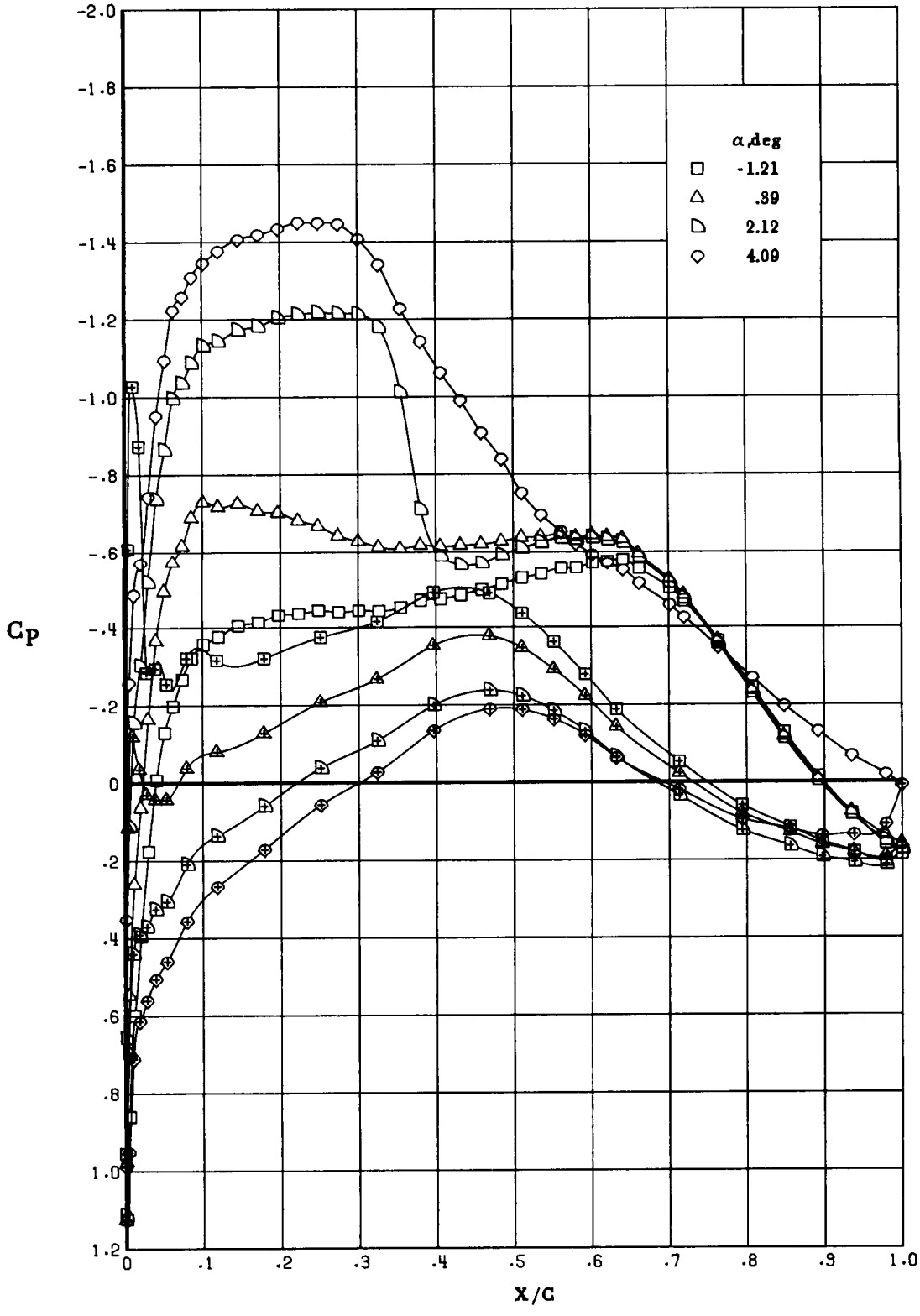

(a) Concluded.

Figure 13. Continued.

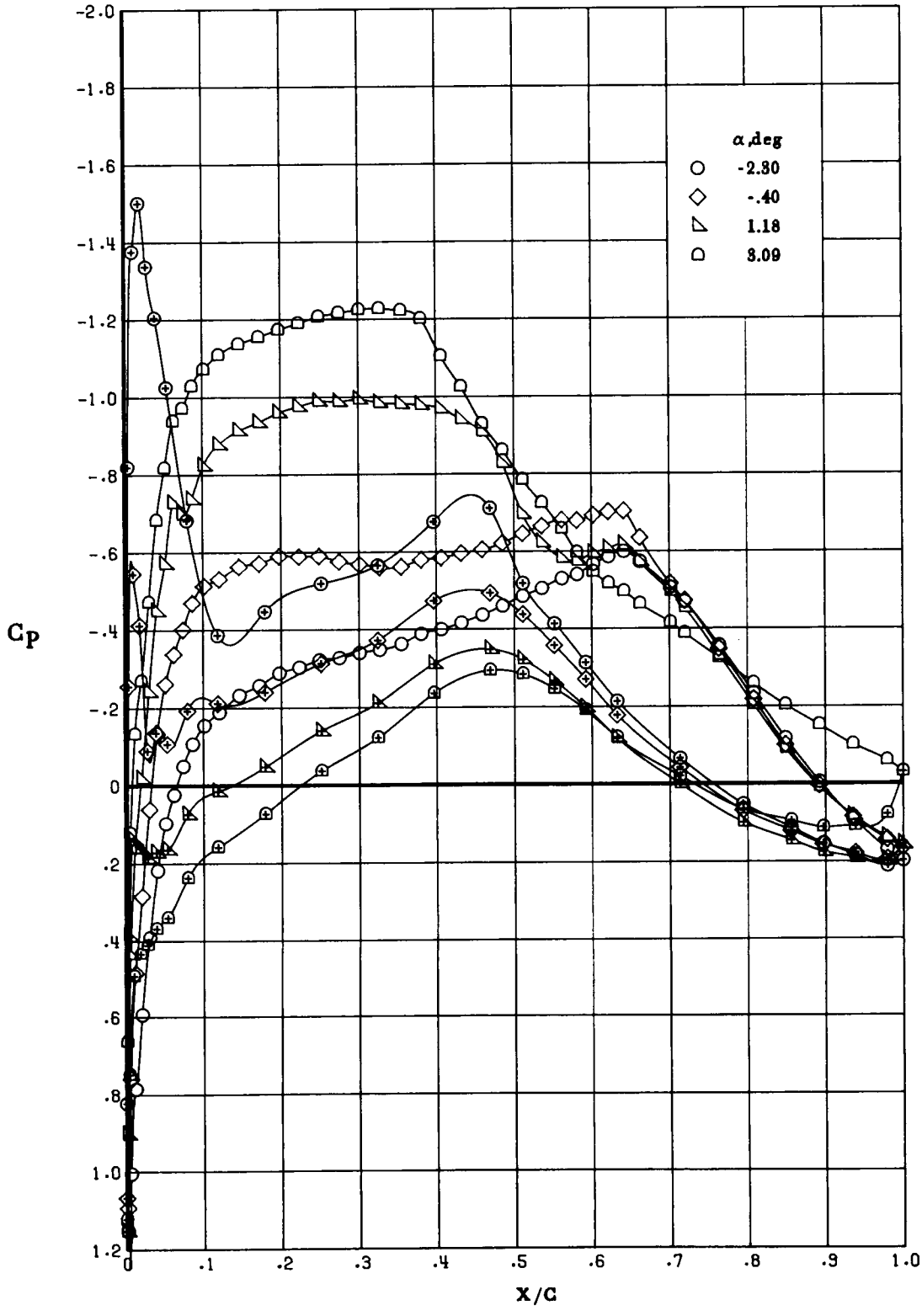

(b) $M_\infty = 0.765$.

Figure 13. Continued.

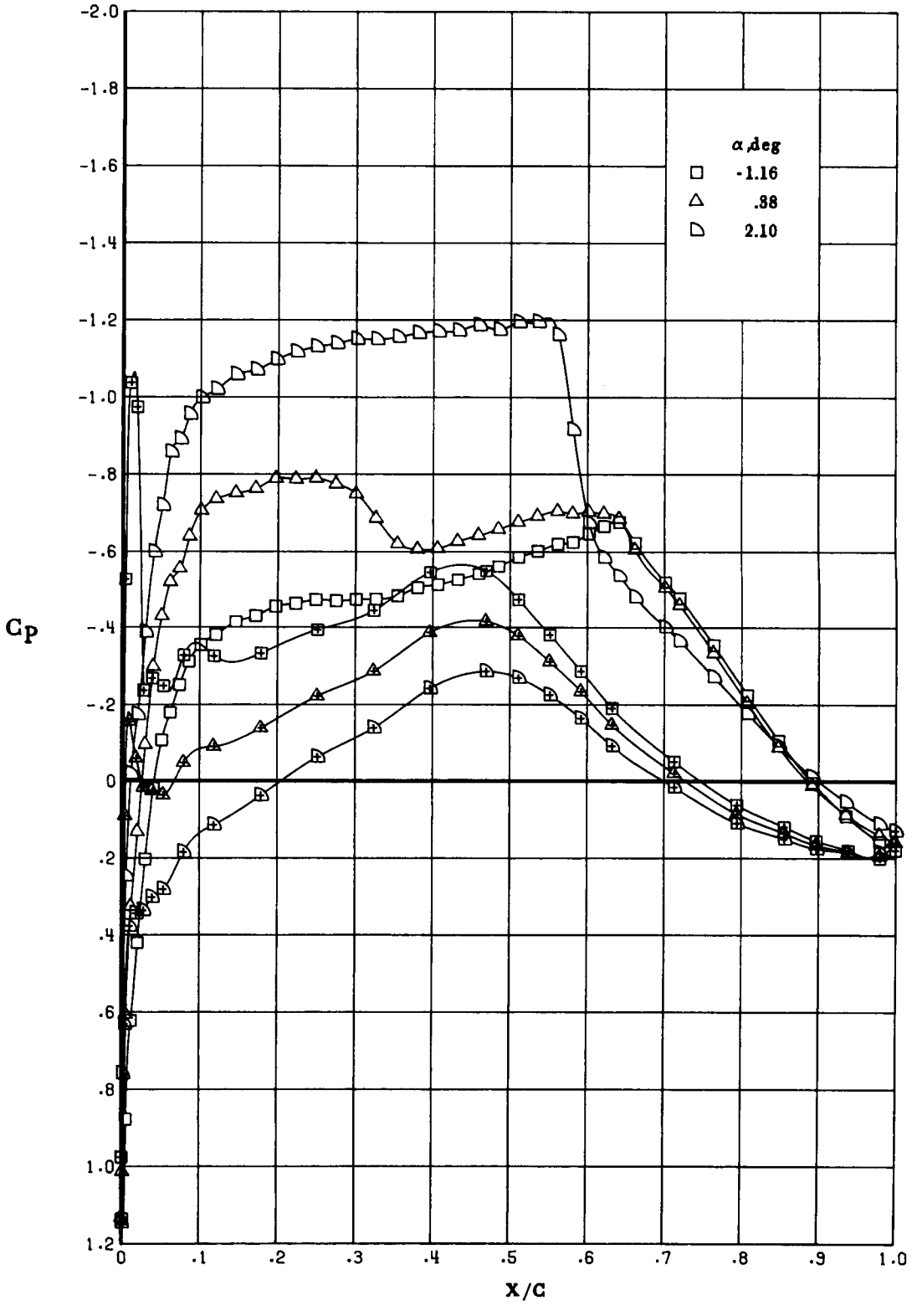

(b) Concluded.

Figure 13. Concluded.

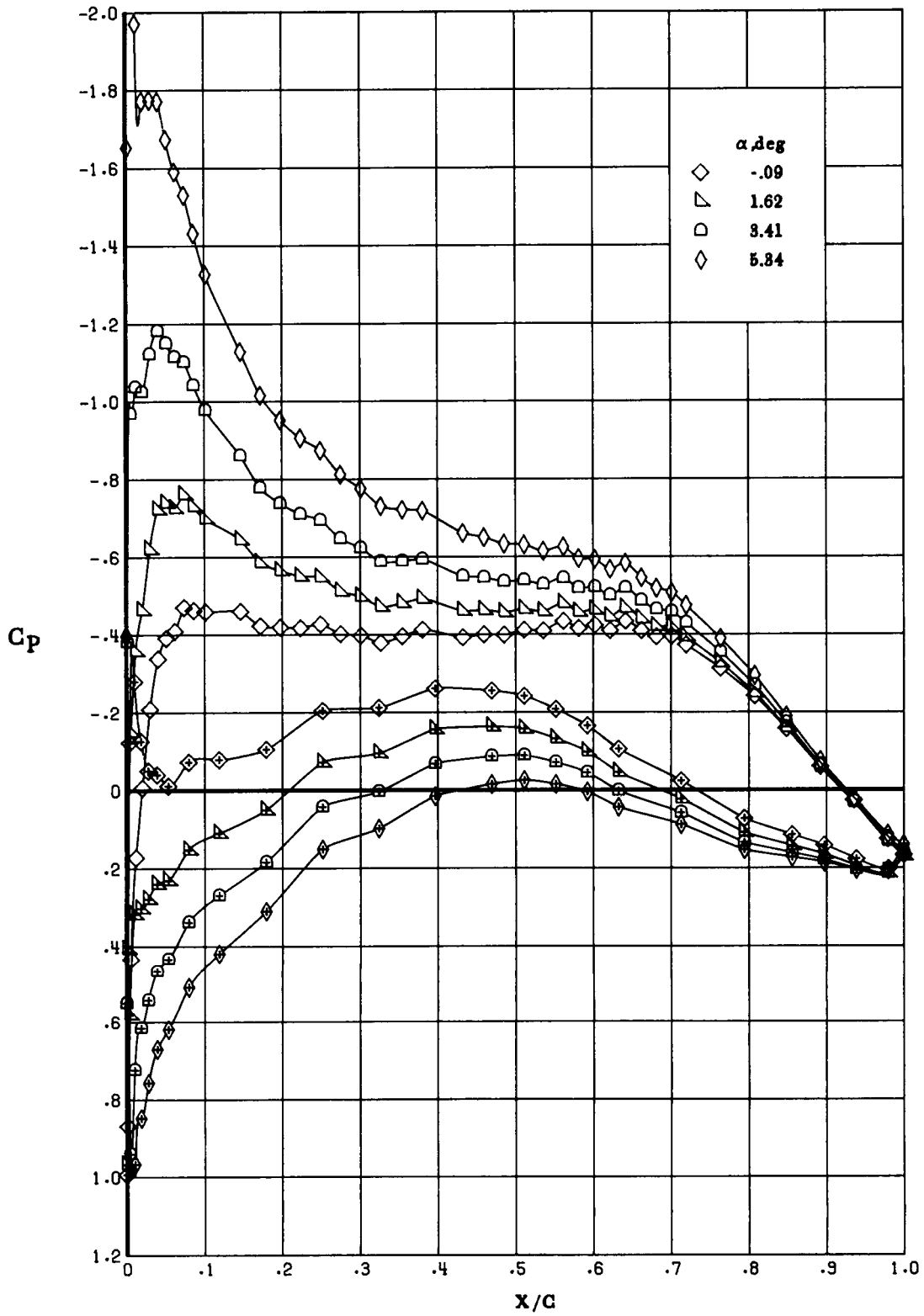

(a) $M_\infty = 0.30$.

Figure 14. Effect of α on chordwise pressure distribution at $R_c = 10 \times 10^6$. Open symbols denote upper surface; "+" within symbol denotes lower surface.

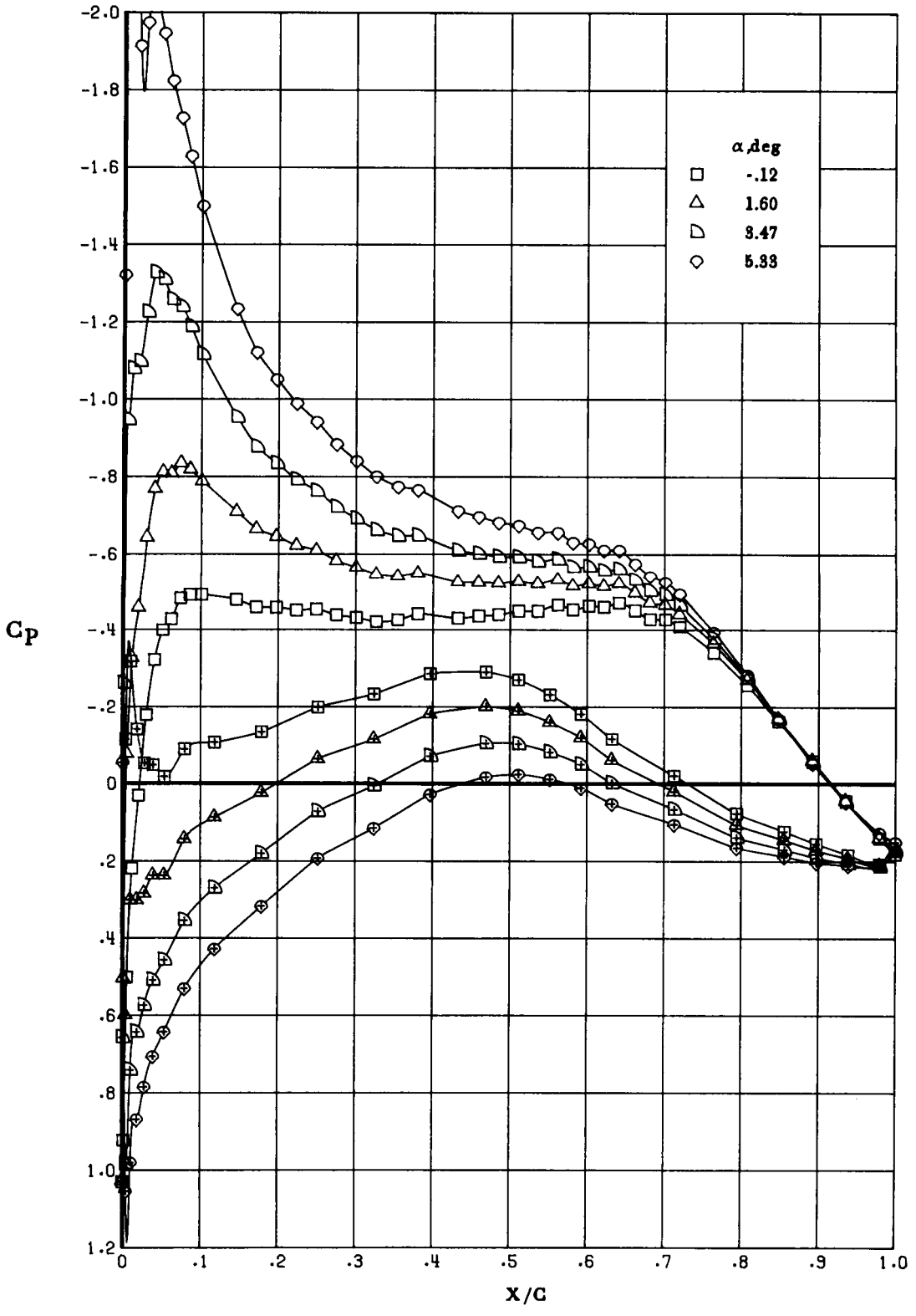

(b) $M_\infty = 0.50$.

Figure 14. Continued.

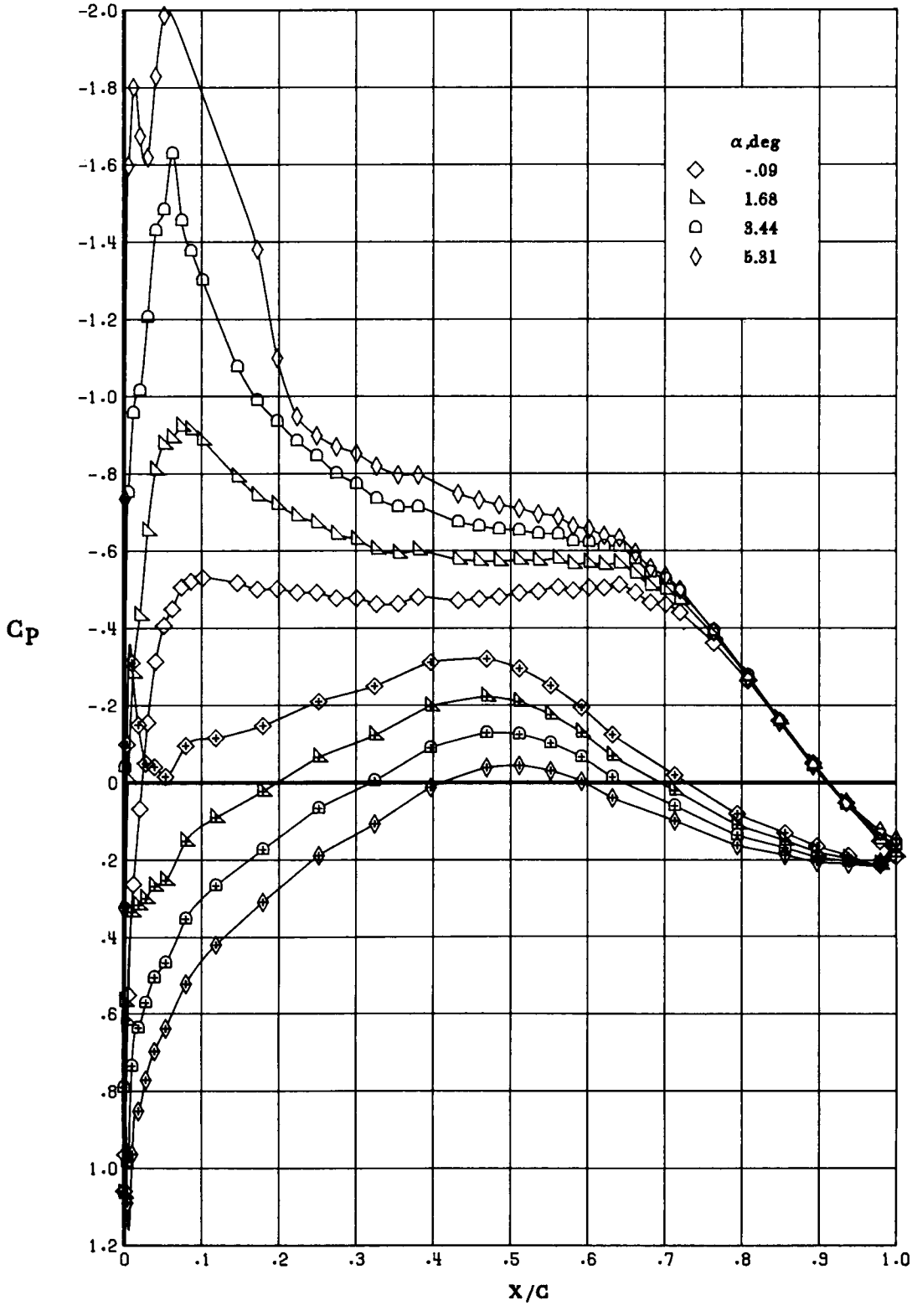

(c) $M_\infty = 0.60$.

Figure 14. Continued.

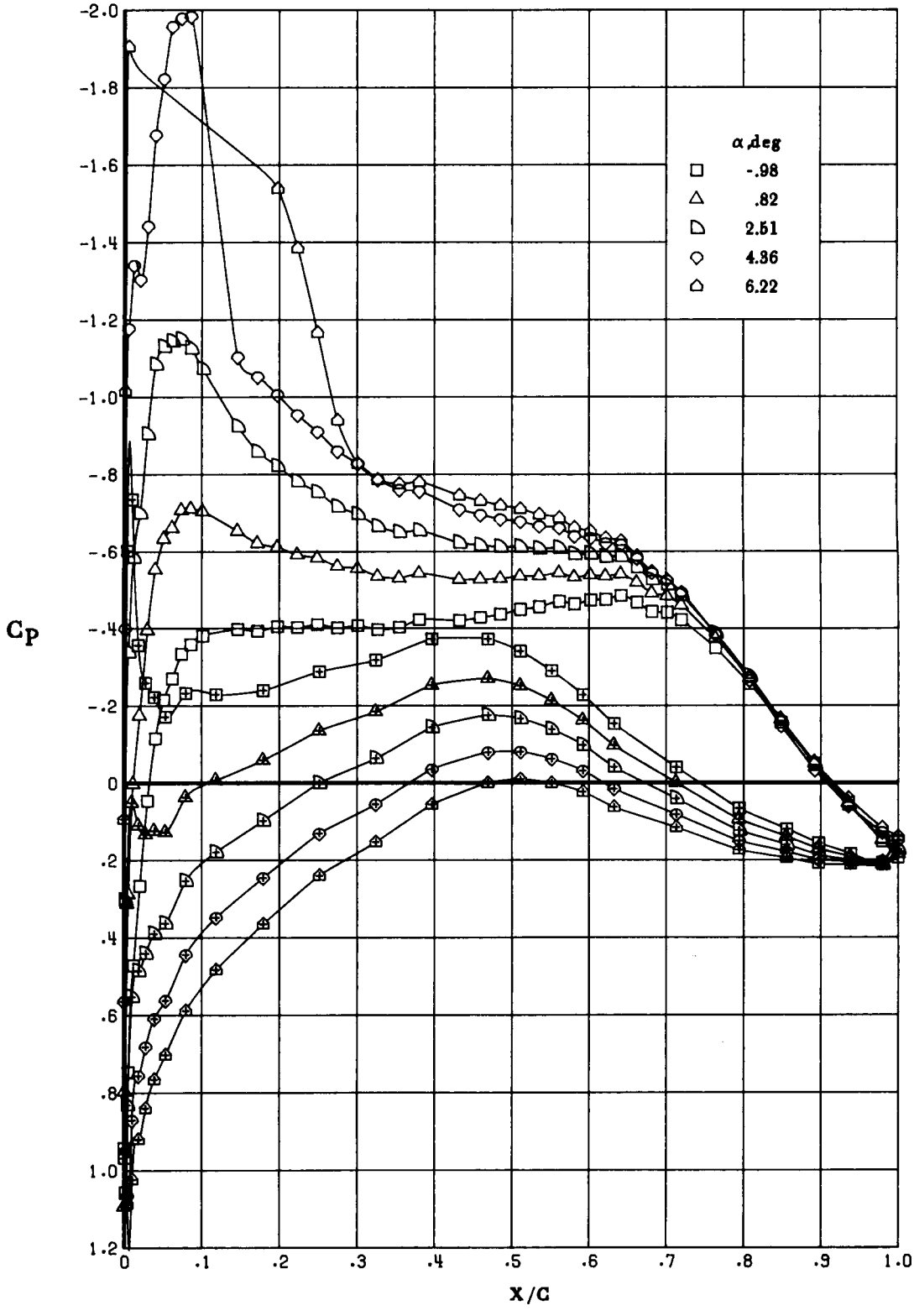

(c) Concluded.

Figure 14. Continued.

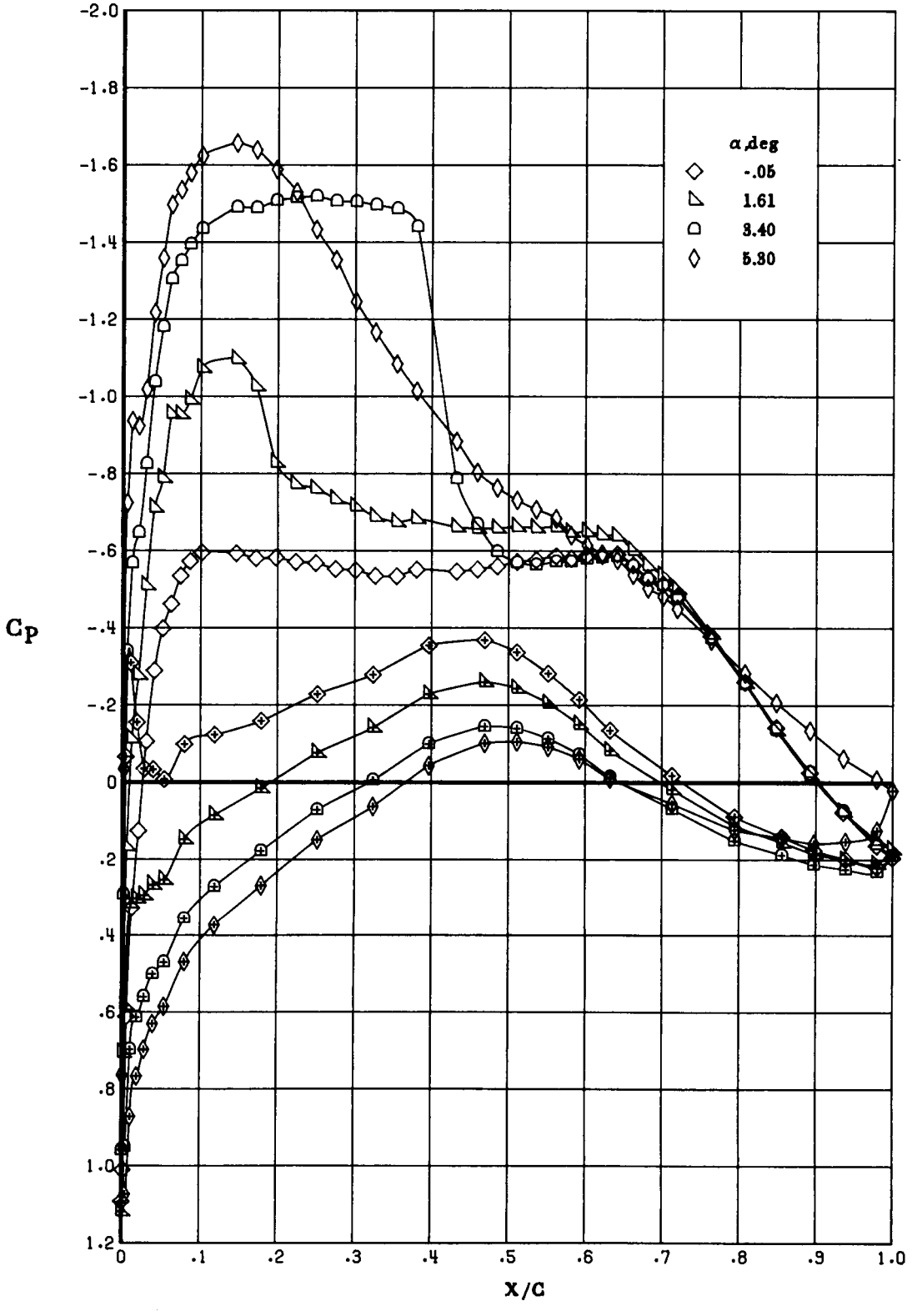

(d) $M_\infty = 0.70$.

Figure 14. Continued.

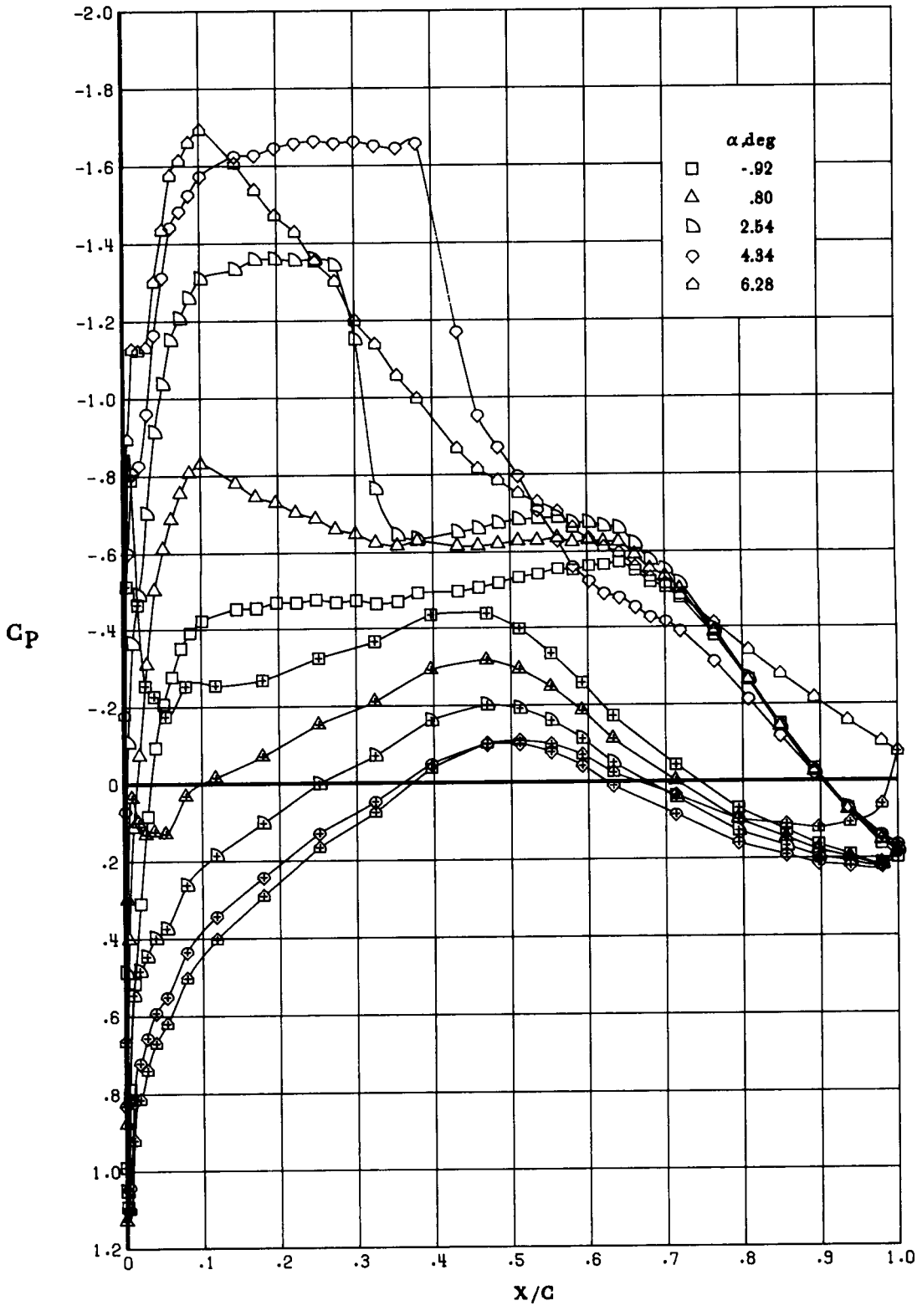

(d) Concluded.

Figure 14. Continued.

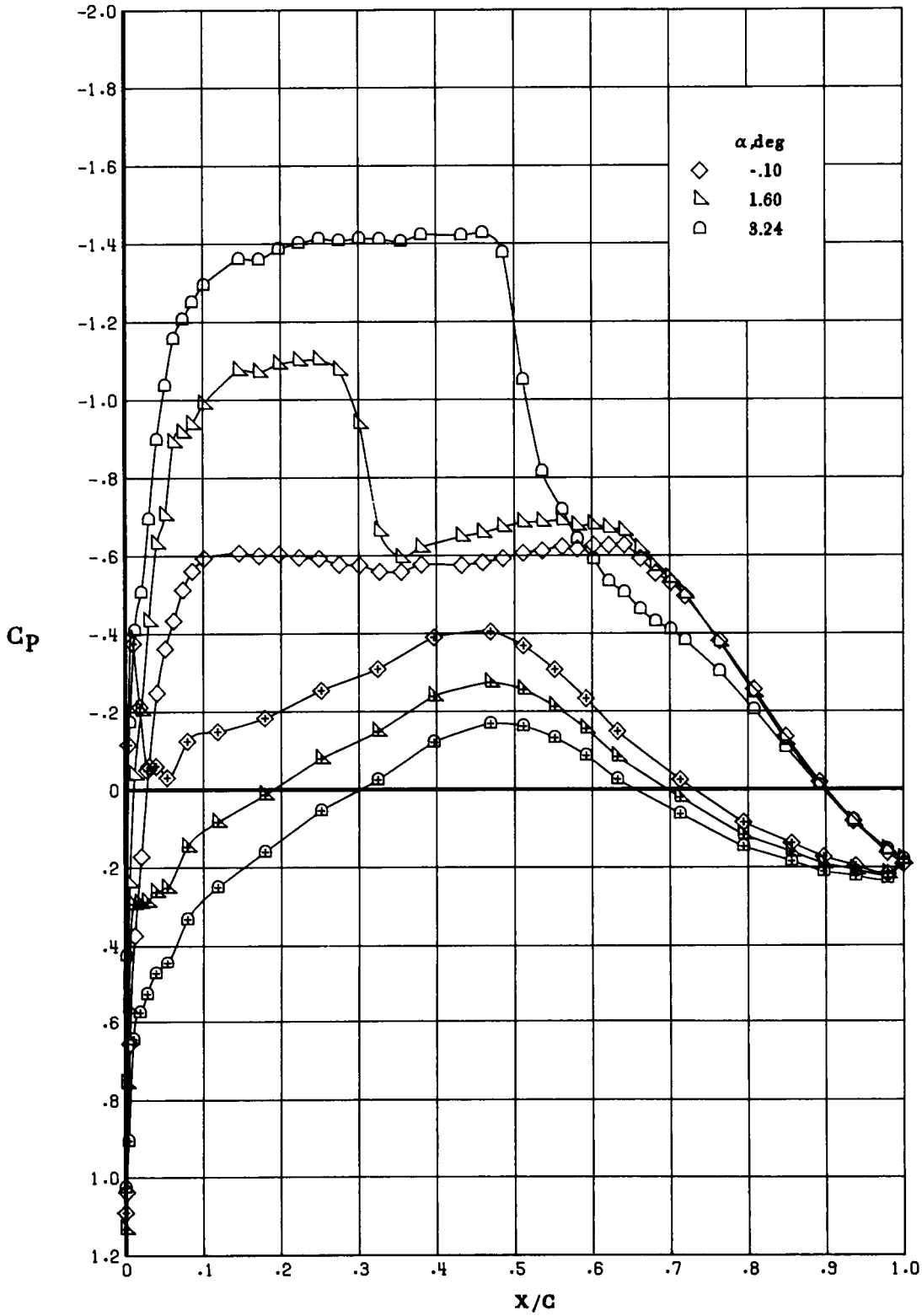

(e) $M_\infty = 0.73$.

Figure 14. Continued.

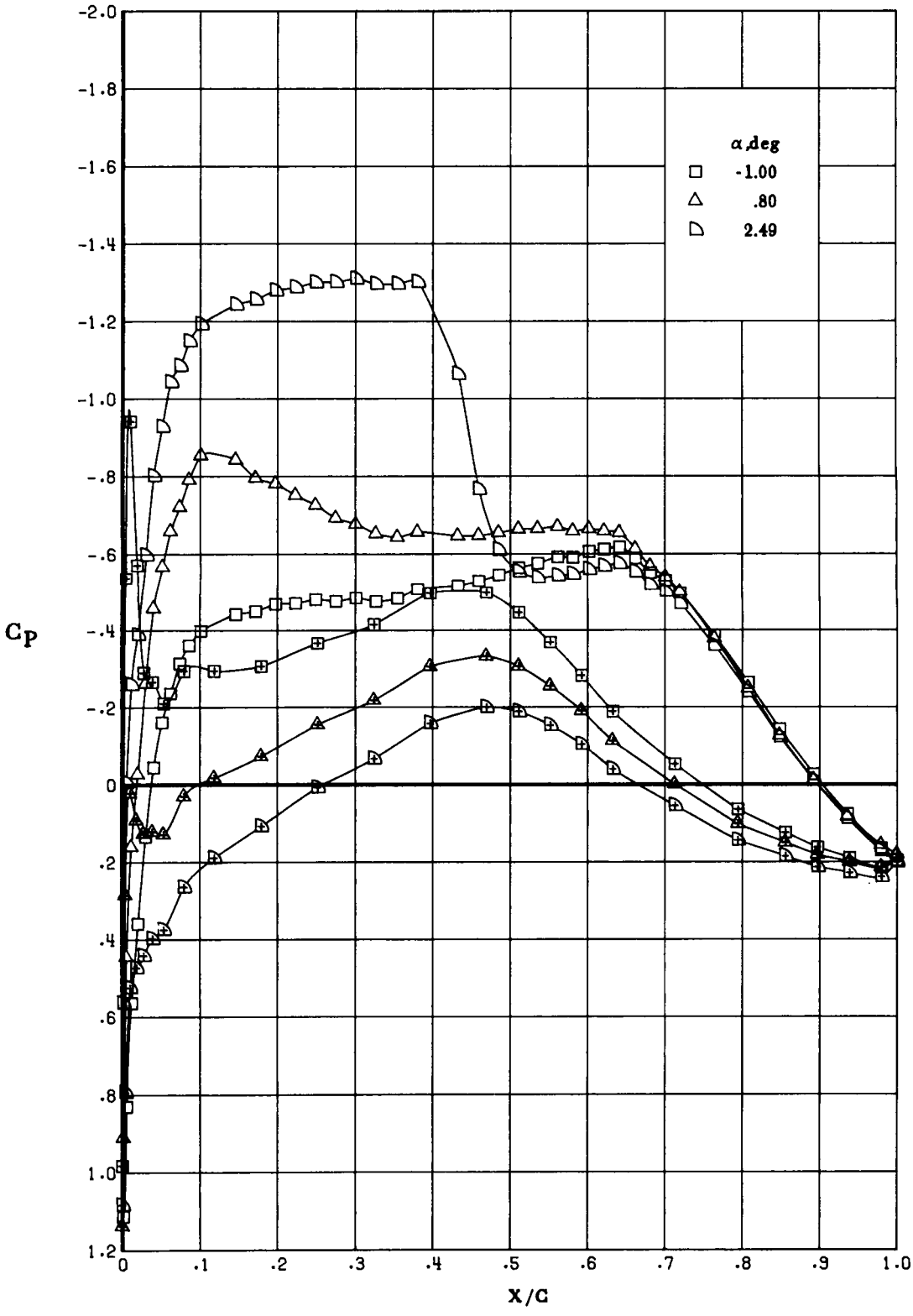

(e) Concluded.

Figure 14. Continued.

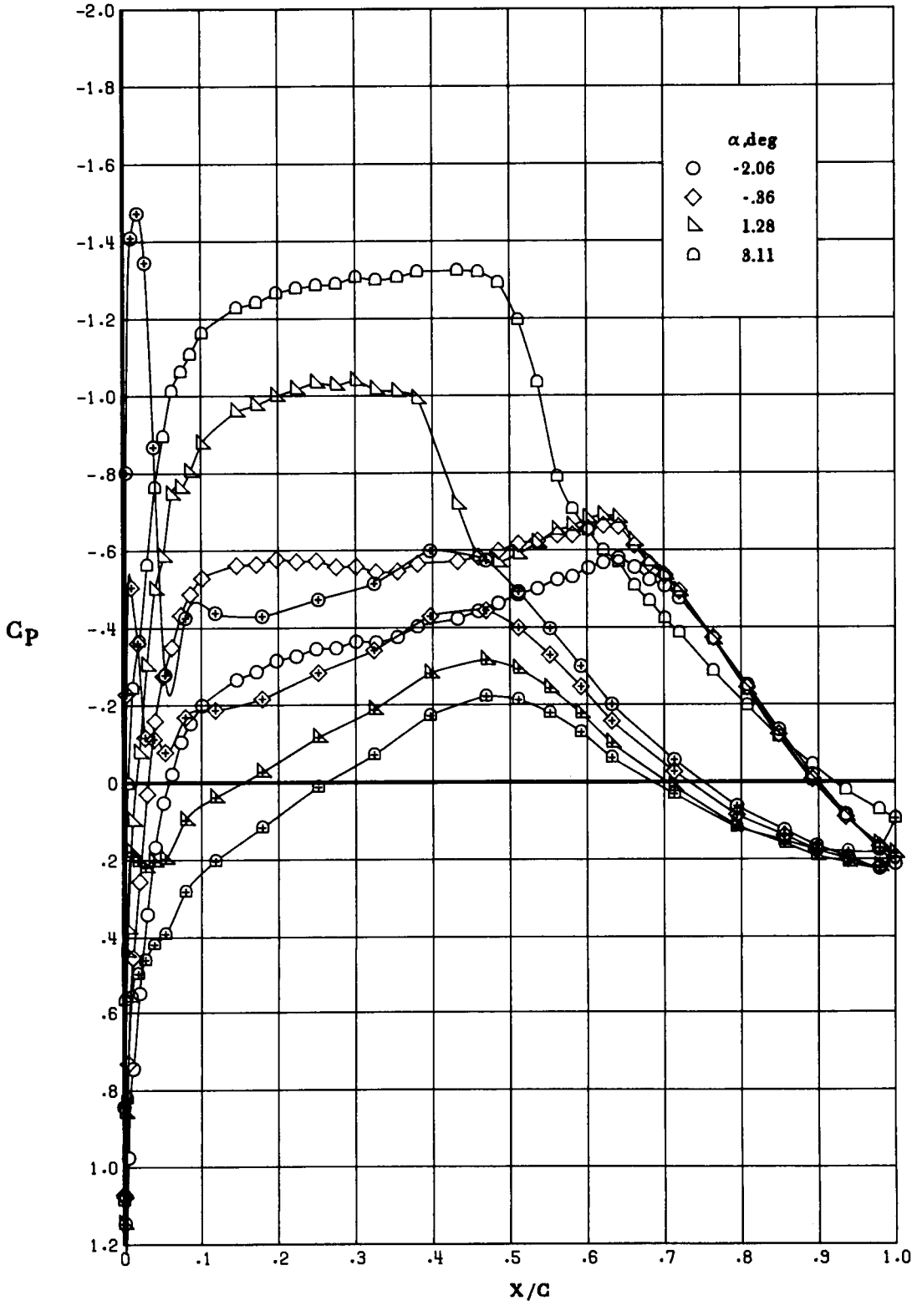

(f) $M_\infty = 0.75$.

Figure 14. Continued.

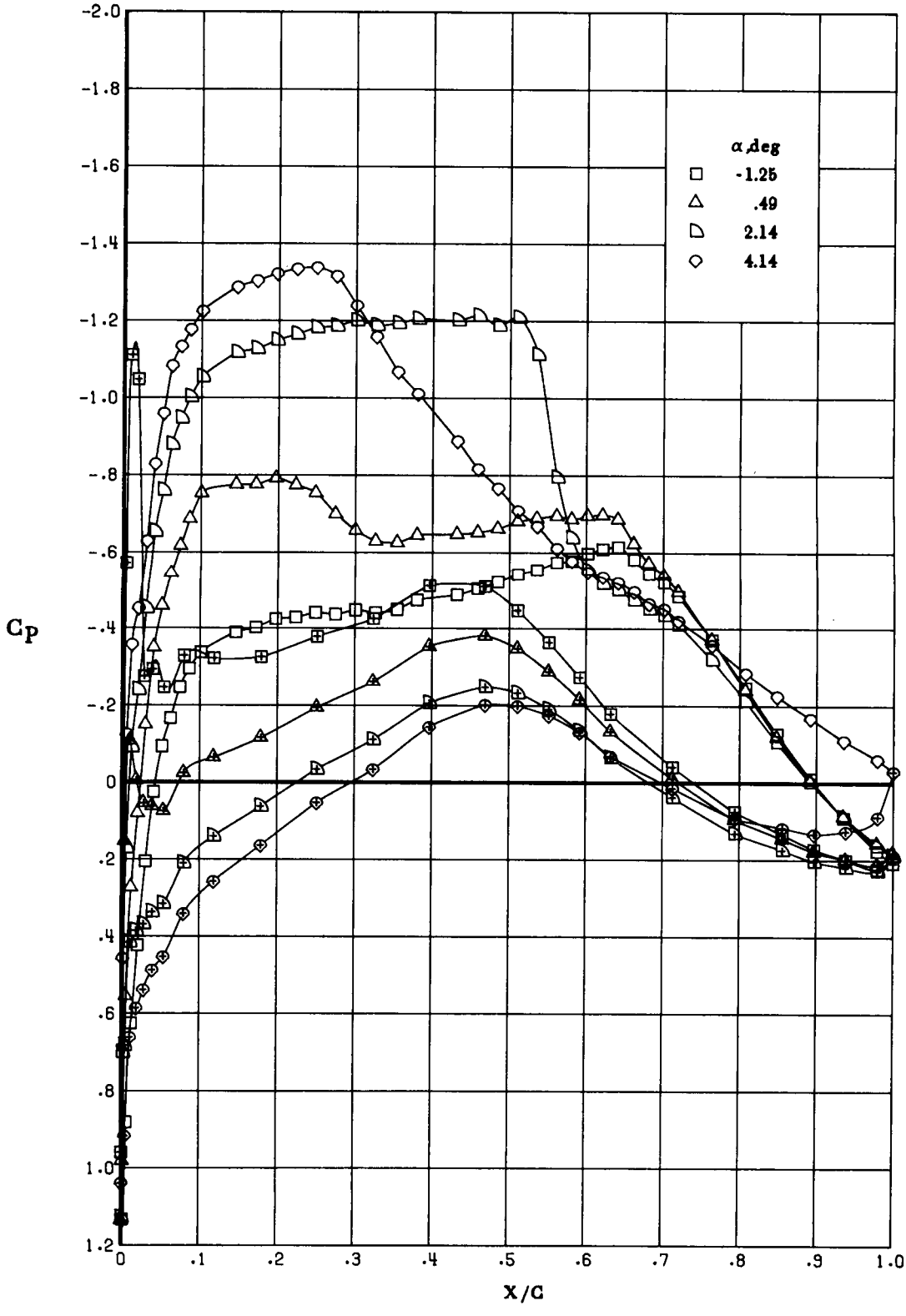

(f) Concluded.

Figure 14. Continued.

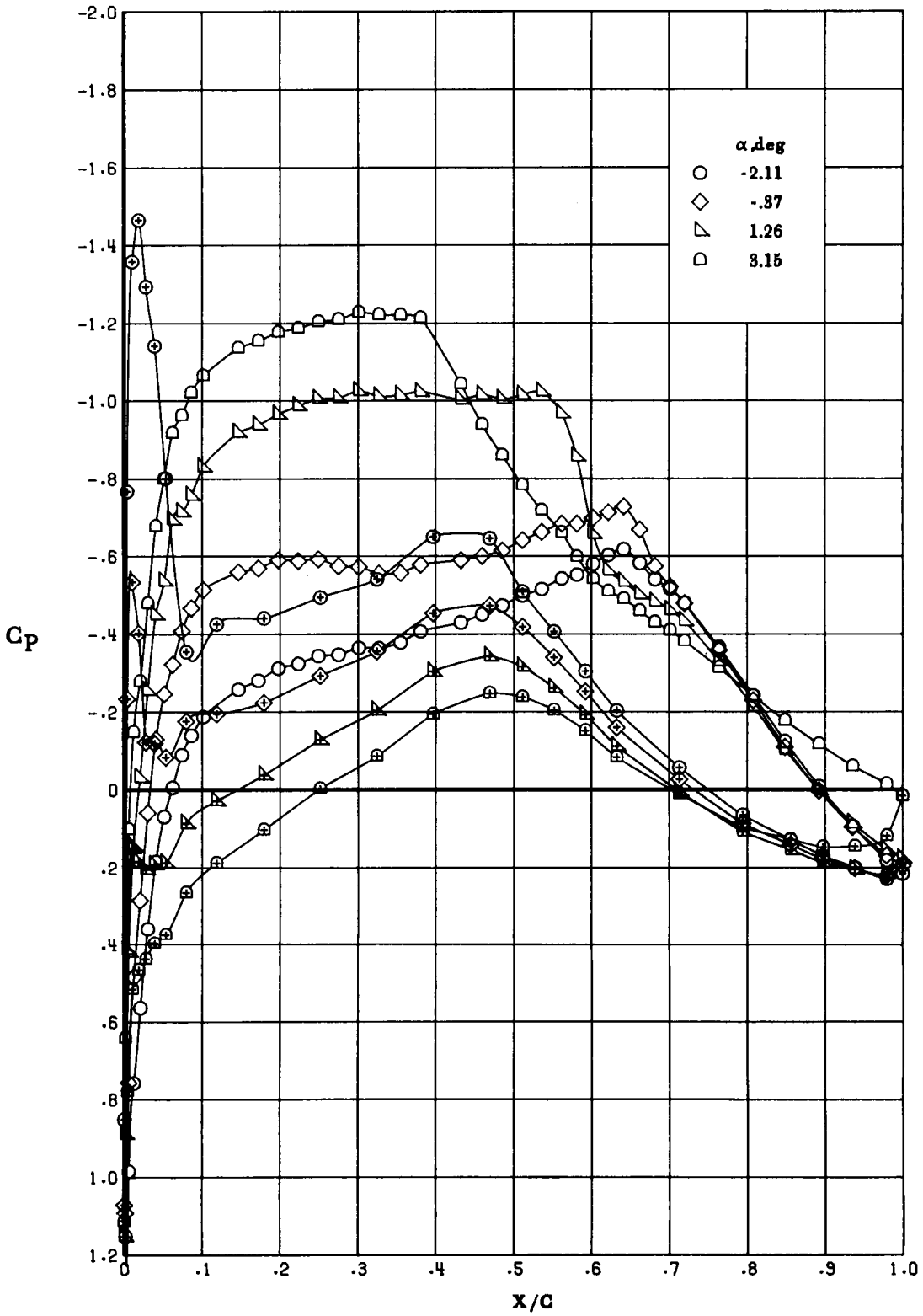

(g) $M_\infty = 0.765$.

Figure 14. Continued.

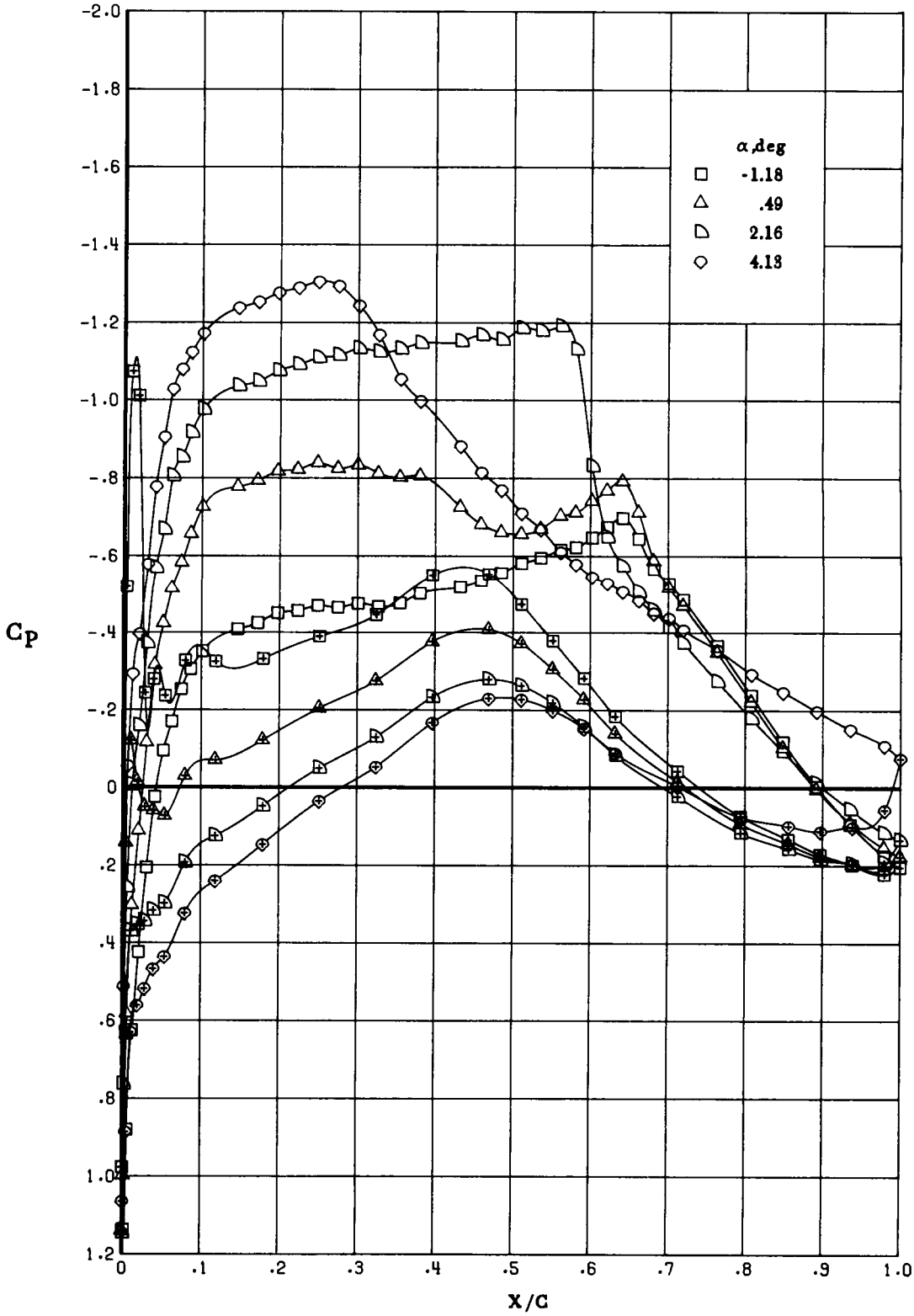

(g) Concluded.

Figure 14. Continued.

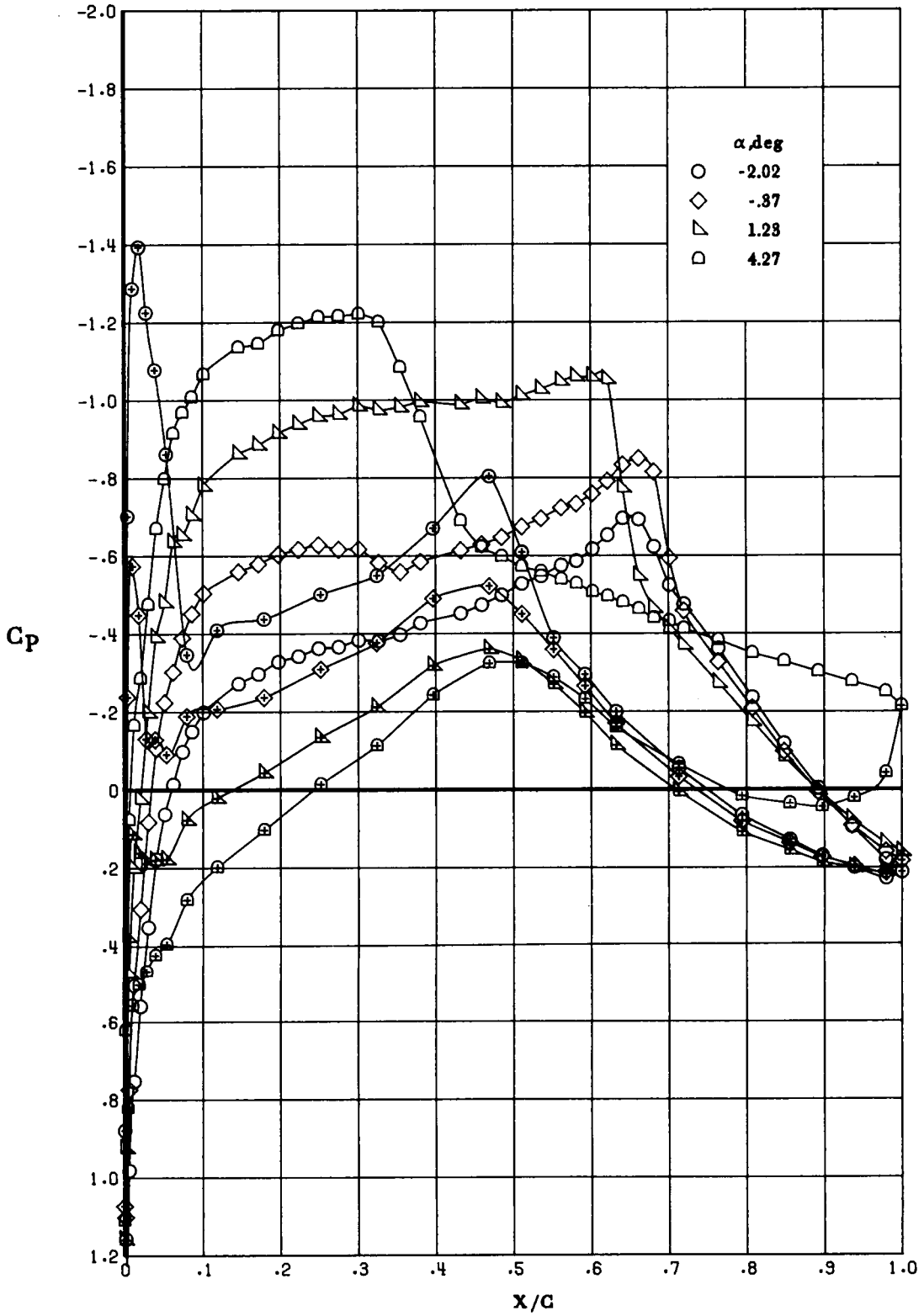

(h) $M_\infty = 0.78$.

Figure 14. Continued.

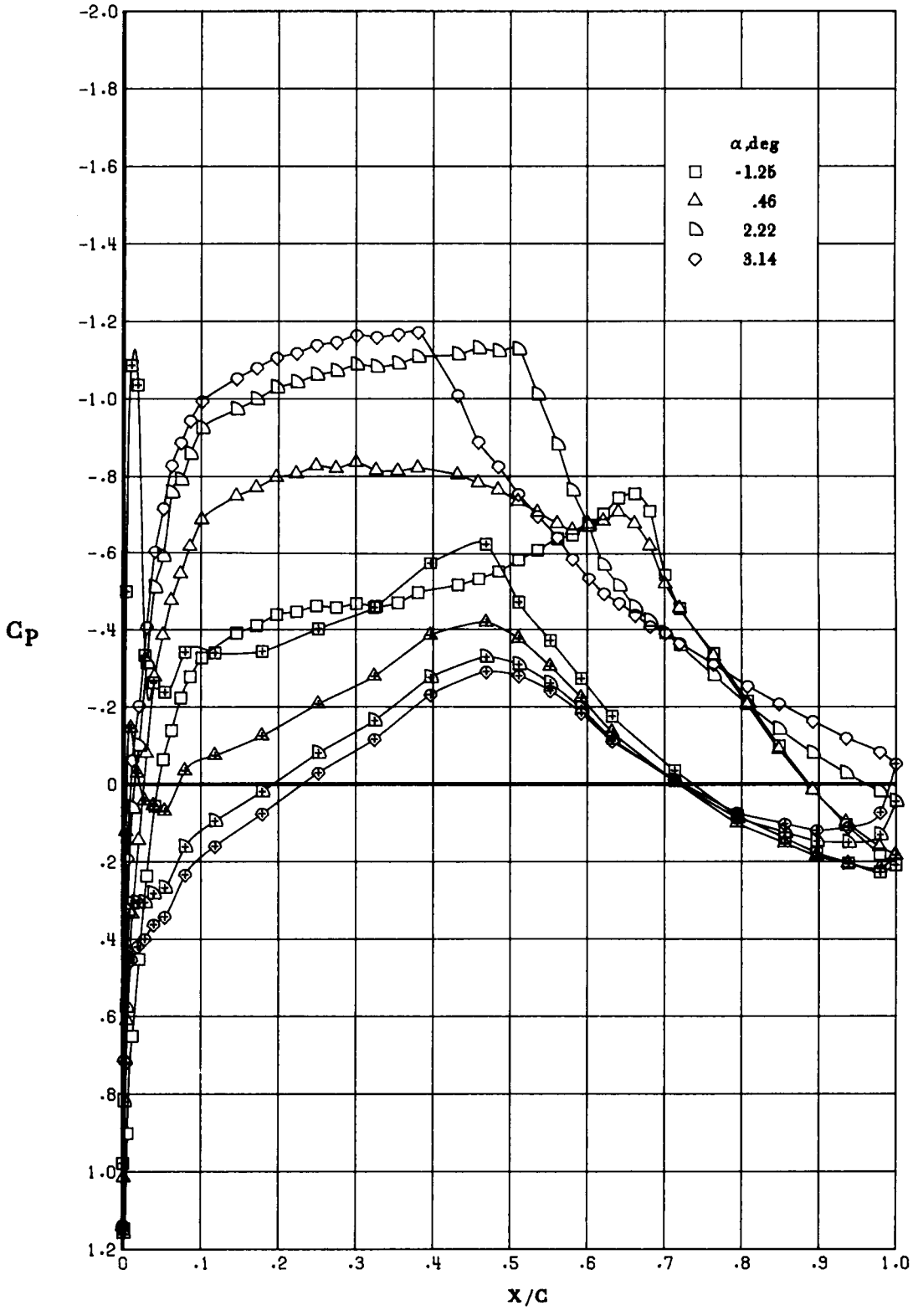

(h) Concluded.

Figure 14. Continued.

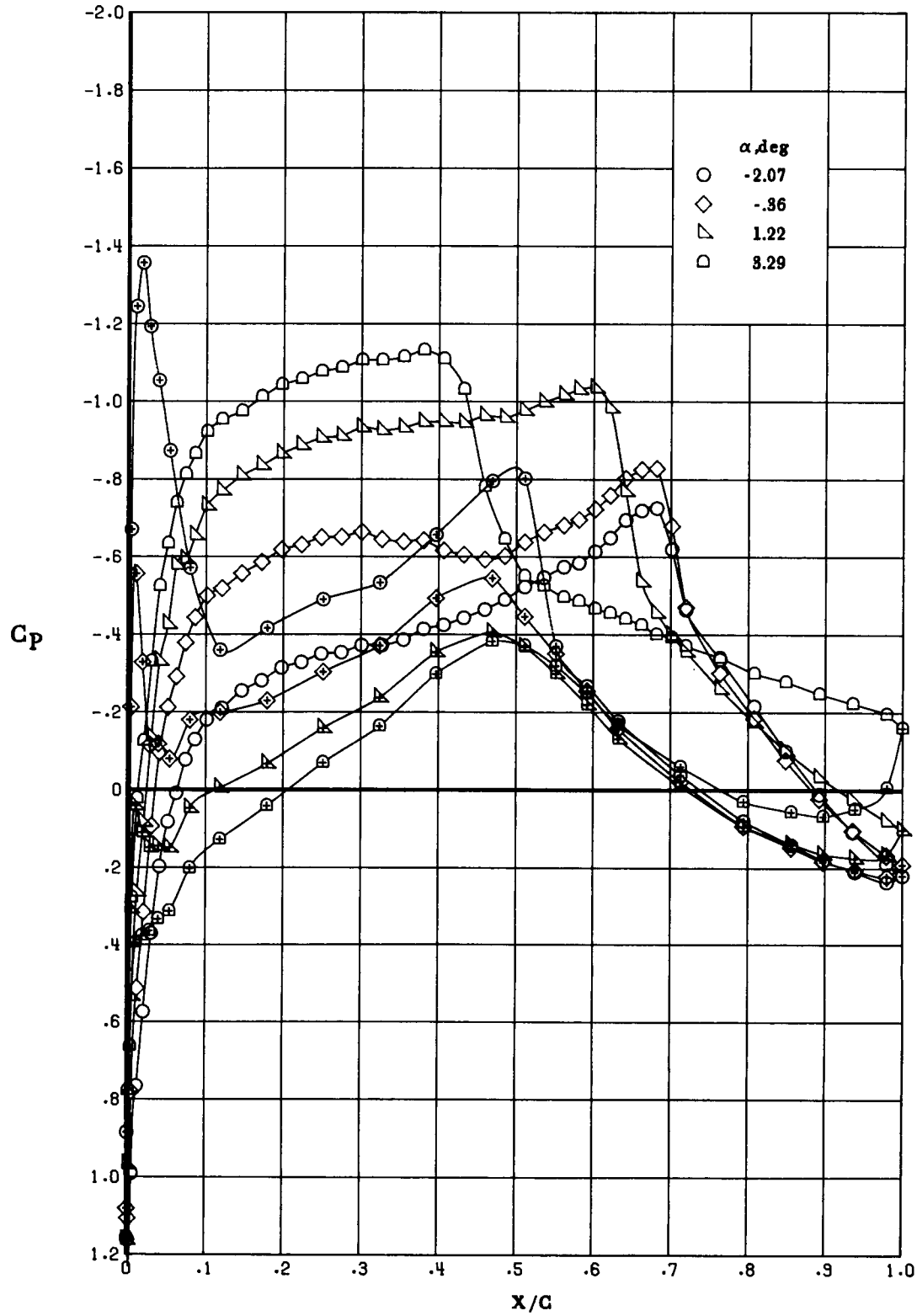

(i) $M_\infty = 0.79$.

Figure 14. Continued.

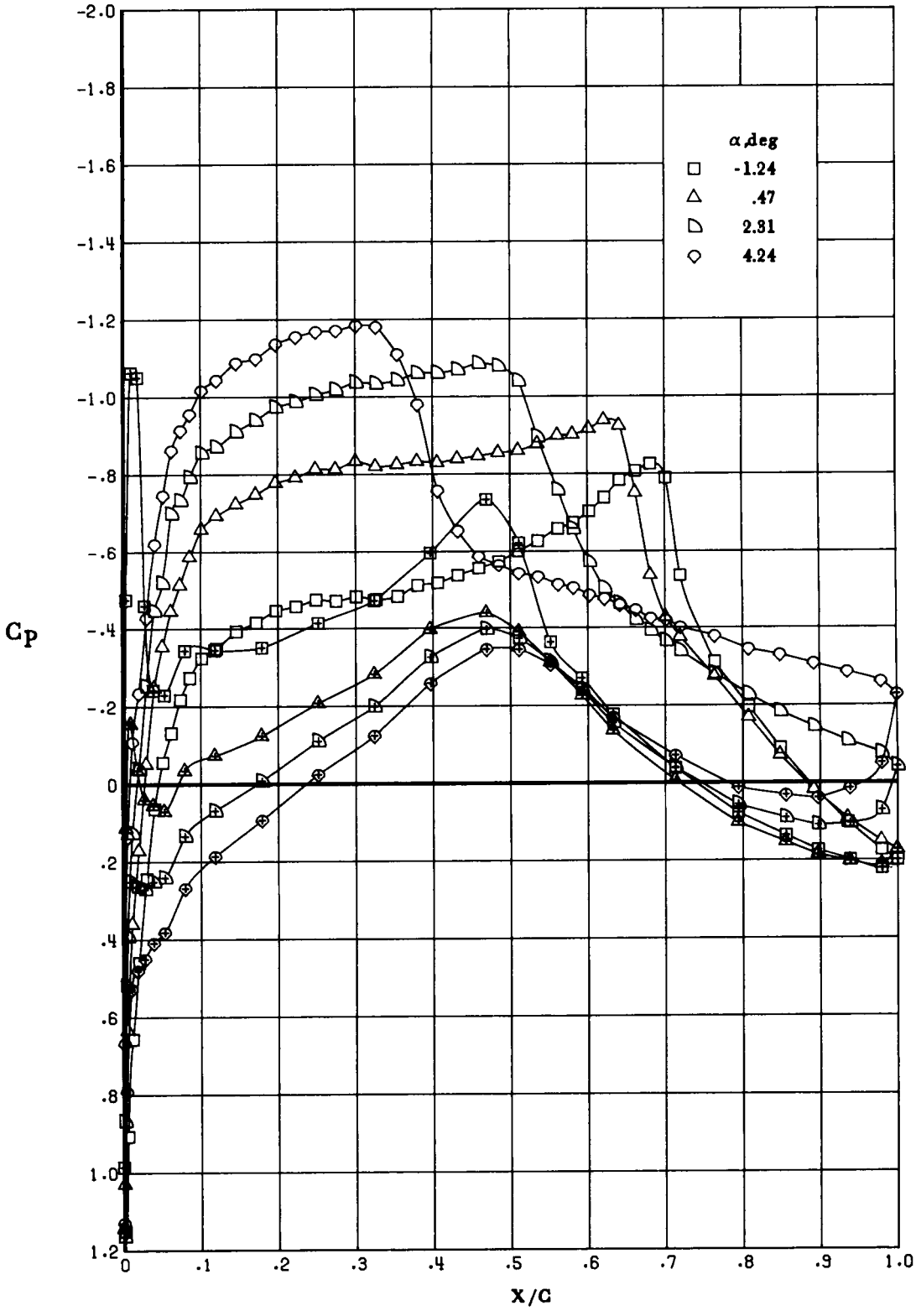

(i) Concluded.

Figure 14. Continued.

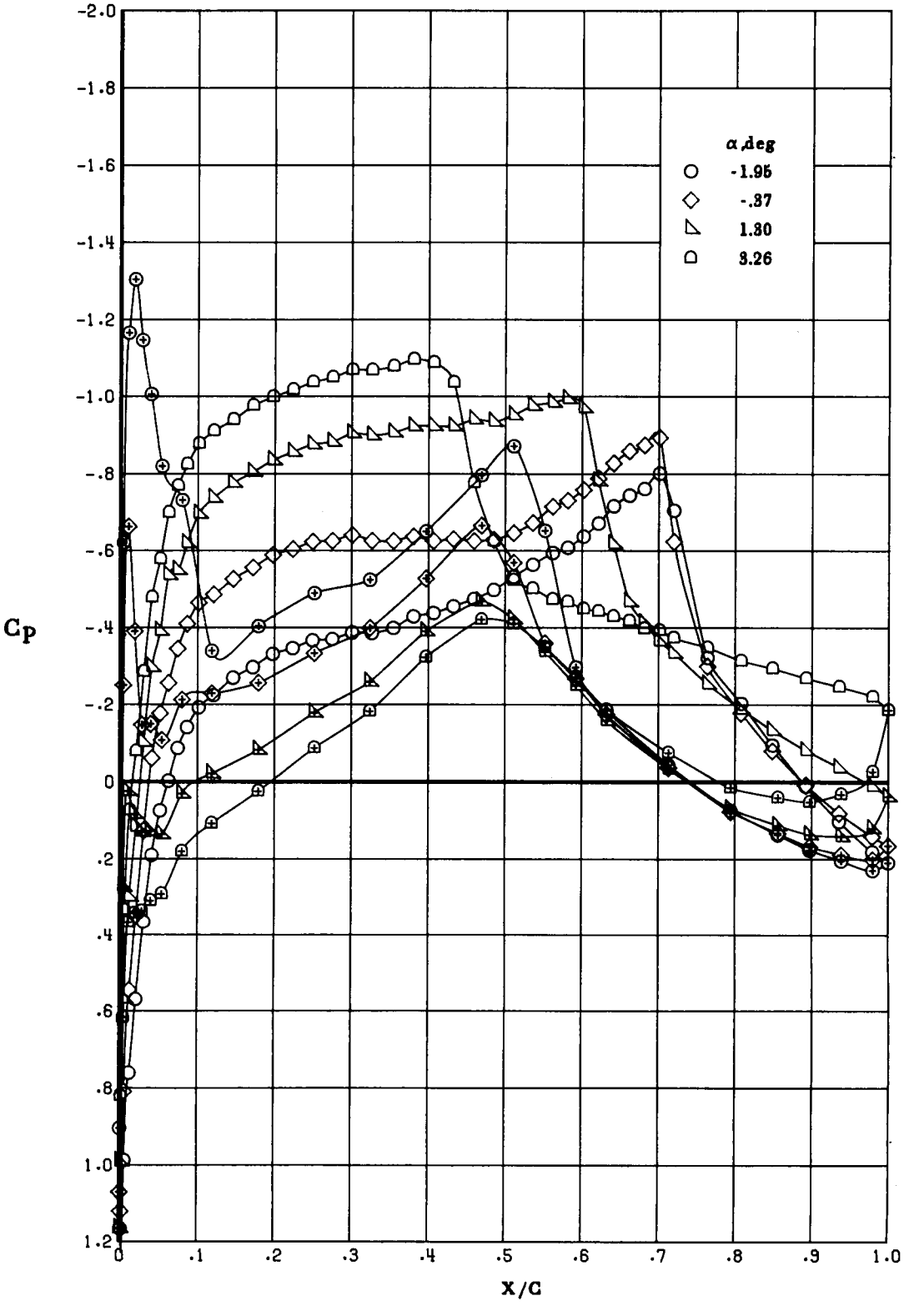

(j) $M_\infty = 0.80$.

Figure 14. Continued.

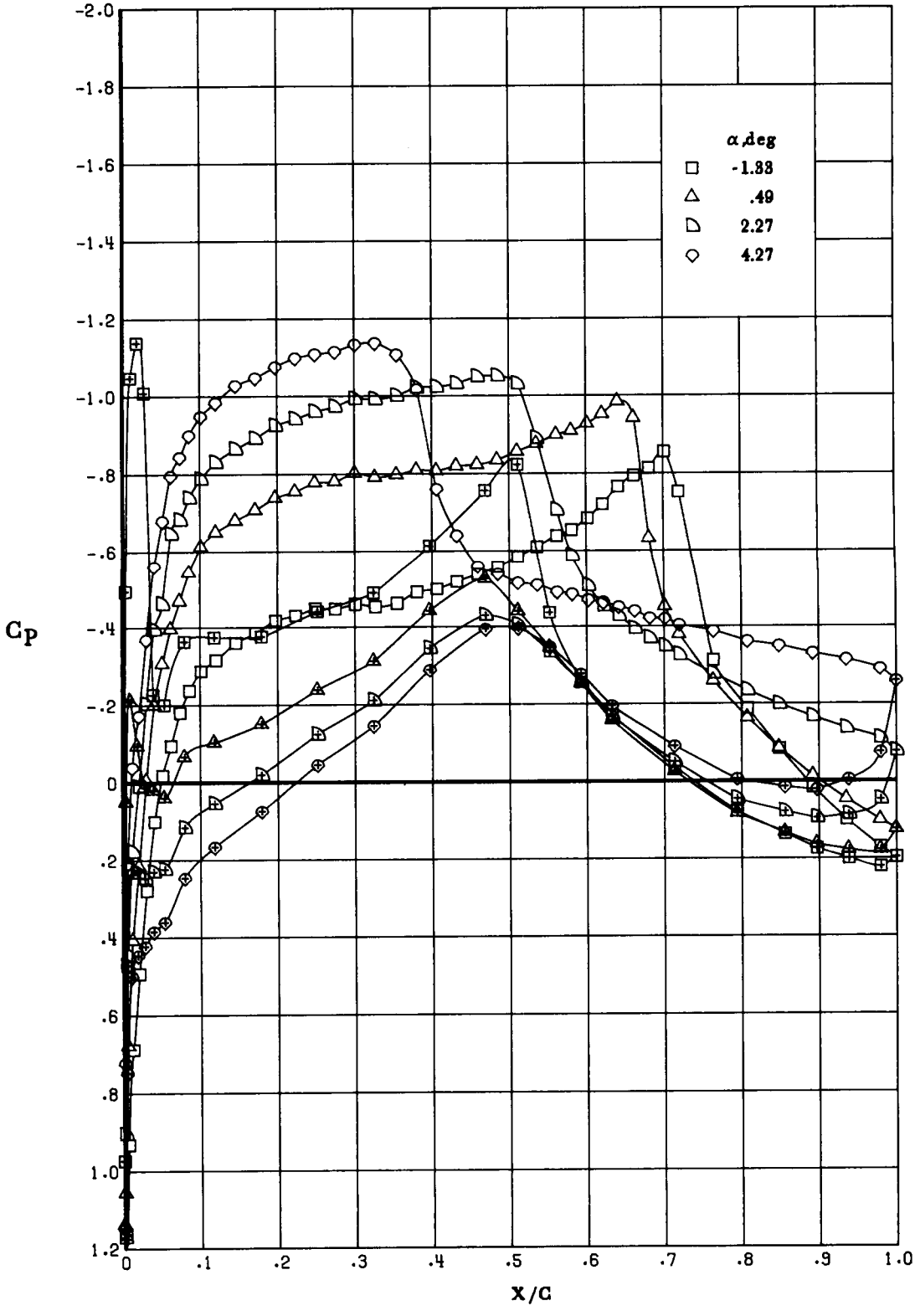

(j) Concluded.

Figure 14. Concluded.

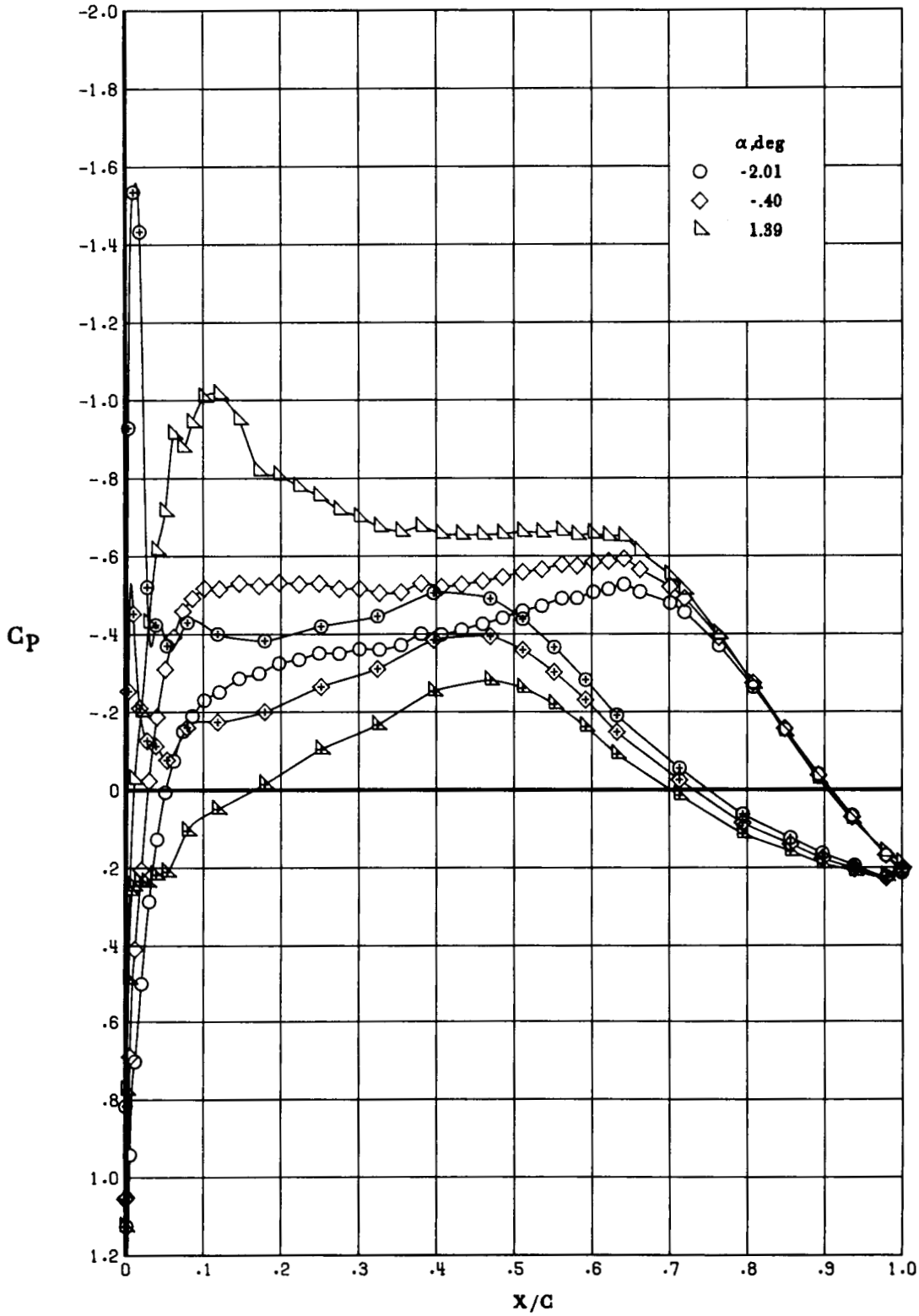

(a) $M_\infty = 0.70$.

Figure 15. Effect of α on chordwise pressure distribution at $R_c = 15 \times 10^6$. Open symbols denote upper surface; "+" within symbol denotes lower surface.

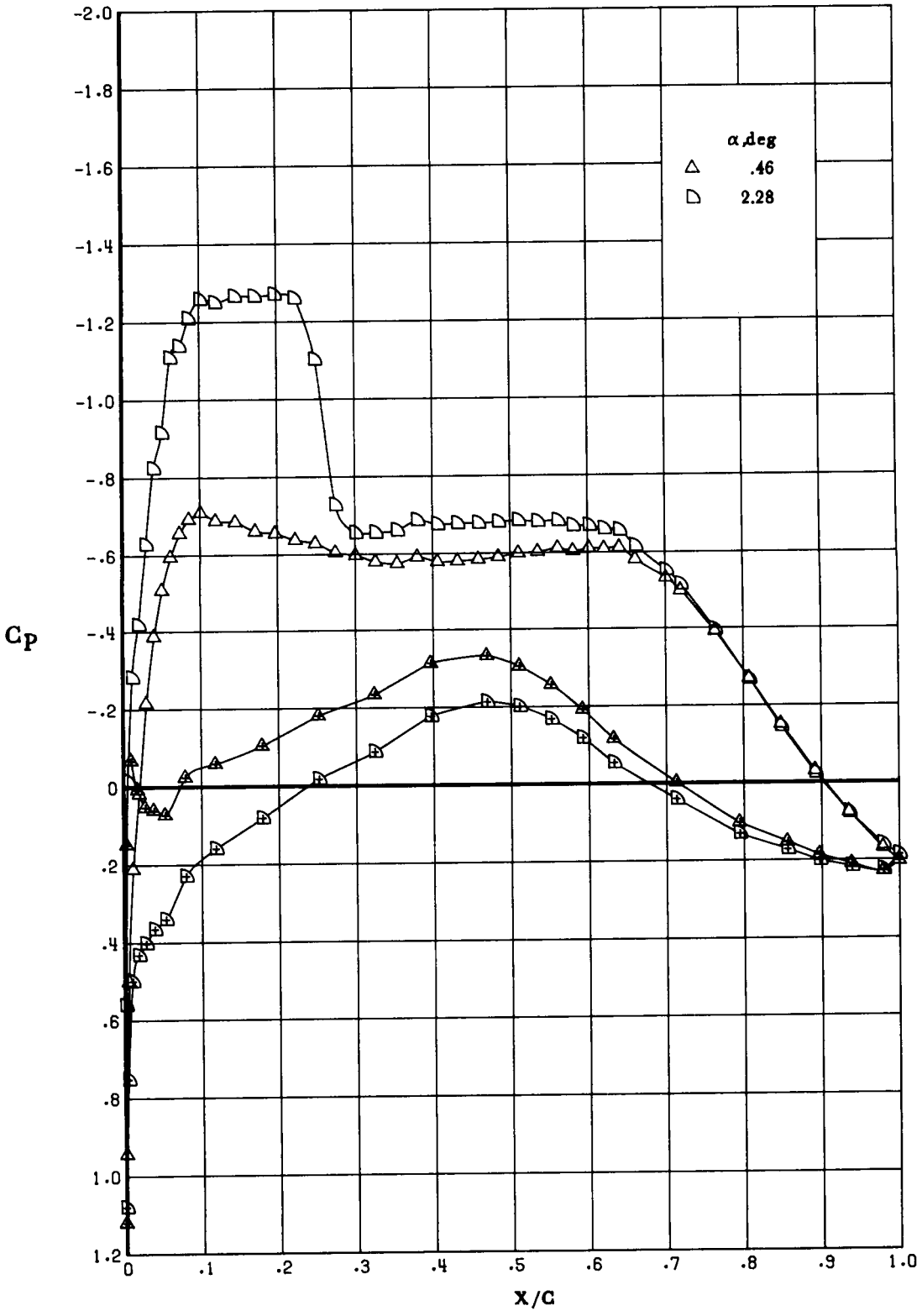

(a) Concluded.

Figure 15. Continued.

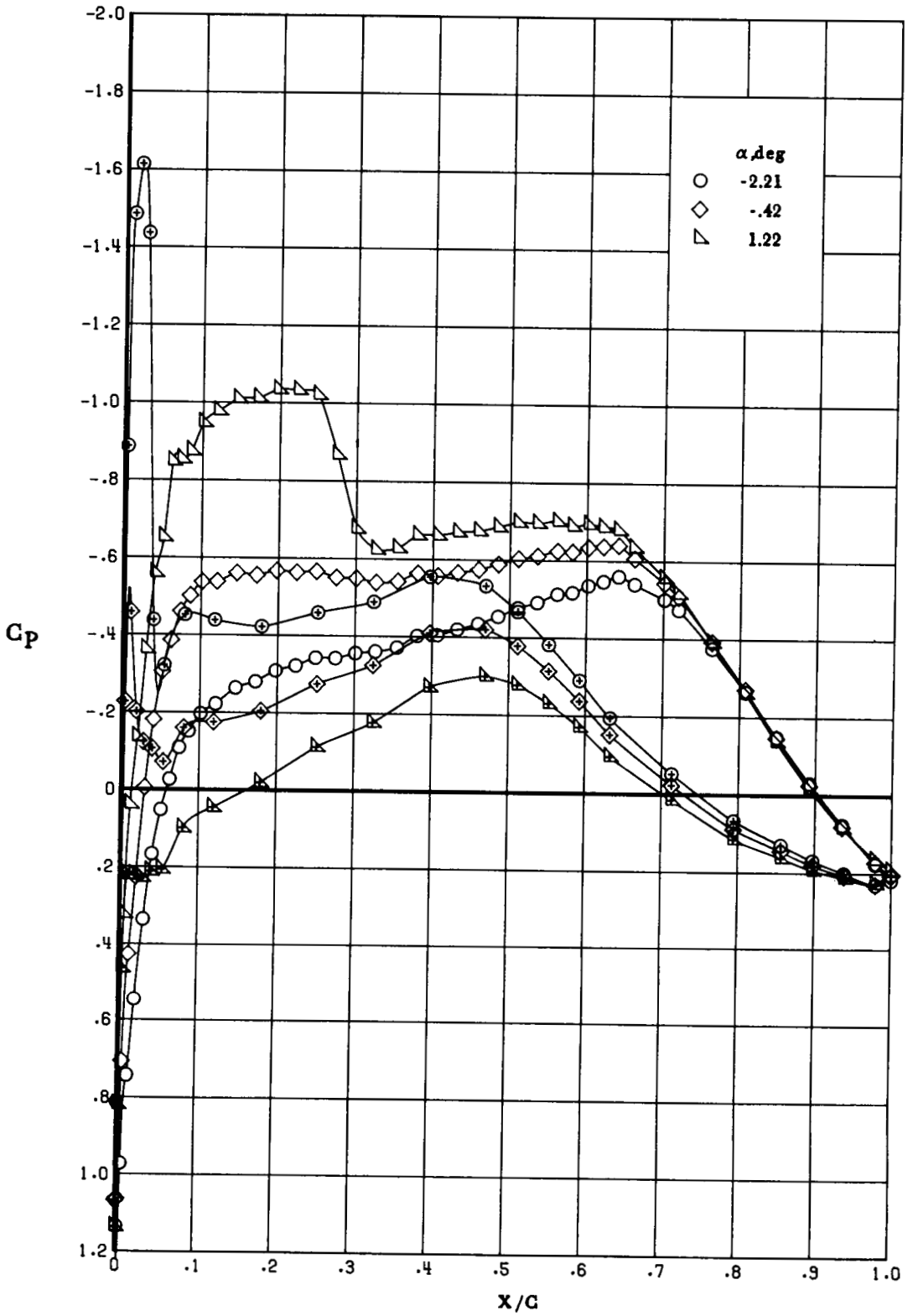

(b) $M_\infty = 0.73$.

Figure 15. Continued.

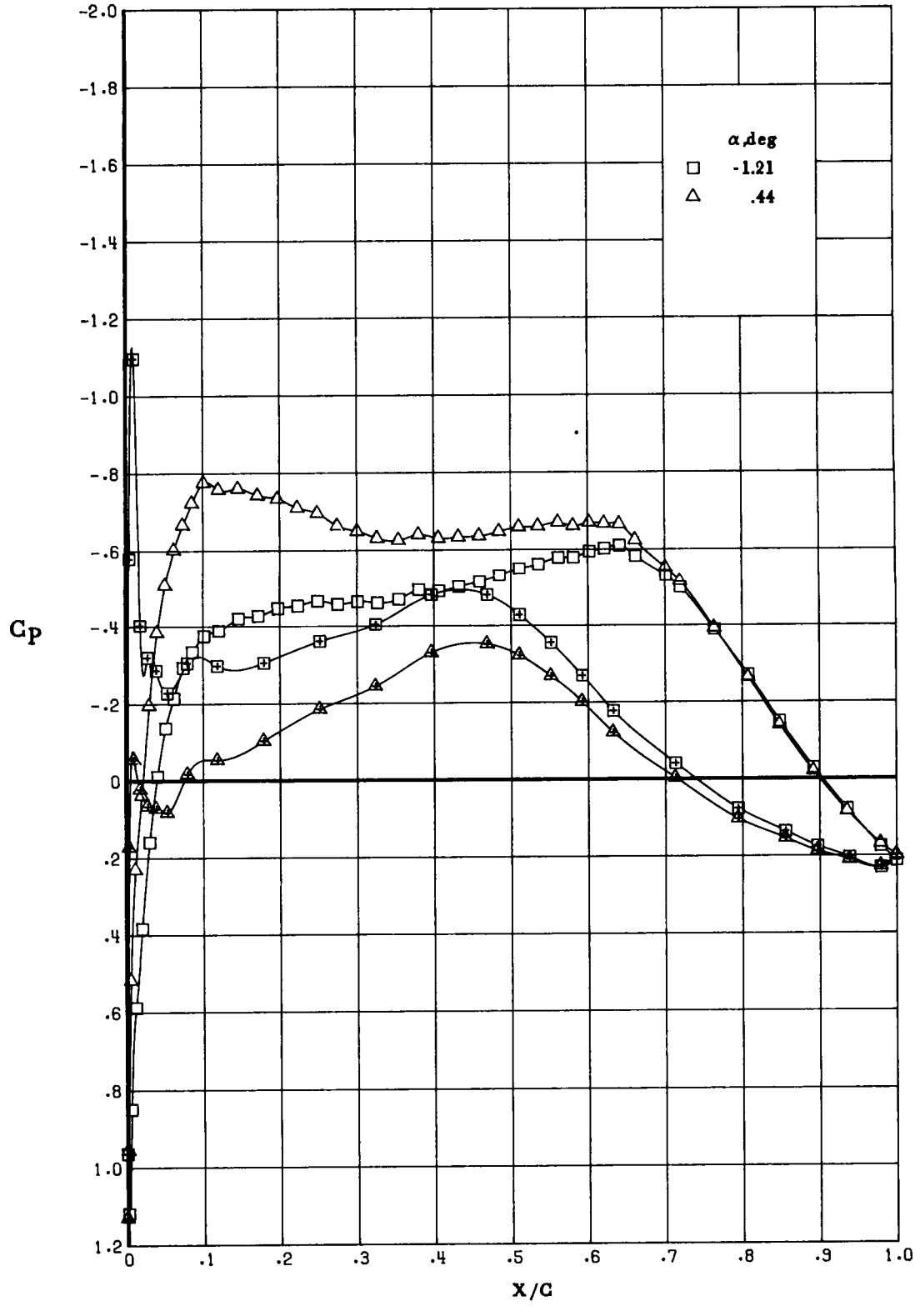

(b) Concluded.

Figure 15. Continued.

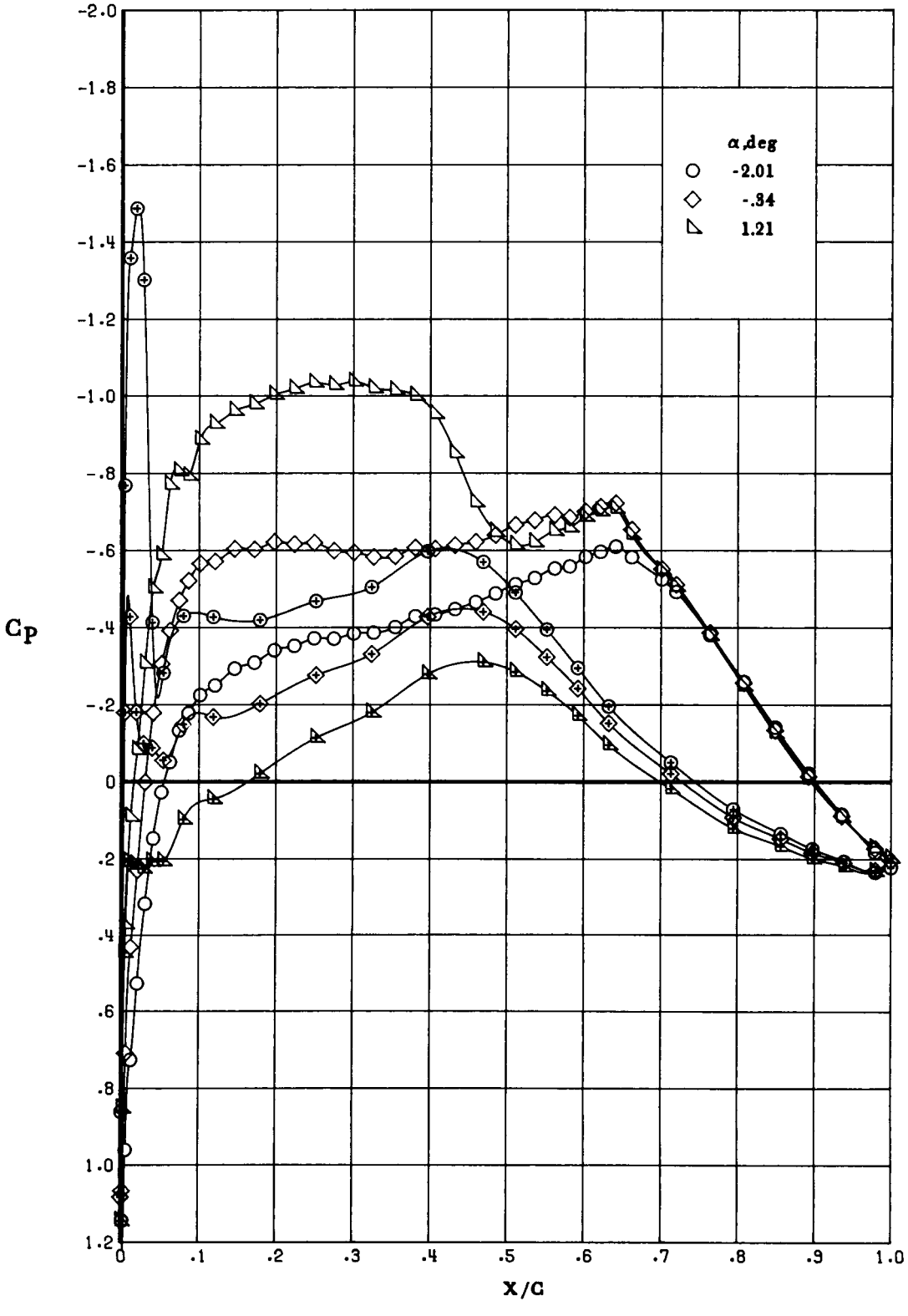

(c) $M_\infty = 0.75$.

Figure 15. Continued.

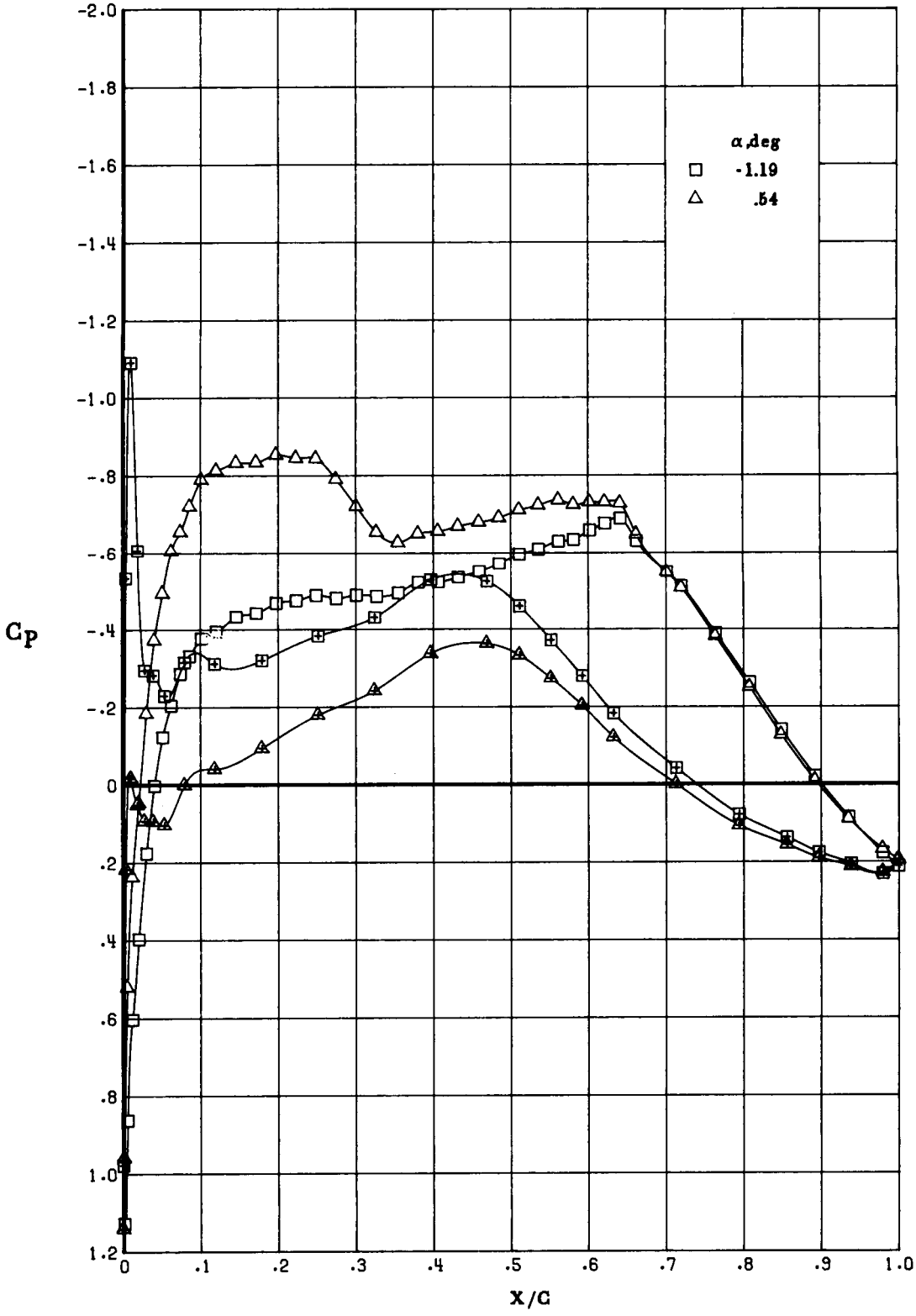

(c) Concluded.

Figure 15. Continued.

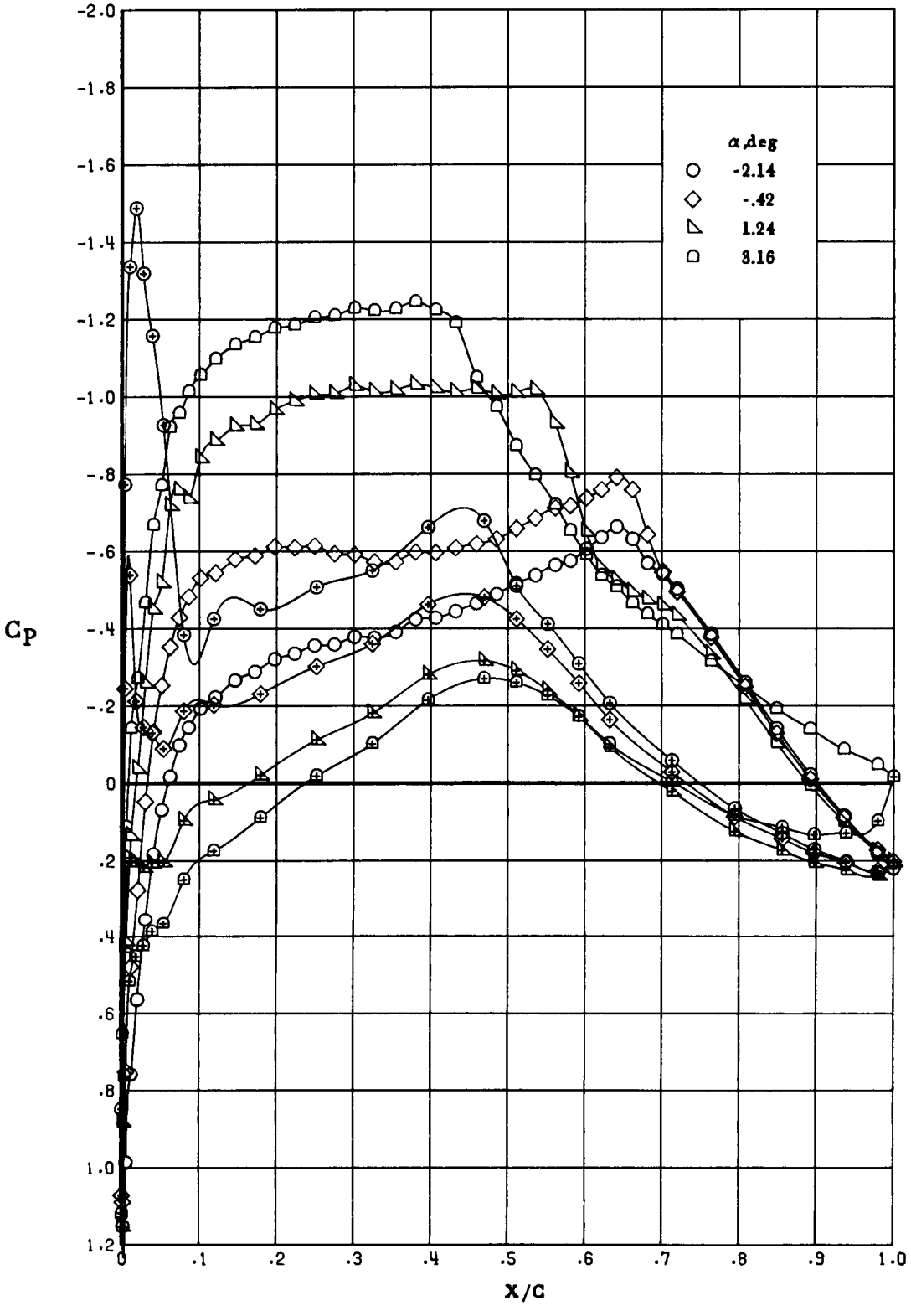

(d) $M_\infty = 0.765$.

Figure 15. Continued.

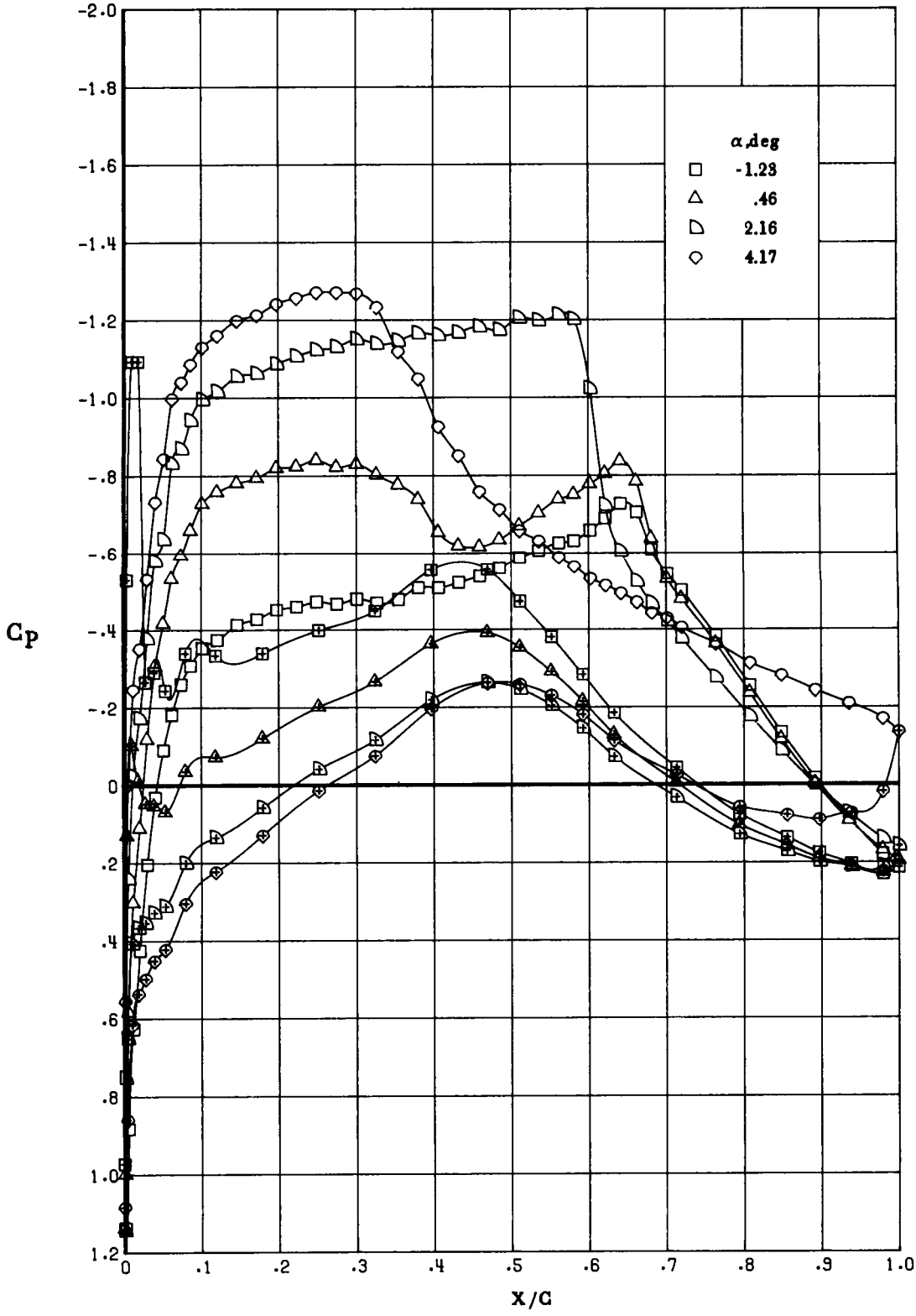

(d) Concluded.

Figure 15. Continued.

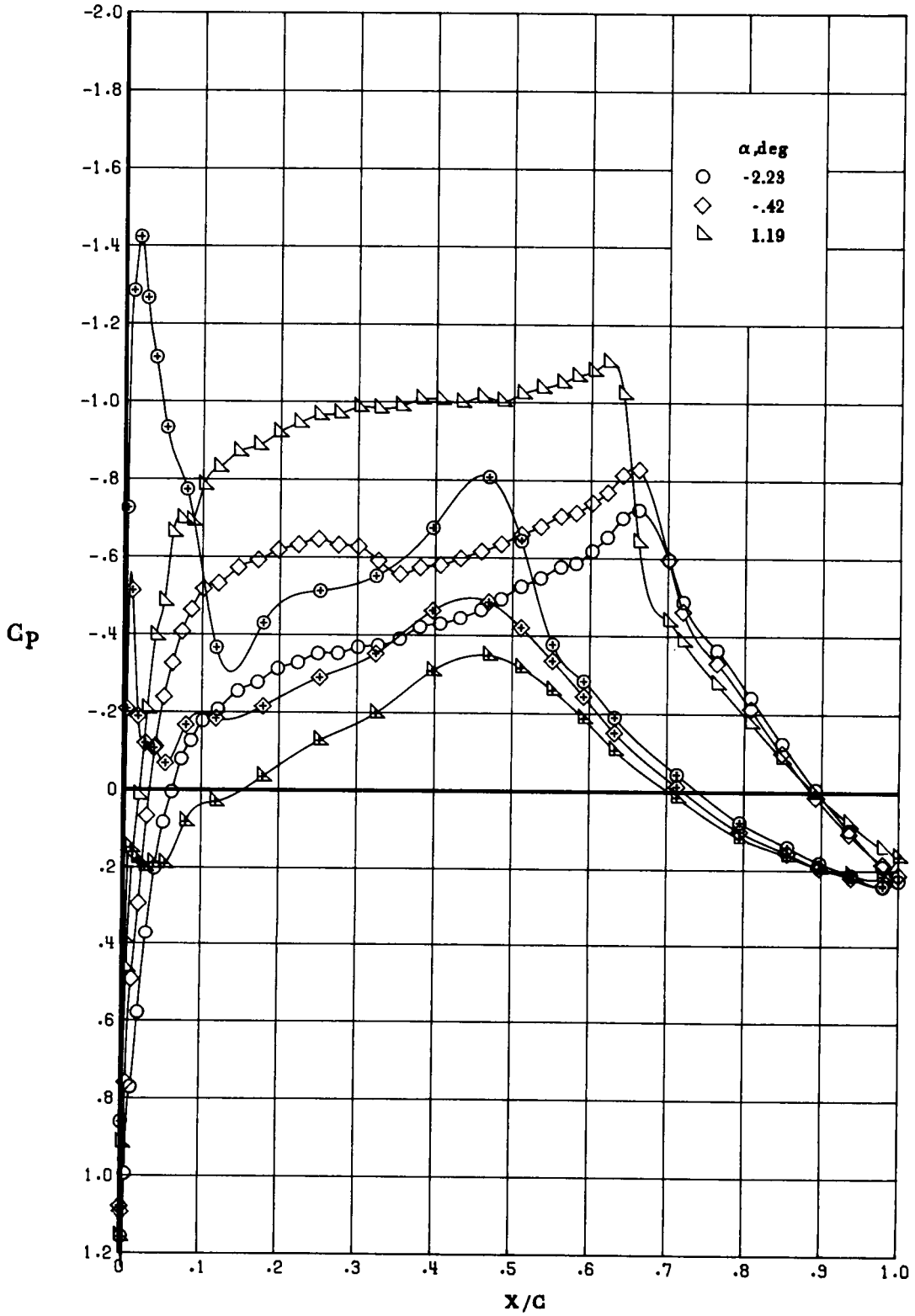

(e) $M_\infty = 0.78$.

Figure 15. Continued.

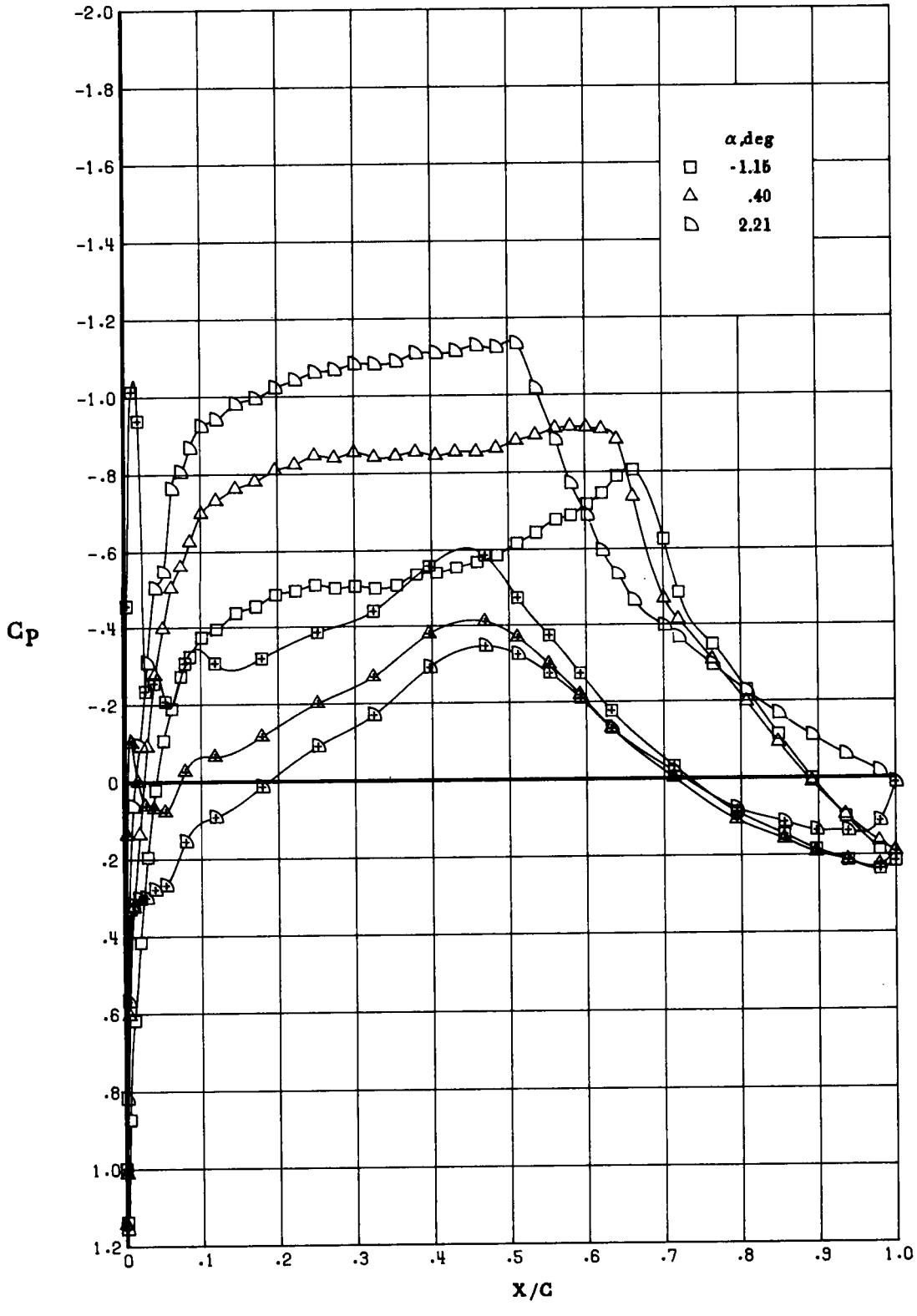

(e) Concluded.

Figure 15. Continued.

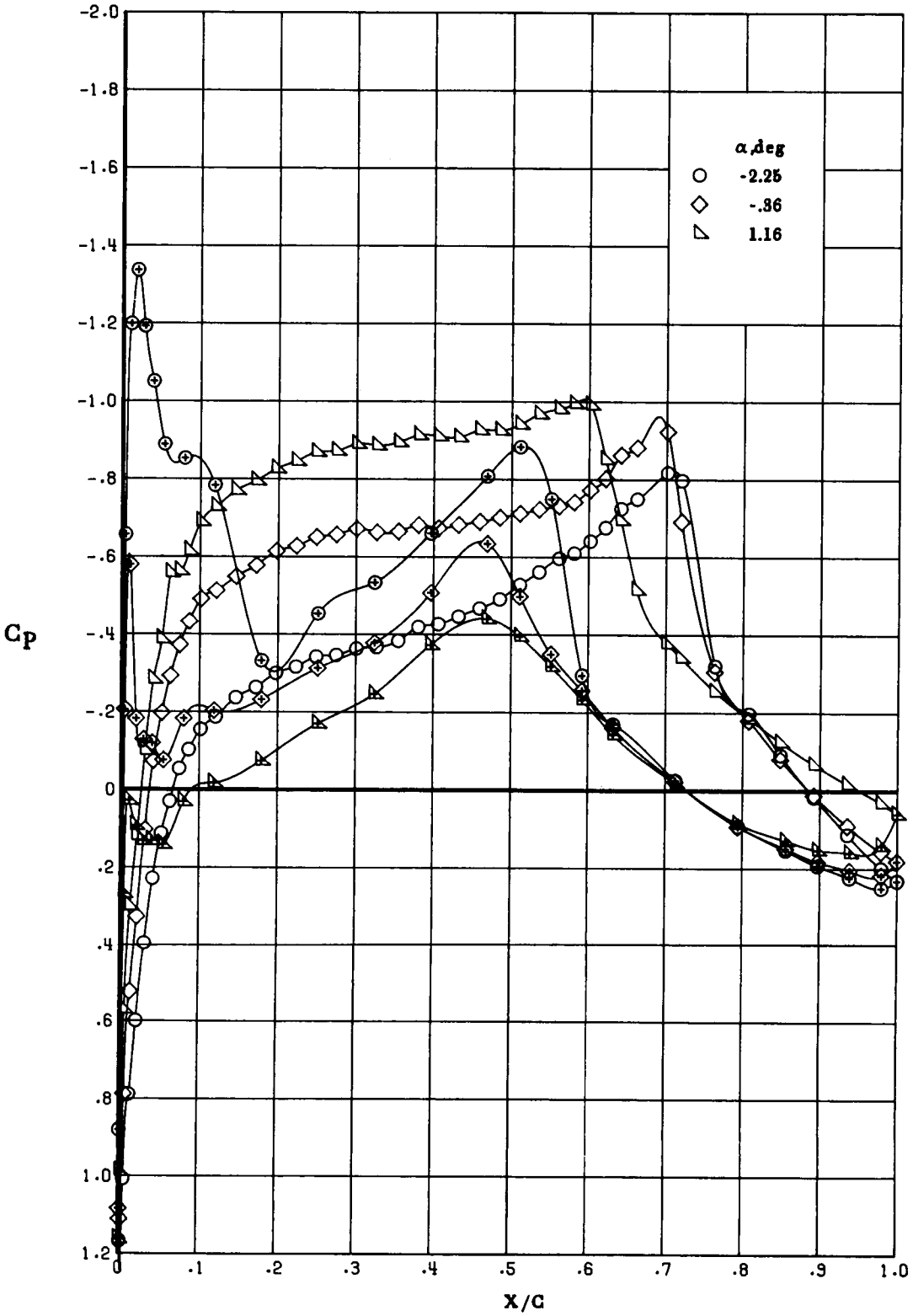

(f) $M_\infty = 0.80$.

Figure 15. Continued.

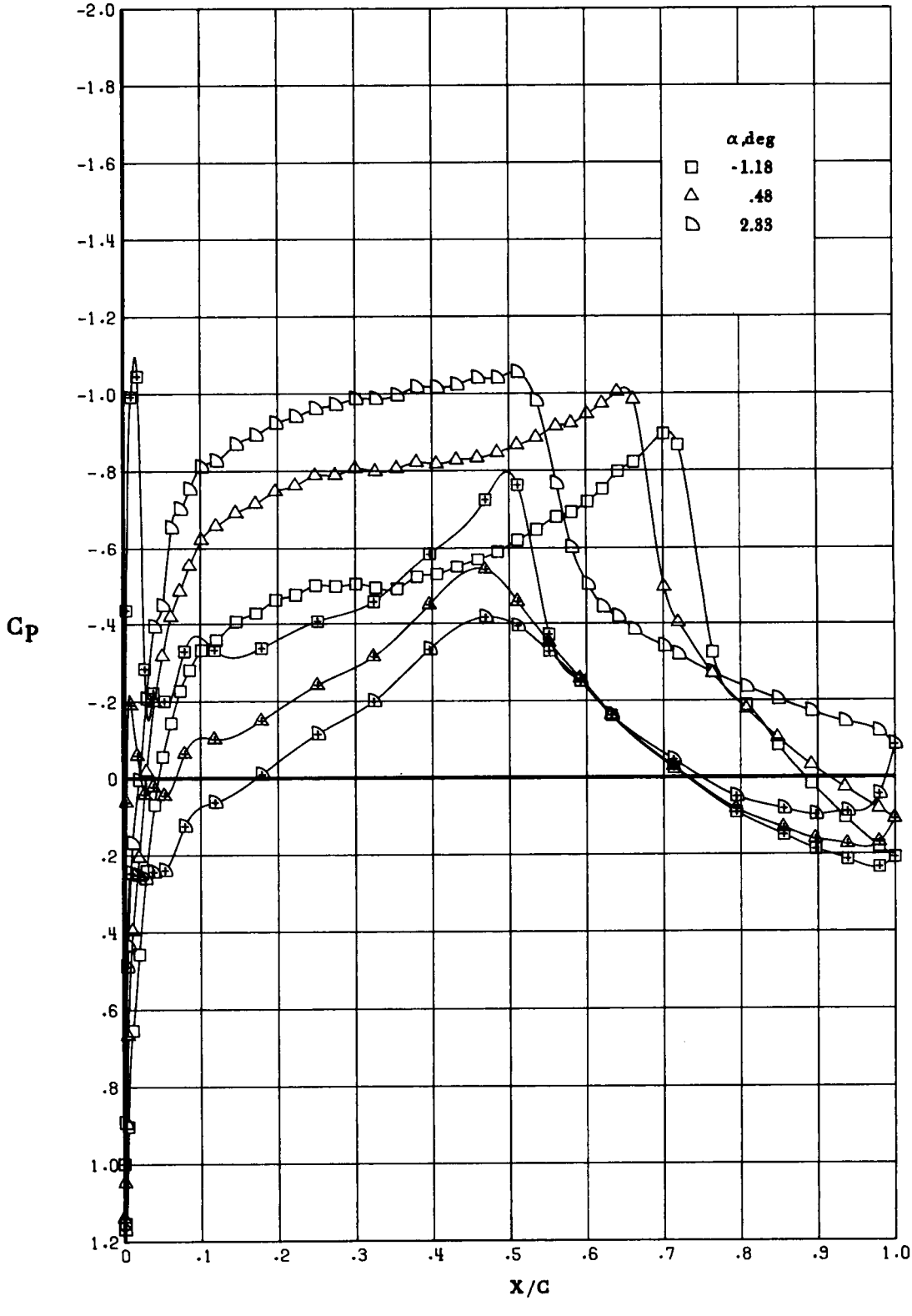

(f) Concluded.

Figure 15. Concluded.

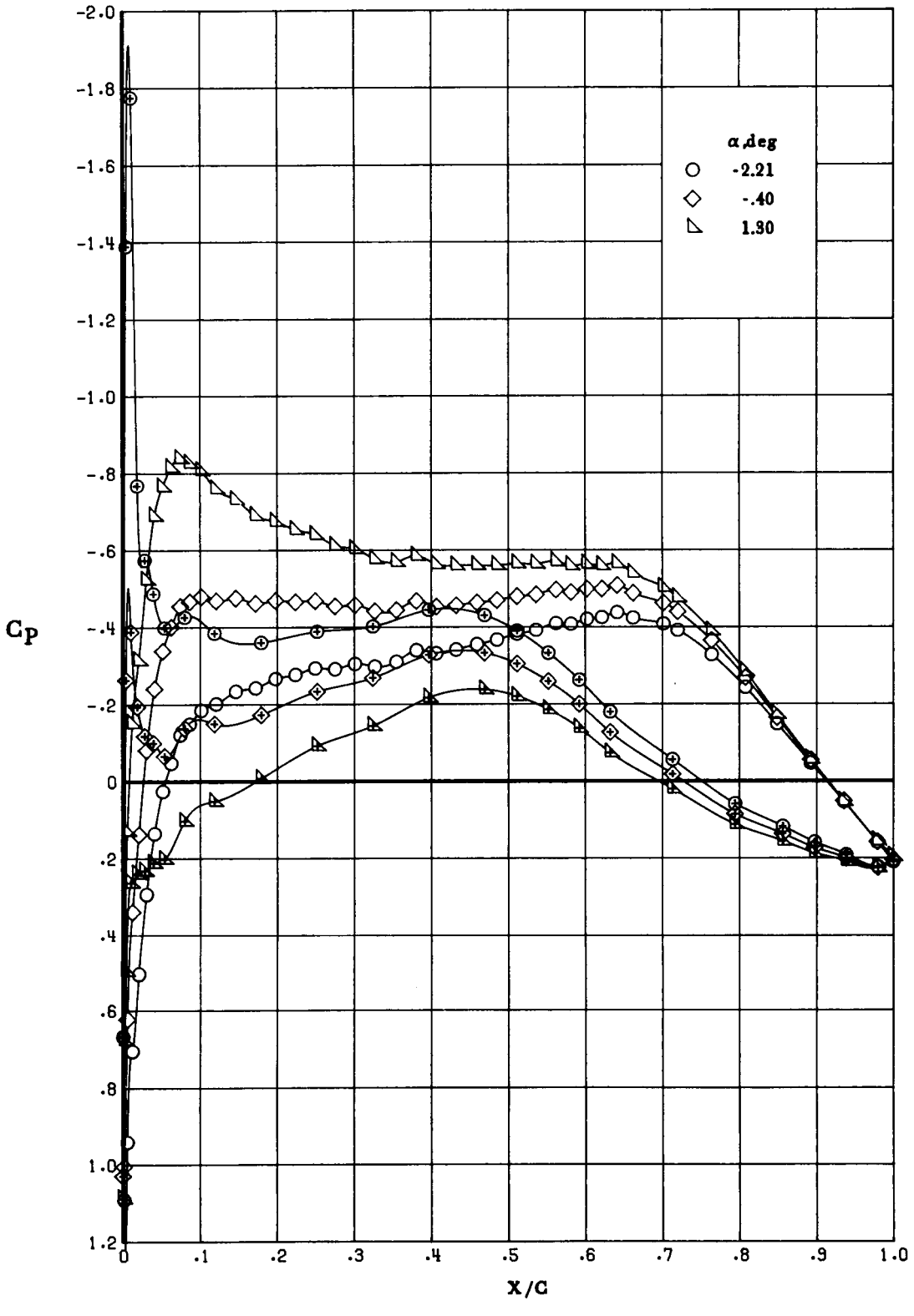

(a) $M_\infty = 0.60$.

Figure 16. Effect of α on chordwise pressure distribution at $R_c = 20 \times 10^6$. Open symbols denote upper surface; "+" within symbol denotes lower surface.

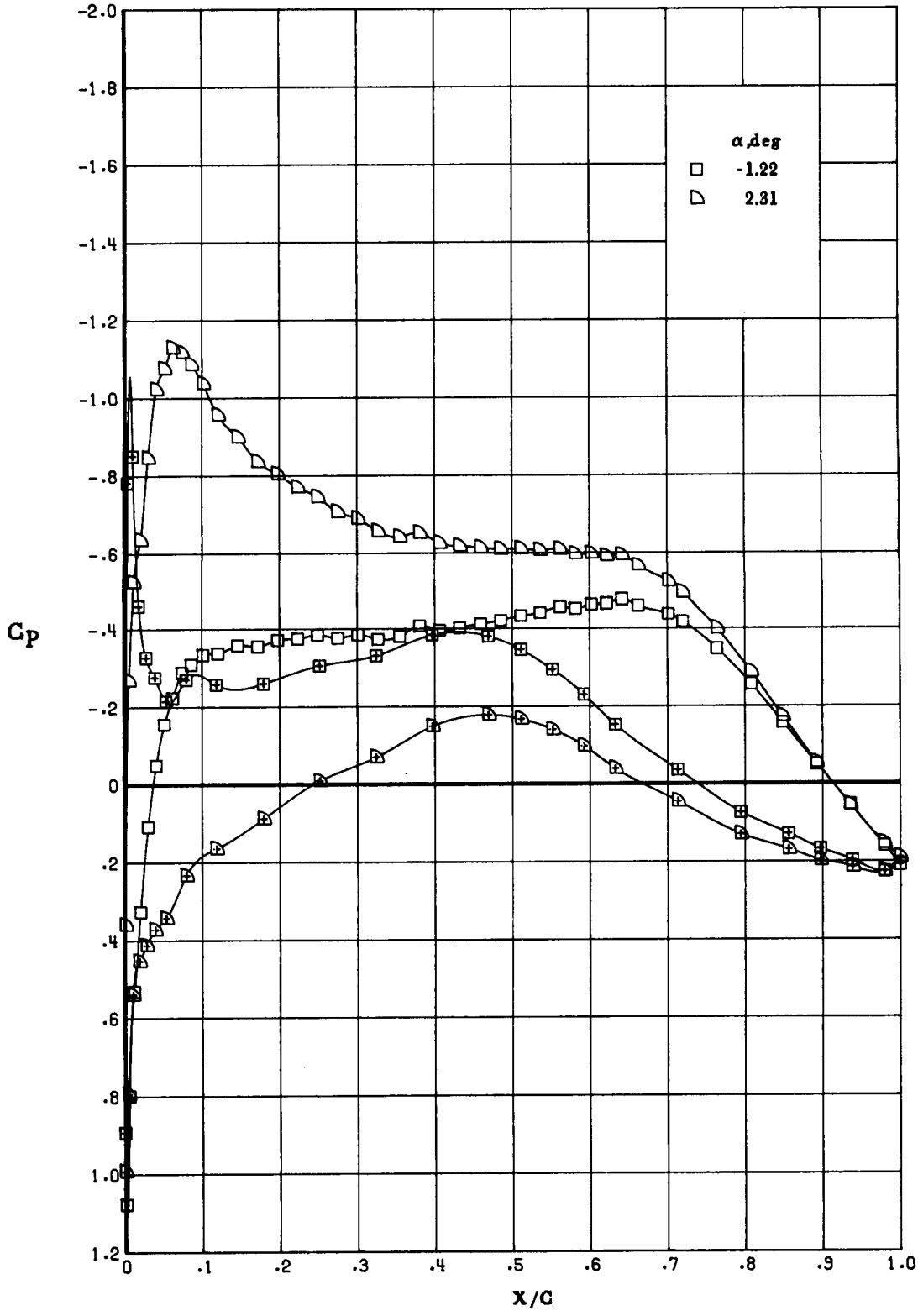

(a) Concluded.

Figure 16. Continued.

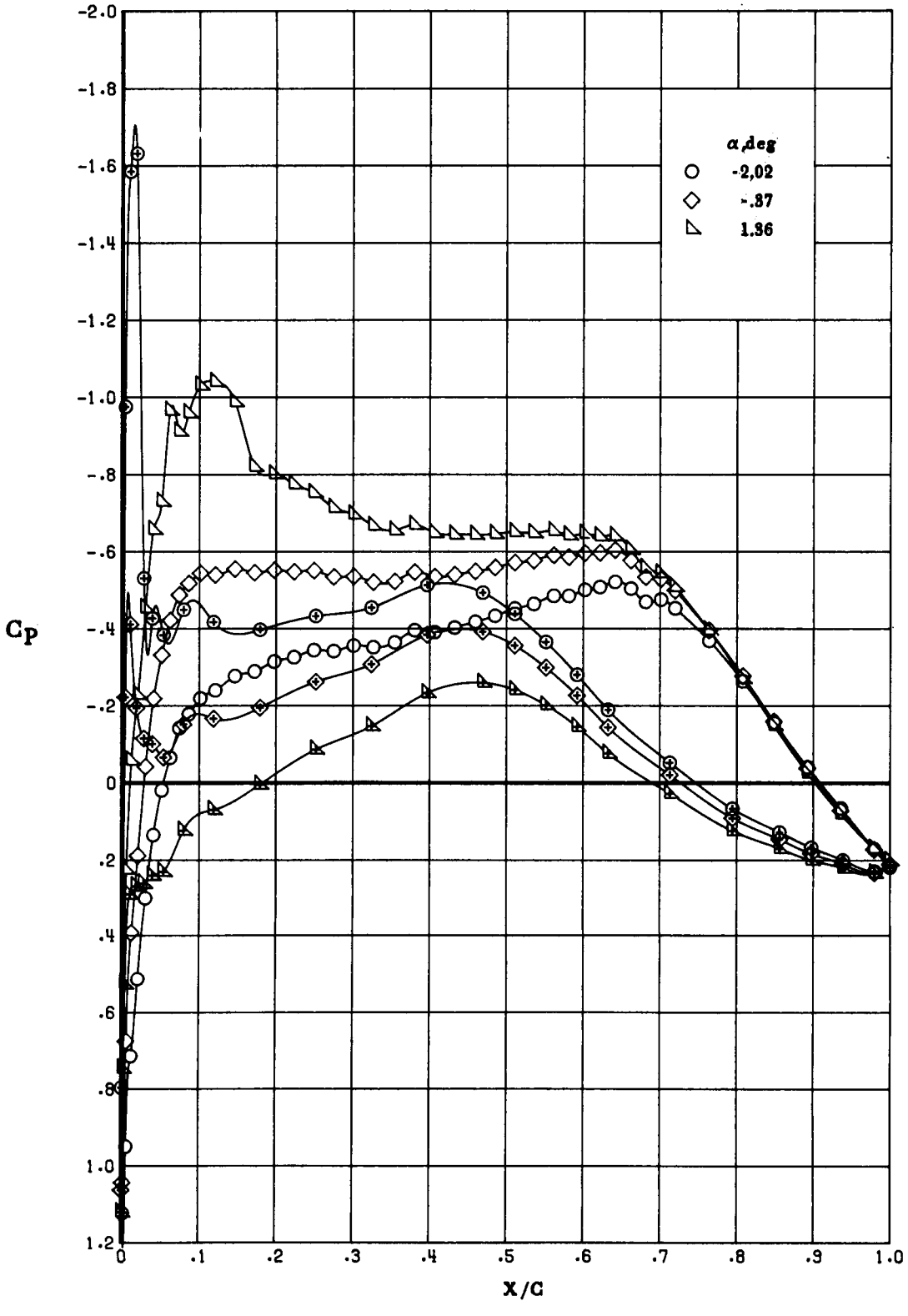

(b) $M_\infty = 0.70$.

Figure 16. Continued.

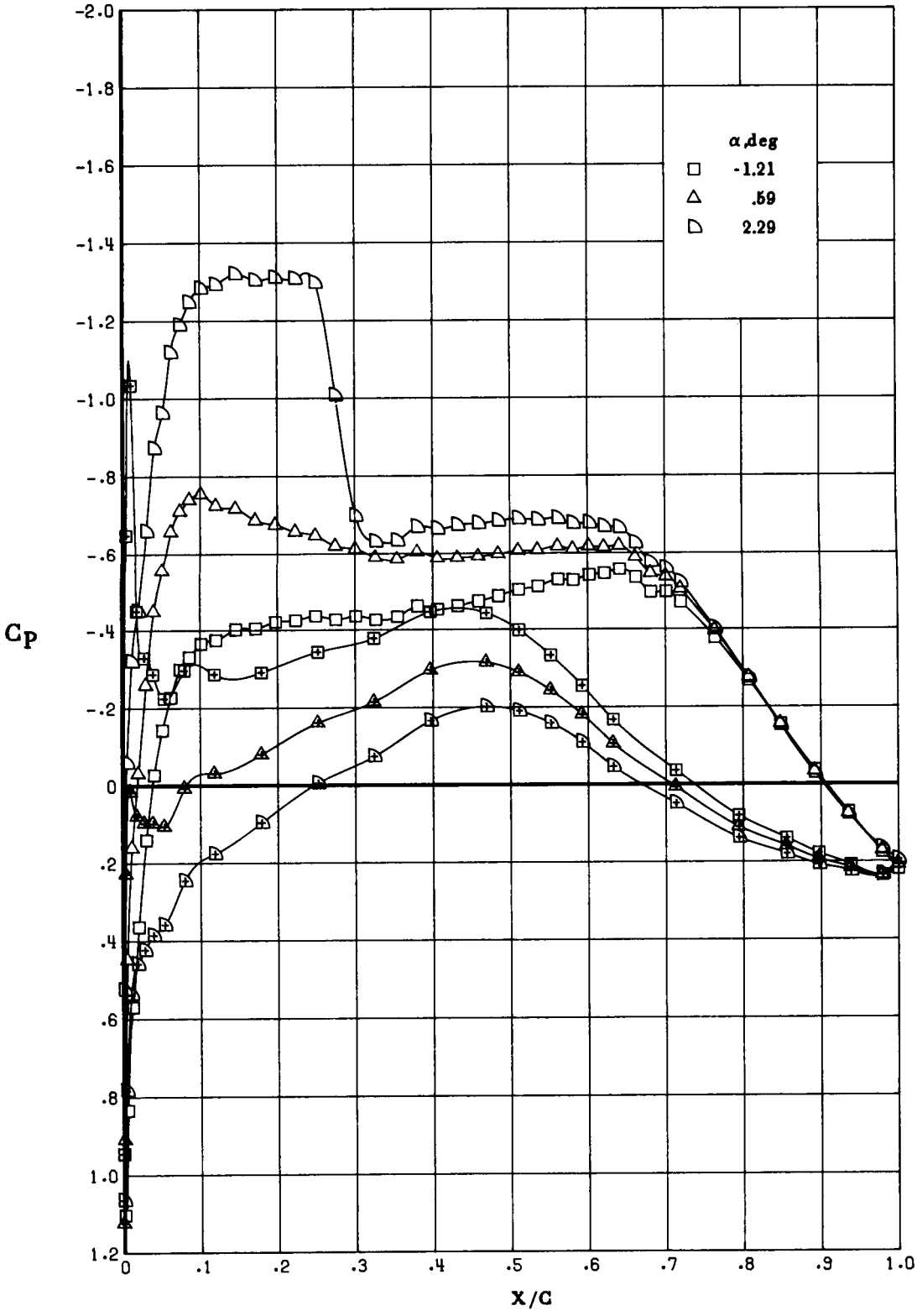

(b) Concluded.

Figure 16. Continued.

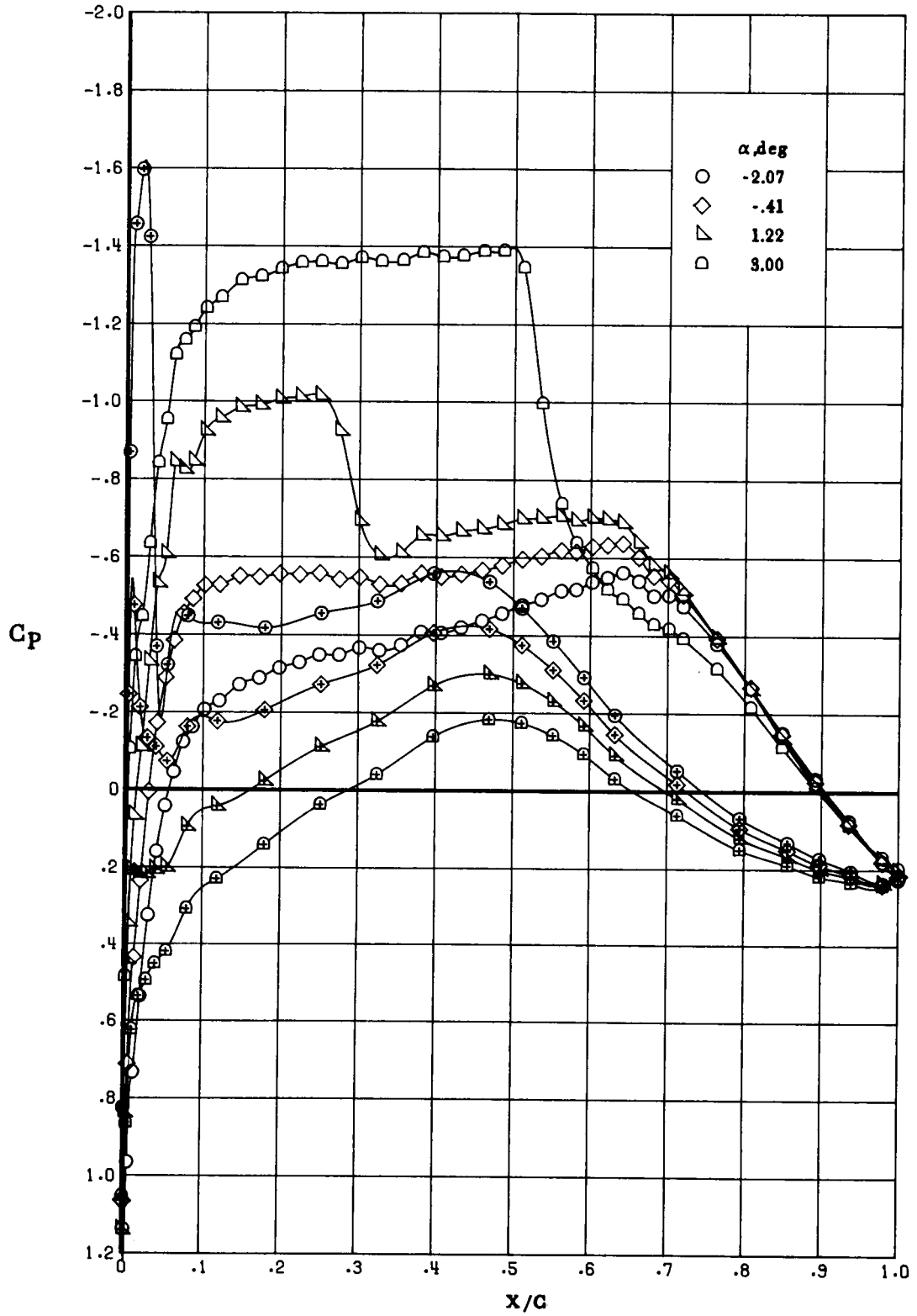

(c) $M_\infty = 0.73$.

Figure 16. Continued.

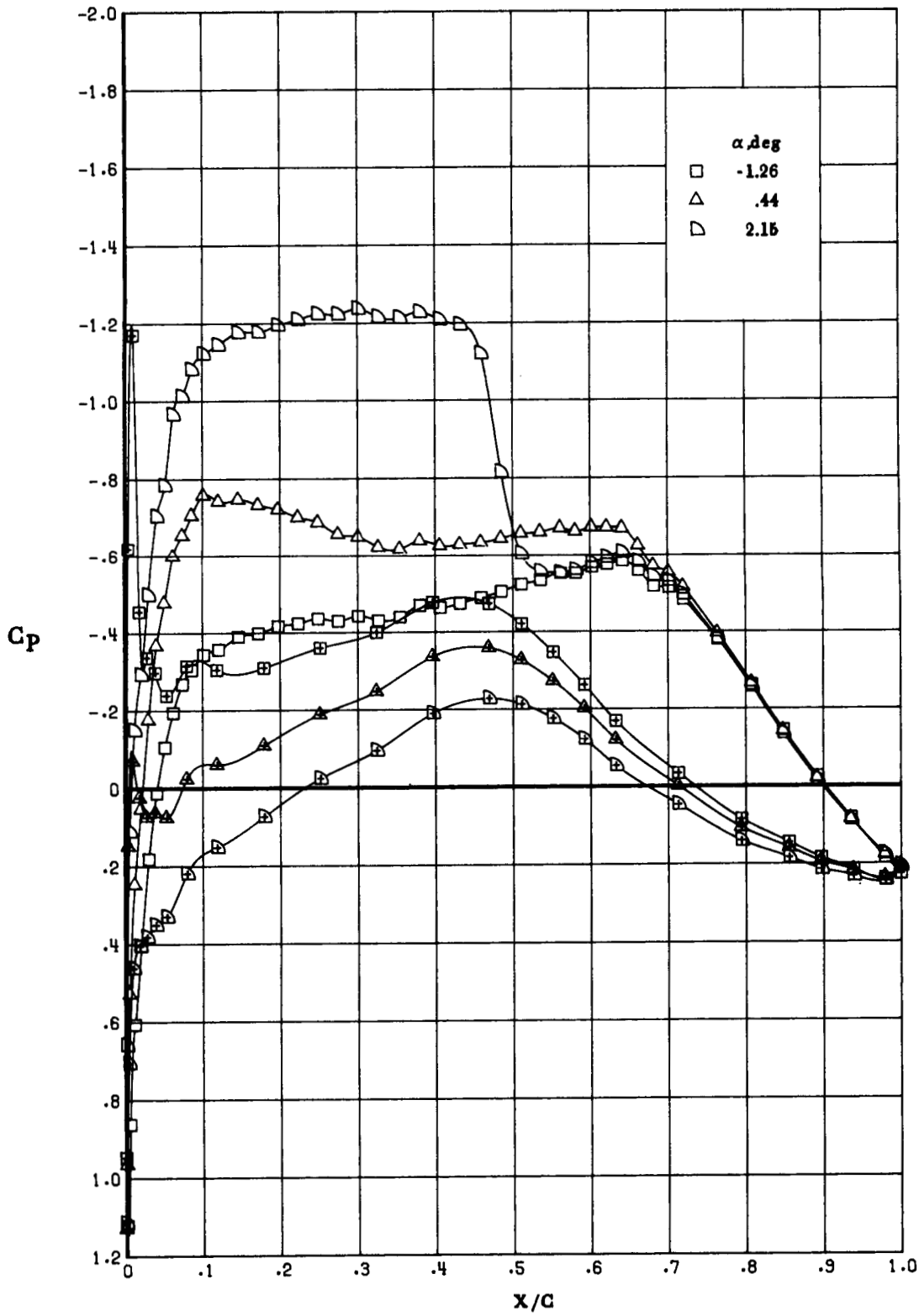

(c) Concluded.

Figure 16. Continued.

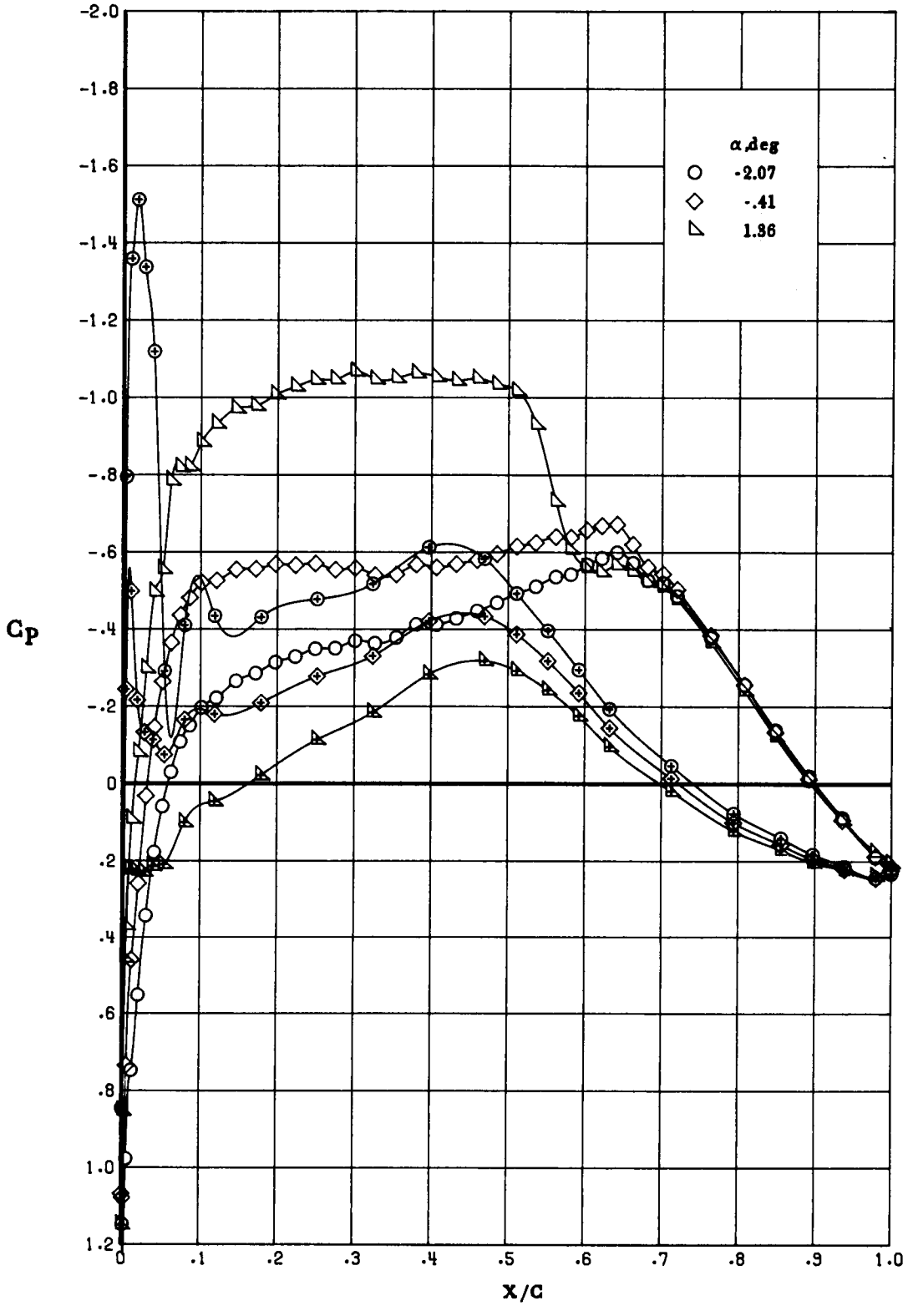

(d) $M_\infty = 0.75$.

Figure 16. Continued.

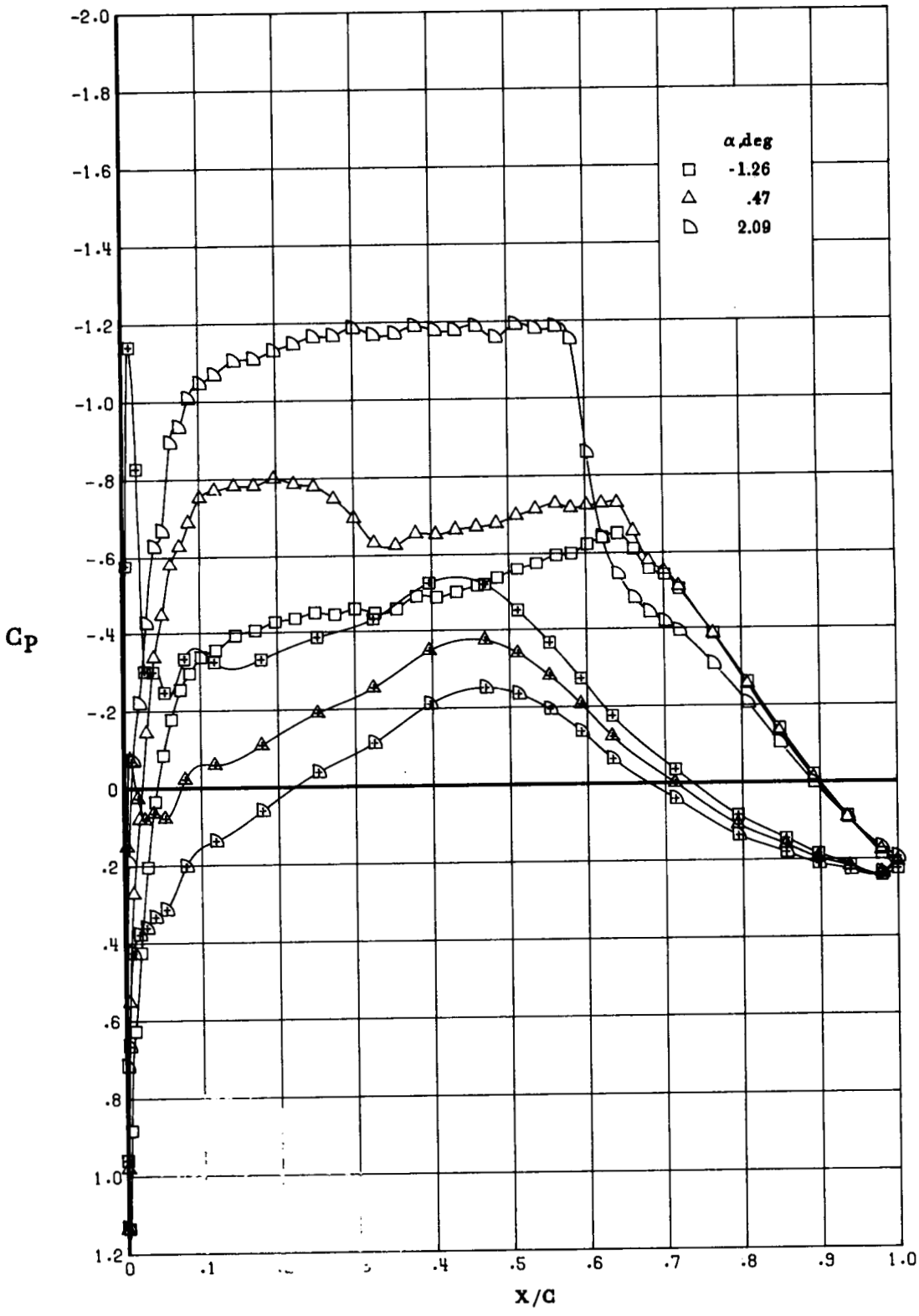

c) Concluded.

Figure 16. Continued.

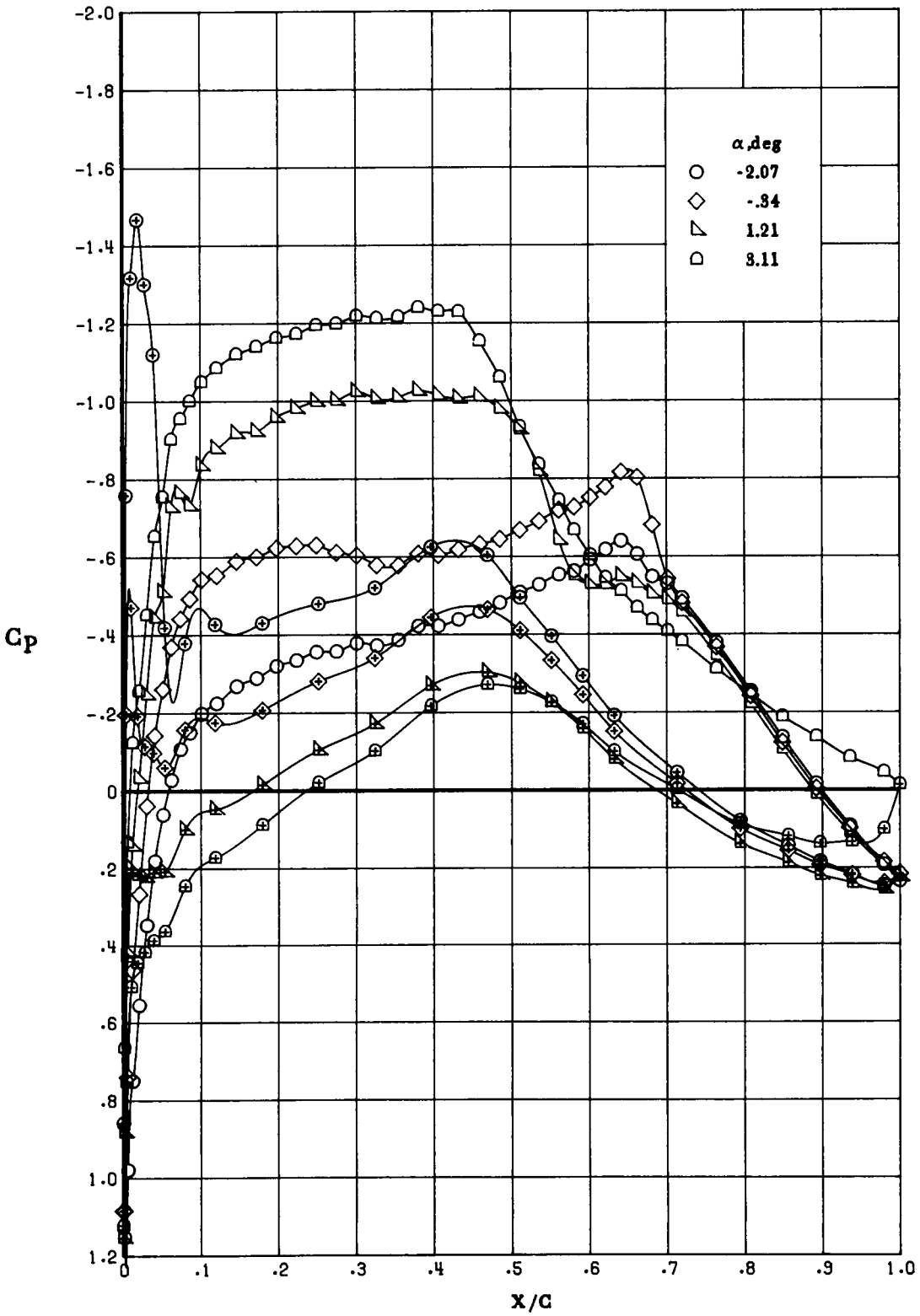

(e) $M_\infty = 0.765$.

Figure 16. Continued.

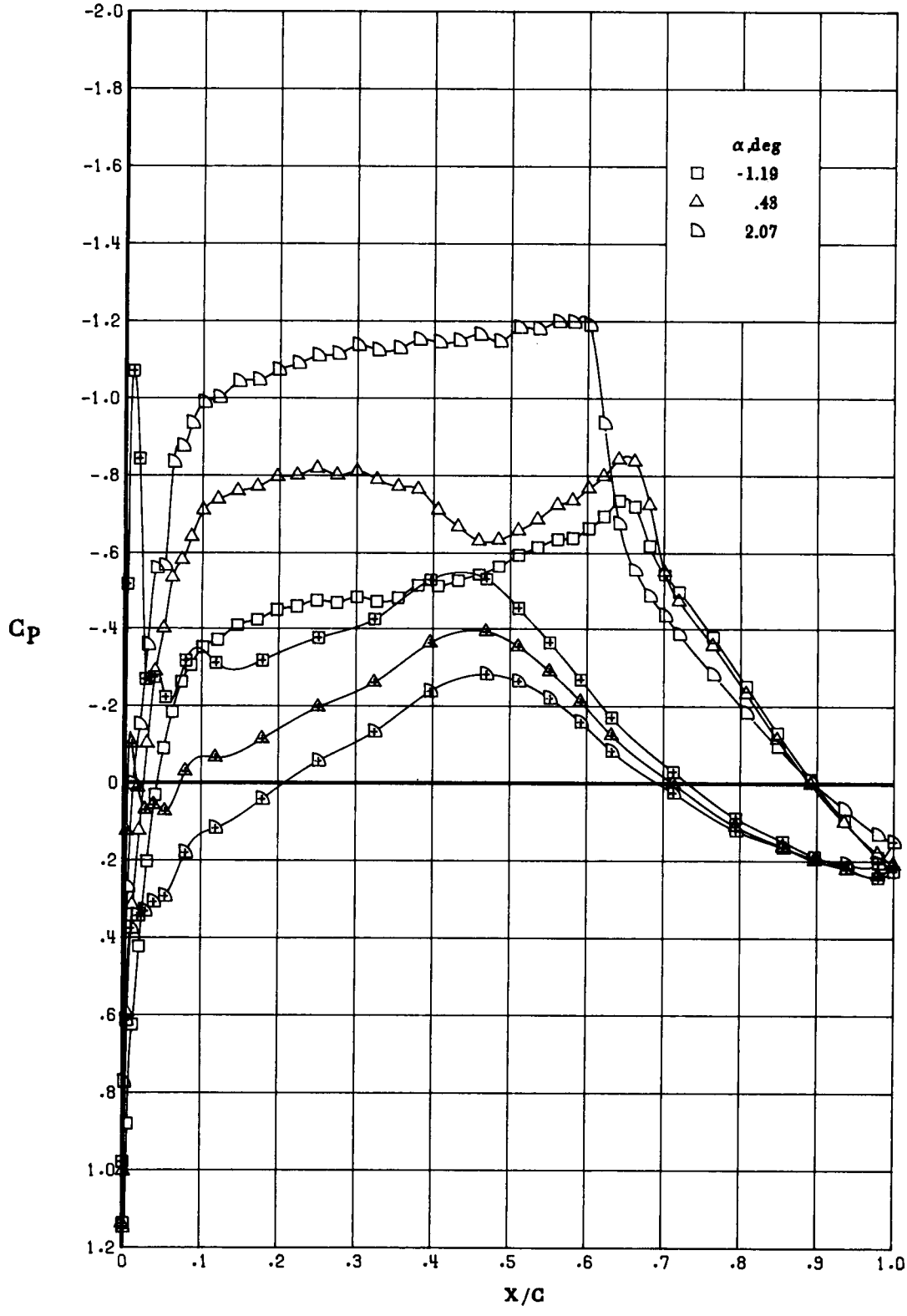

(e) Concluded.

Figure 16. Continued.

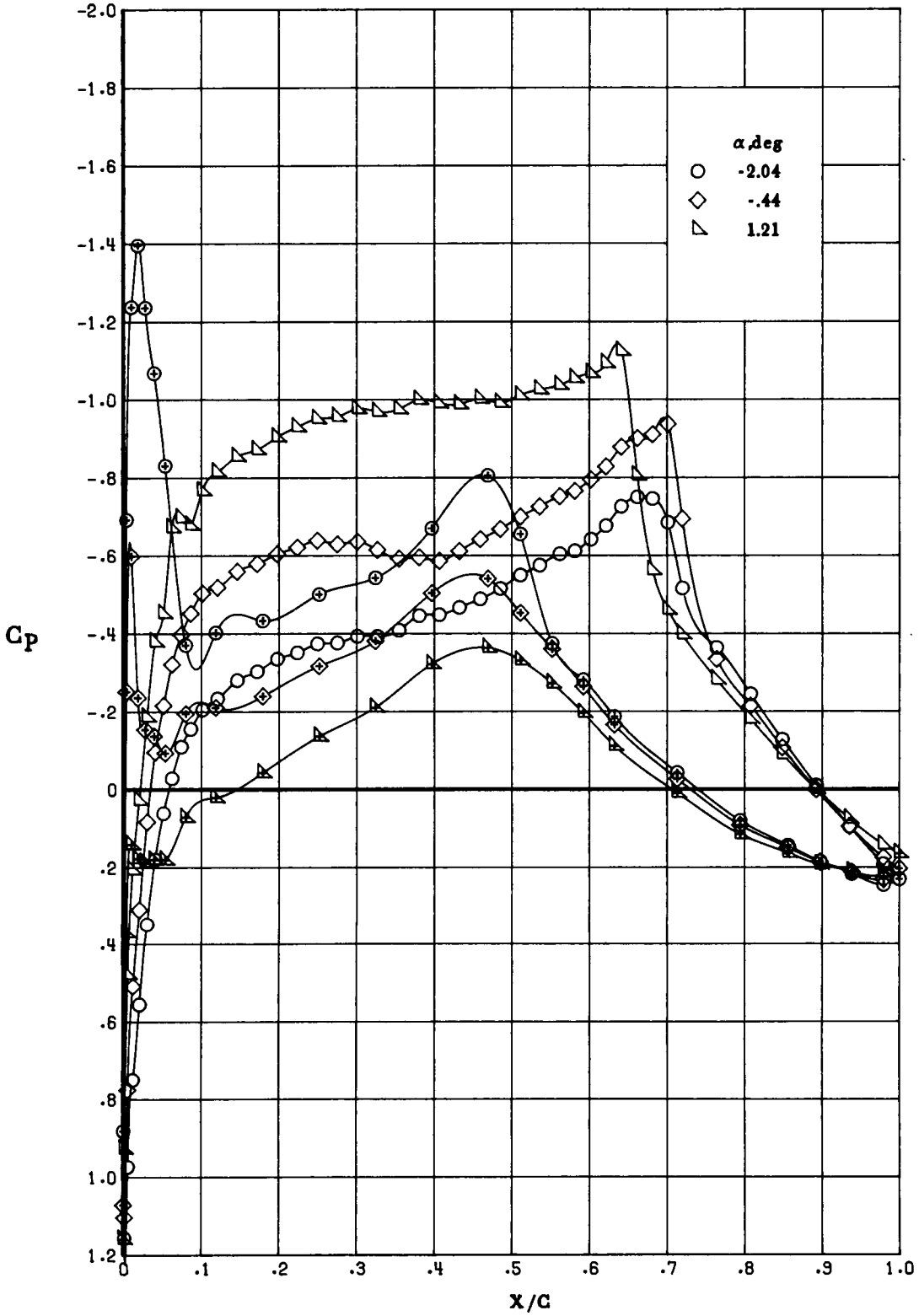

(f) $M_\infty = 0.78$.

Figure 16. Continued.

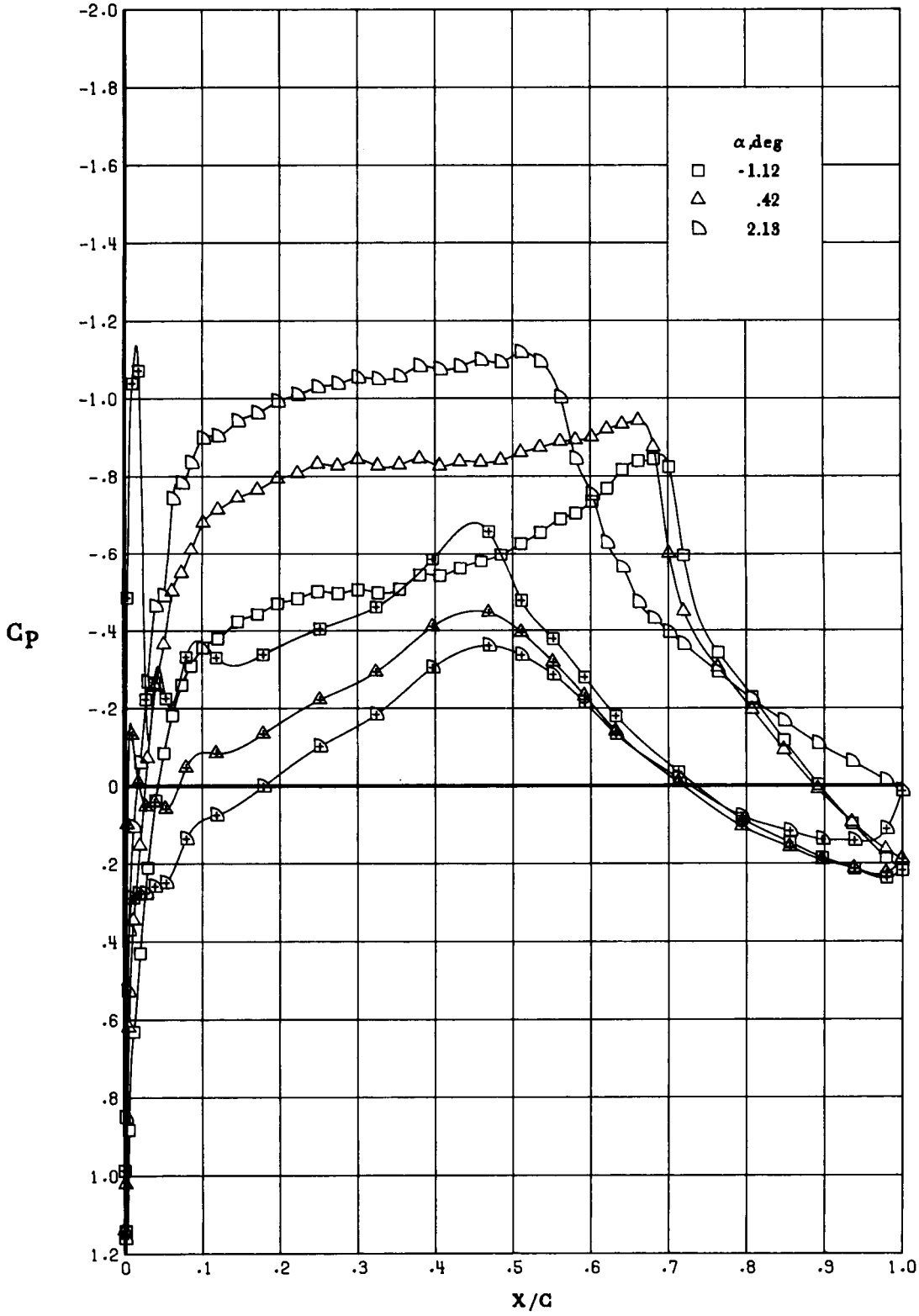

(f) Concluded.

Figure 16. Continued.

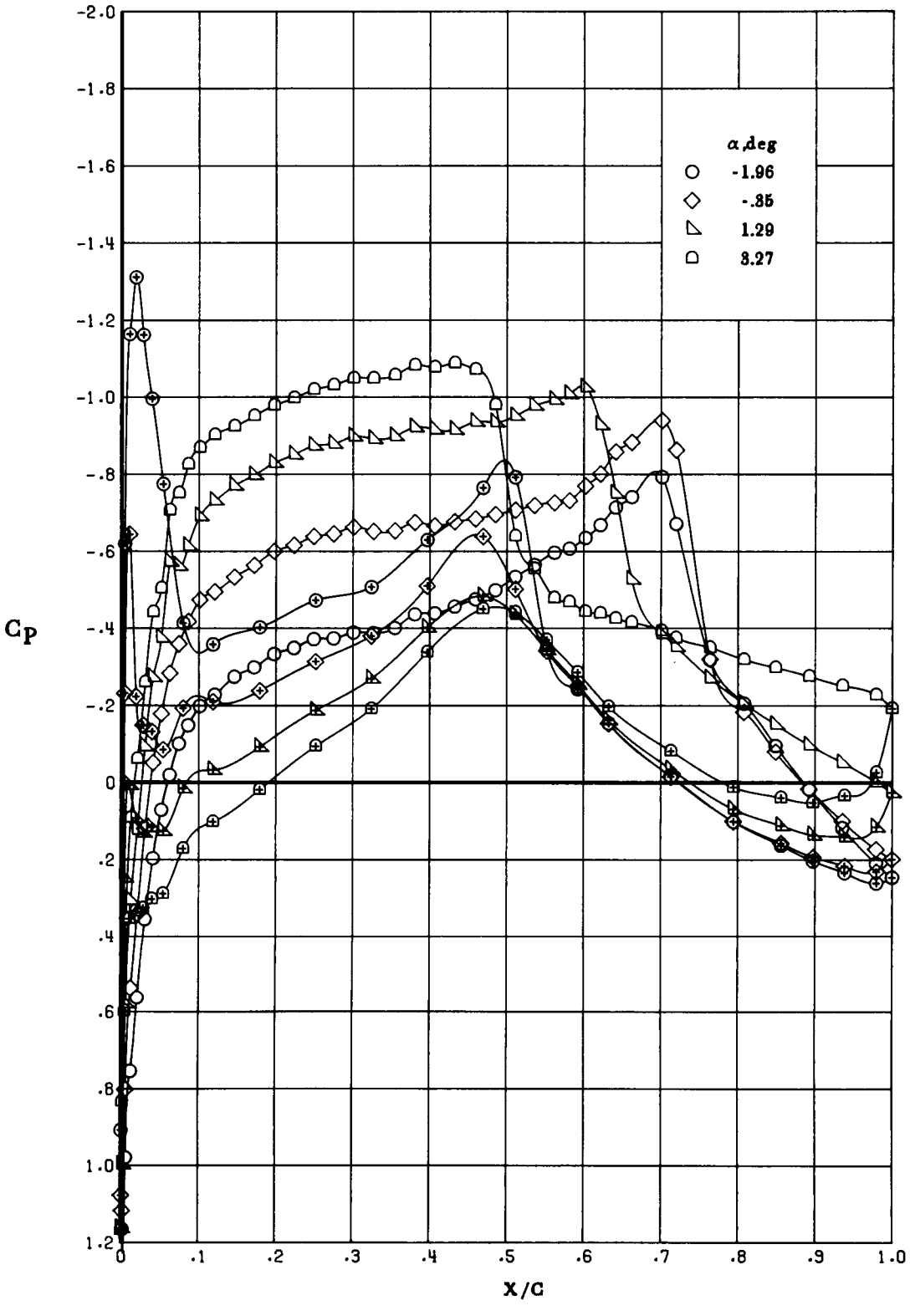

(g) $M_\infty = 0.80$.

Figure 16. Continued.

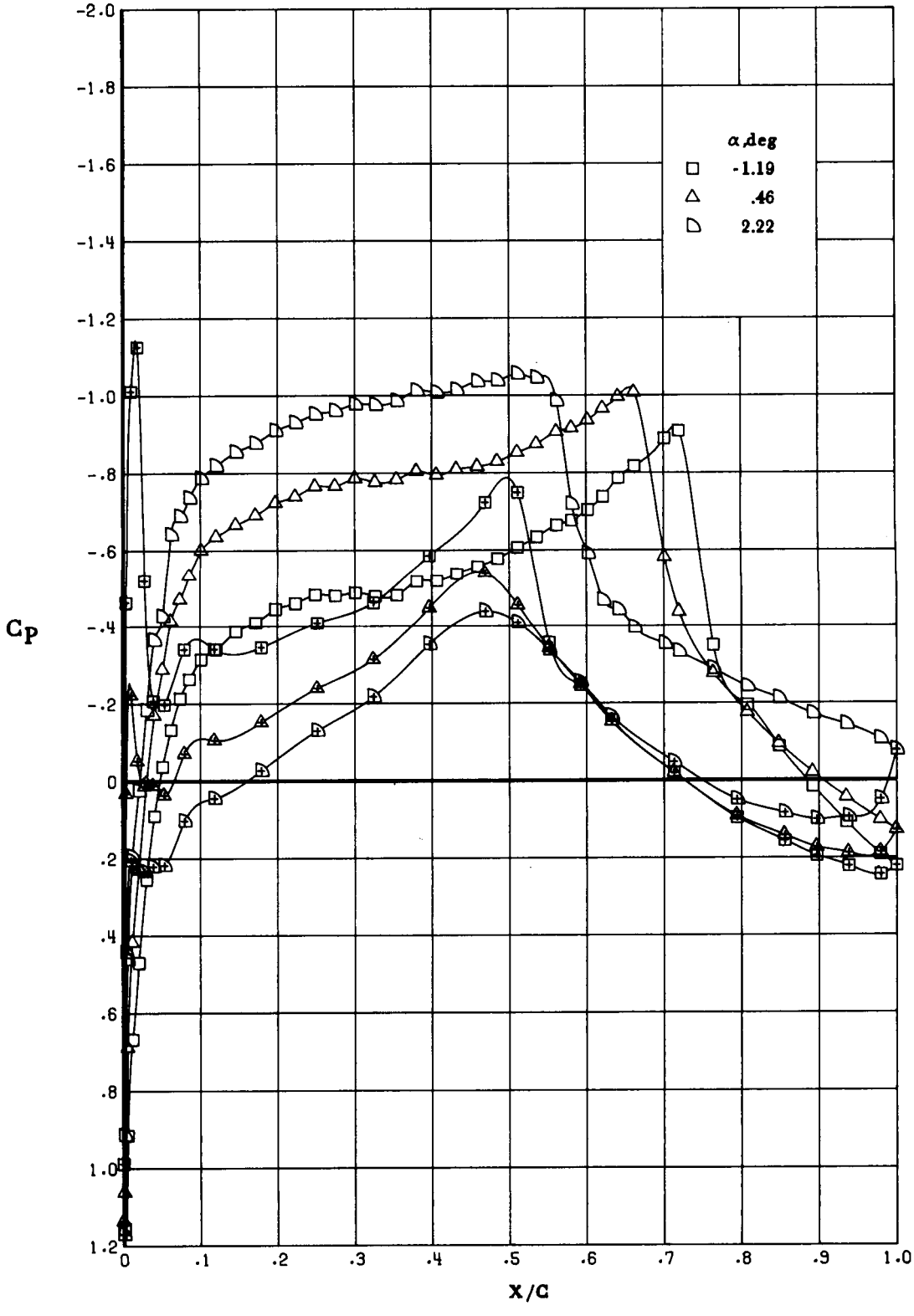

(g) Concluded.

Figure 16. Concluded.

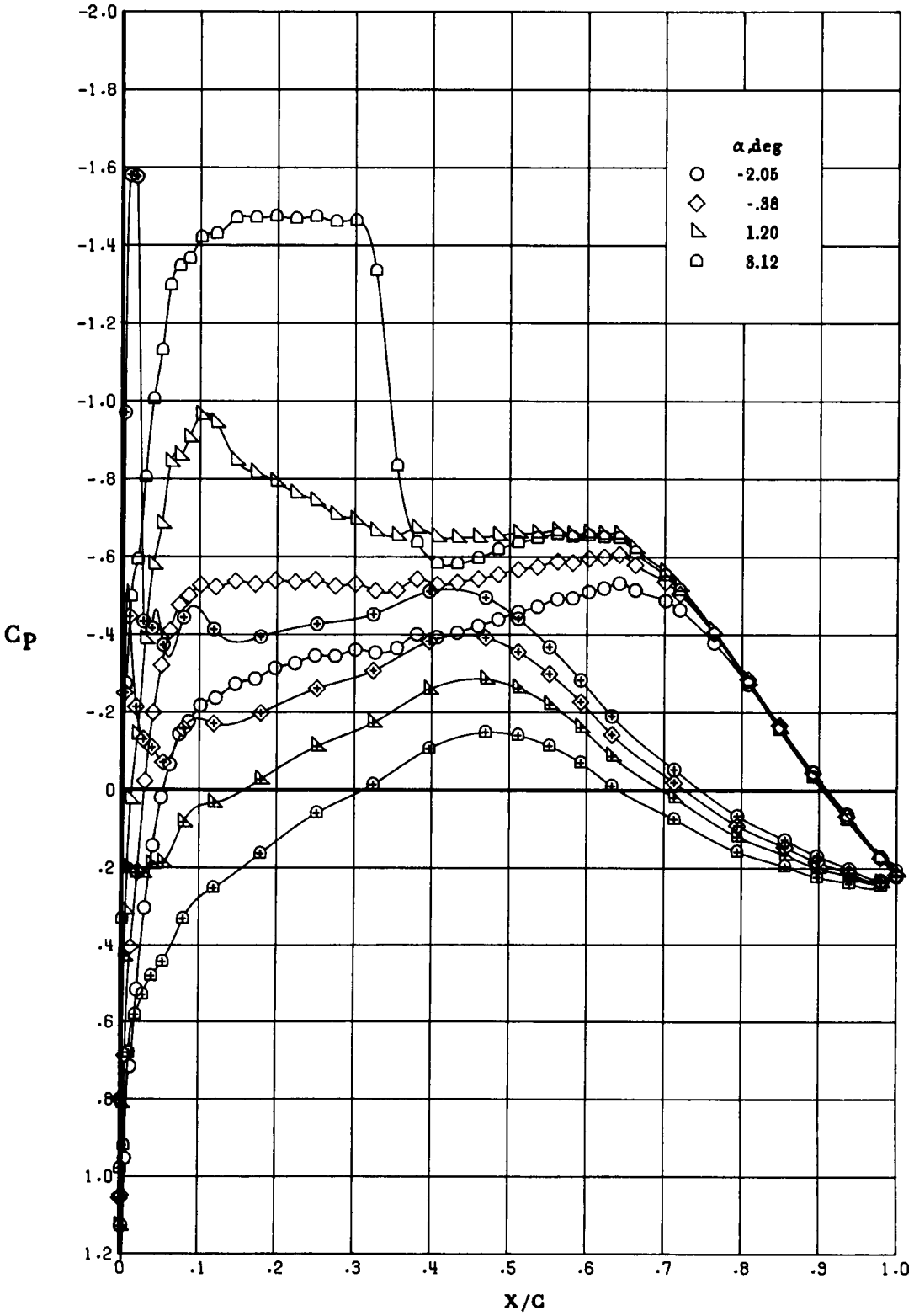

(a) $M_\infty = 0.70$.

Figure 17. Effect of α on chordwise pressure distribution at $R_c = 30 \times 10^6$. Open symbols denote upper surface; "+" within symbol denotes lower surface.

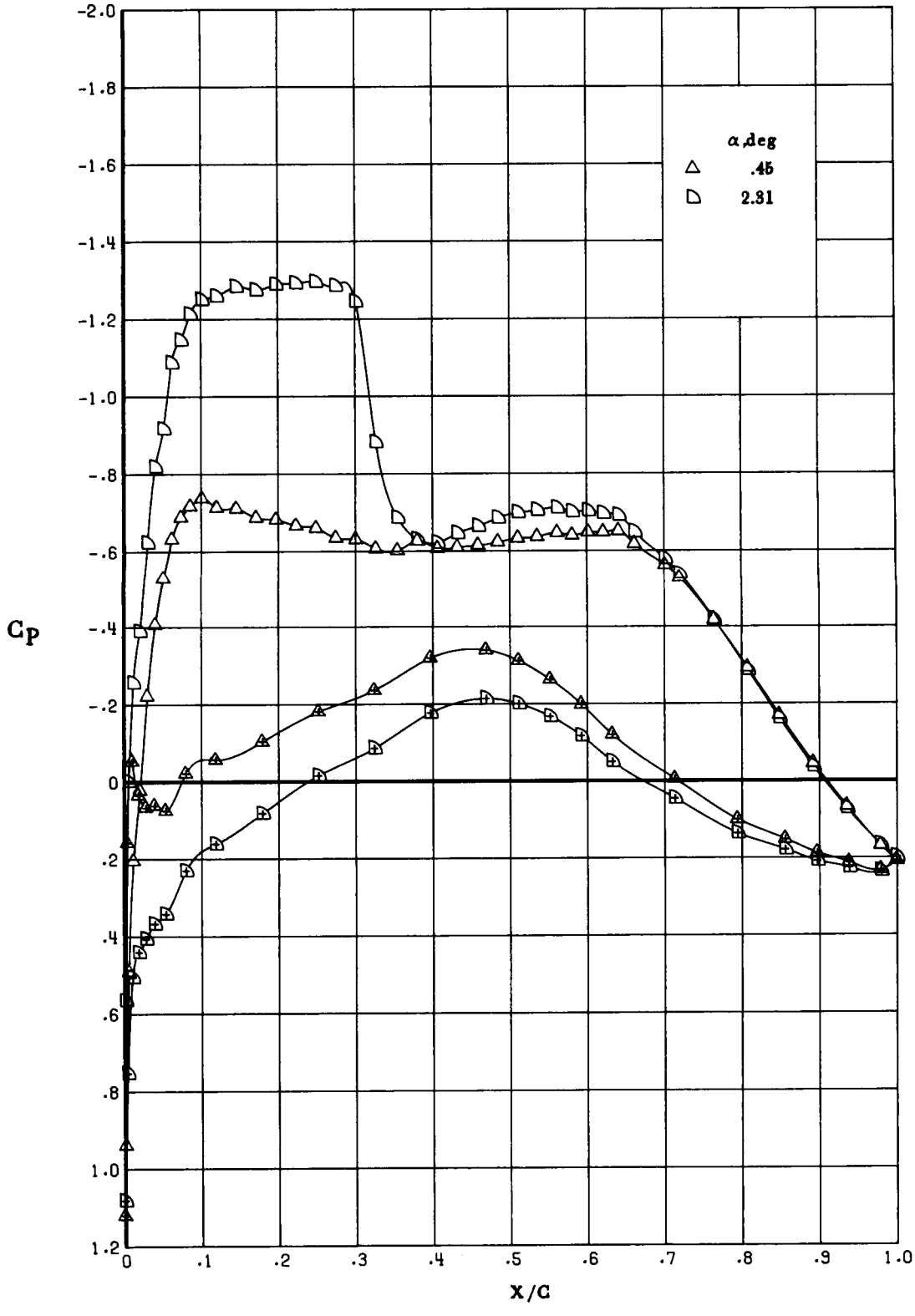

(a) Concluded.

Figure 17. Continued.

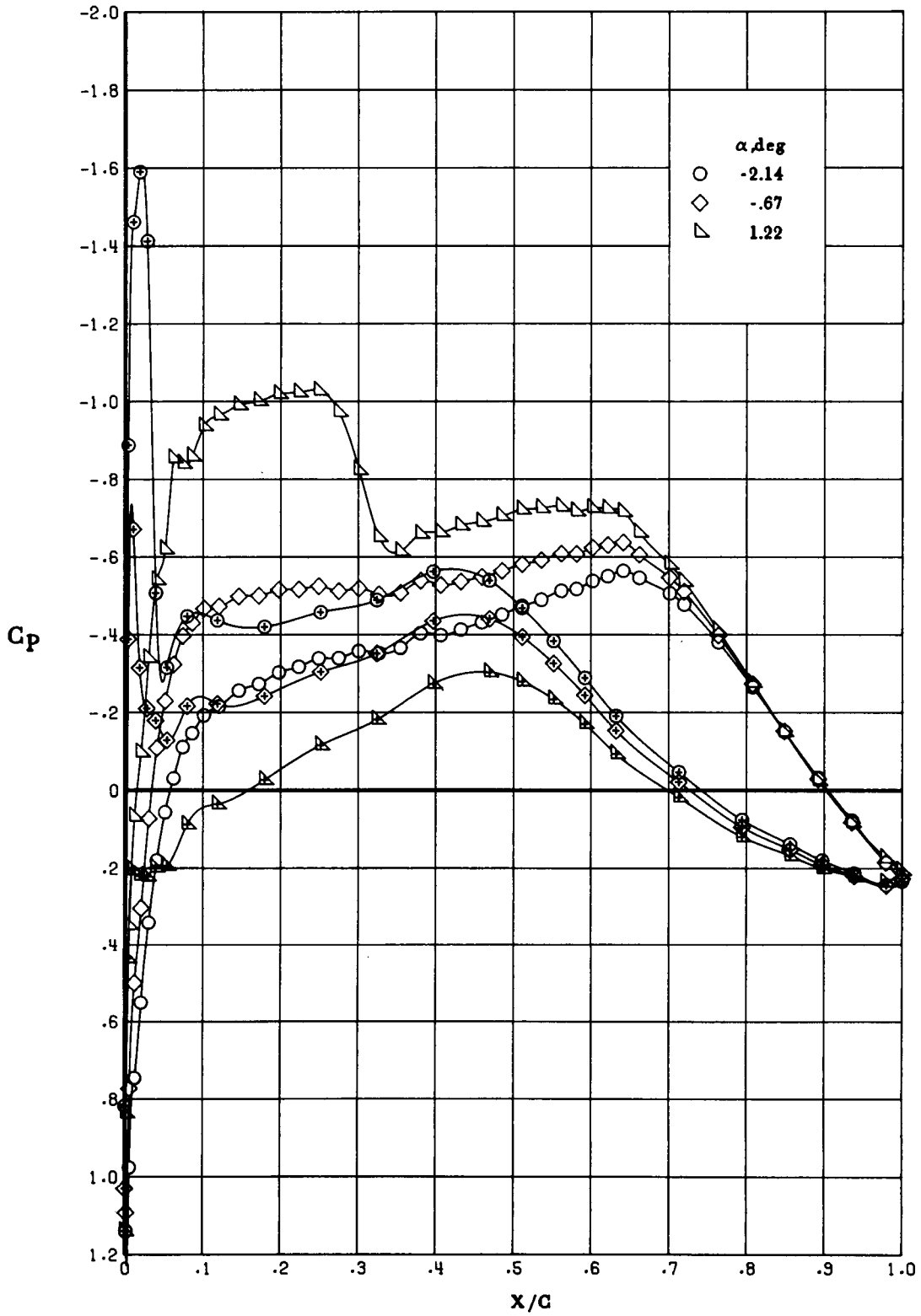

(b) $M_\infty = 0.73$.

Figure 17. Continued.

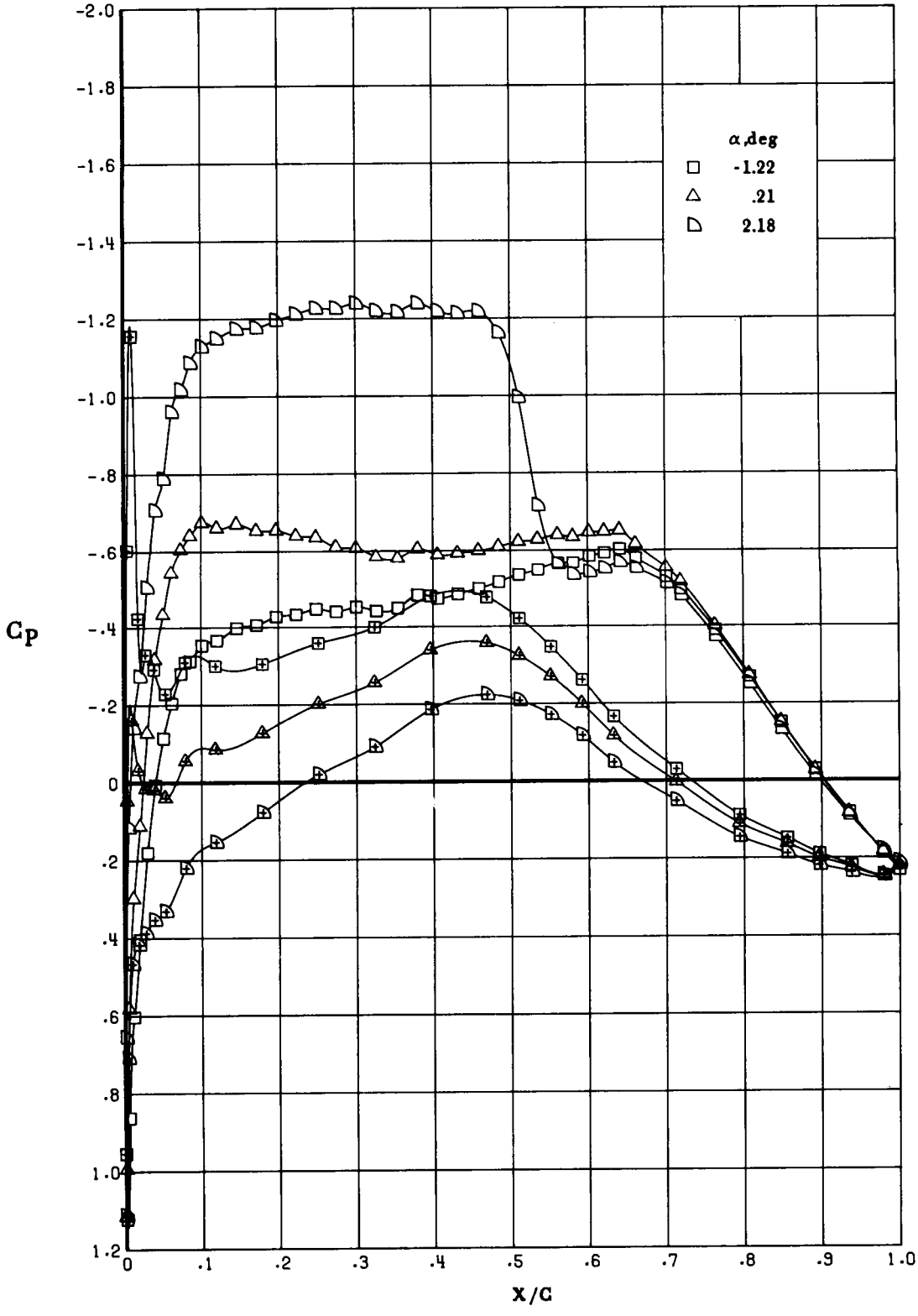

(b) Concluded.

Figure 17. Continued.

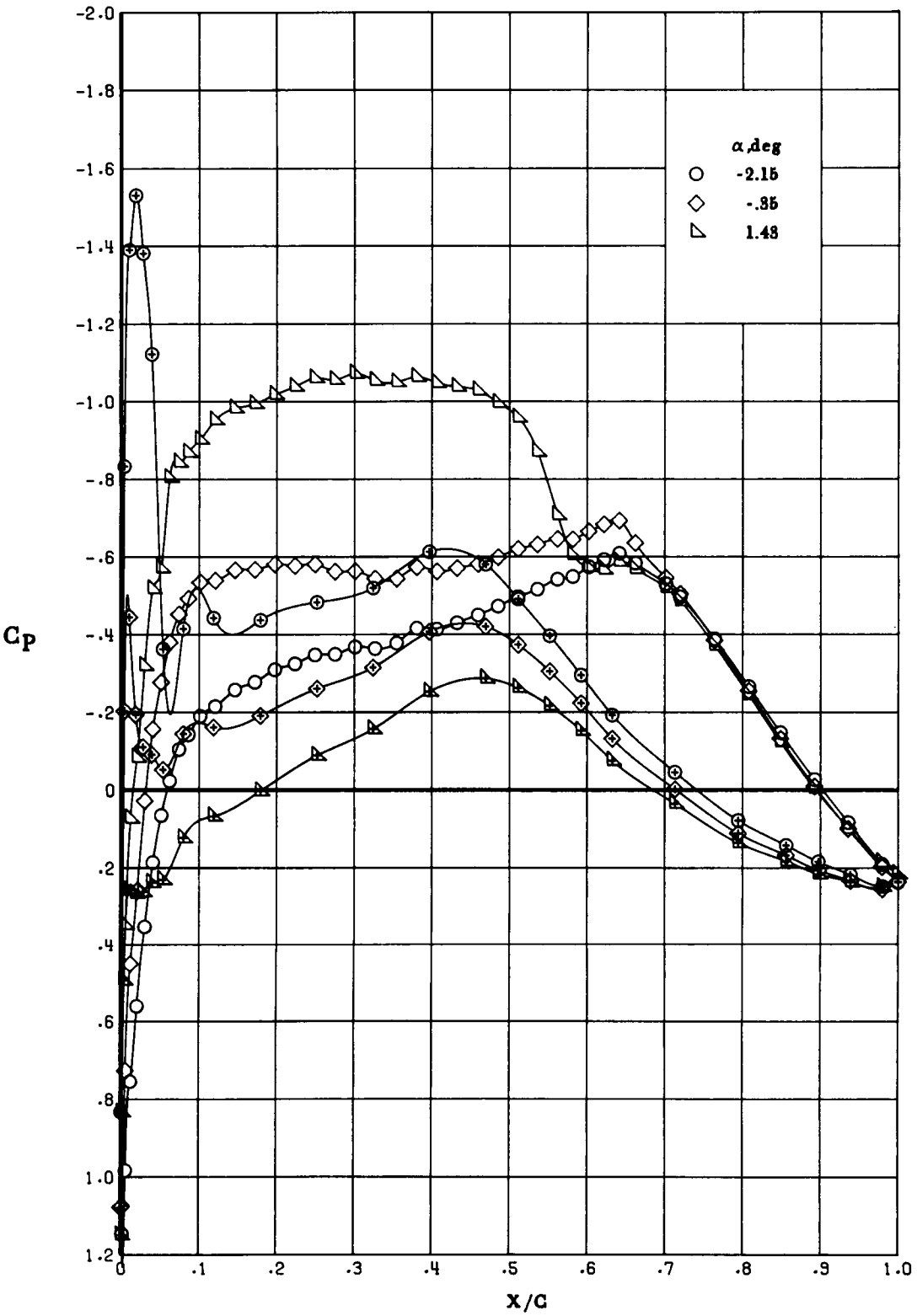

(c) $M_\infty = 0.75$.

Figure 17. Continued.

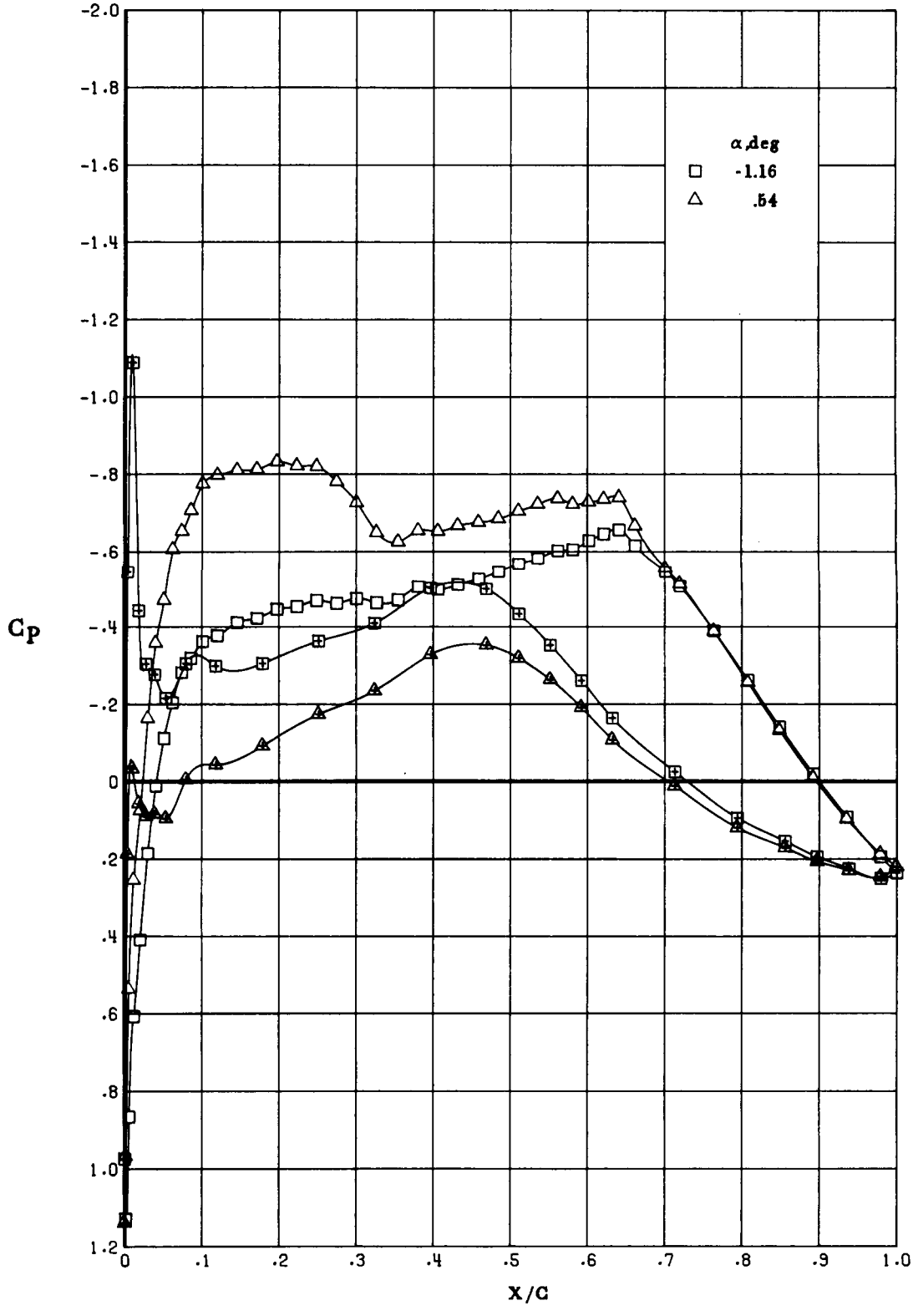

(c) Concluded.

Figure 17. Continued.

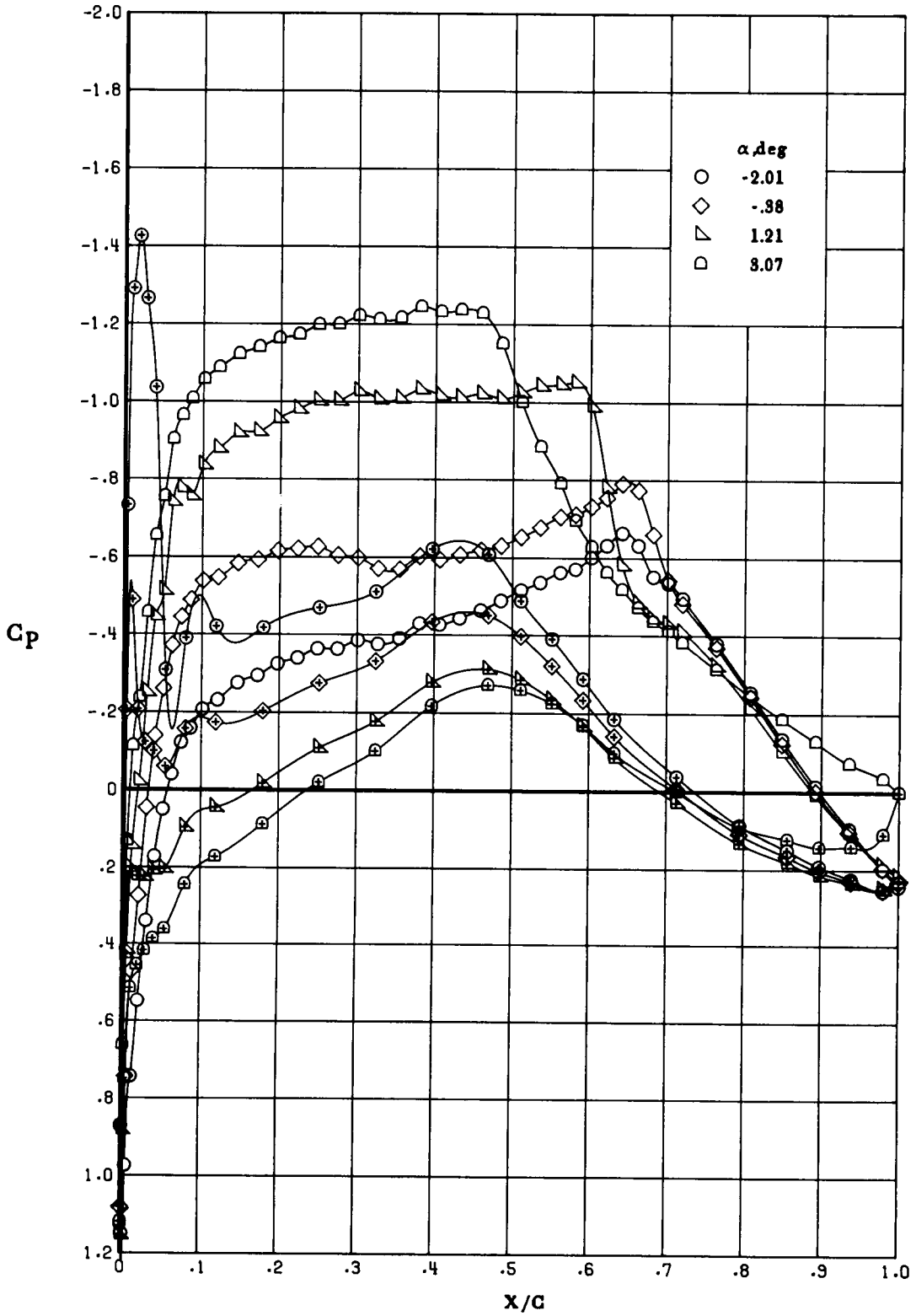

(d) $M_\infty = 0.765$.

Figure 17. Continued.

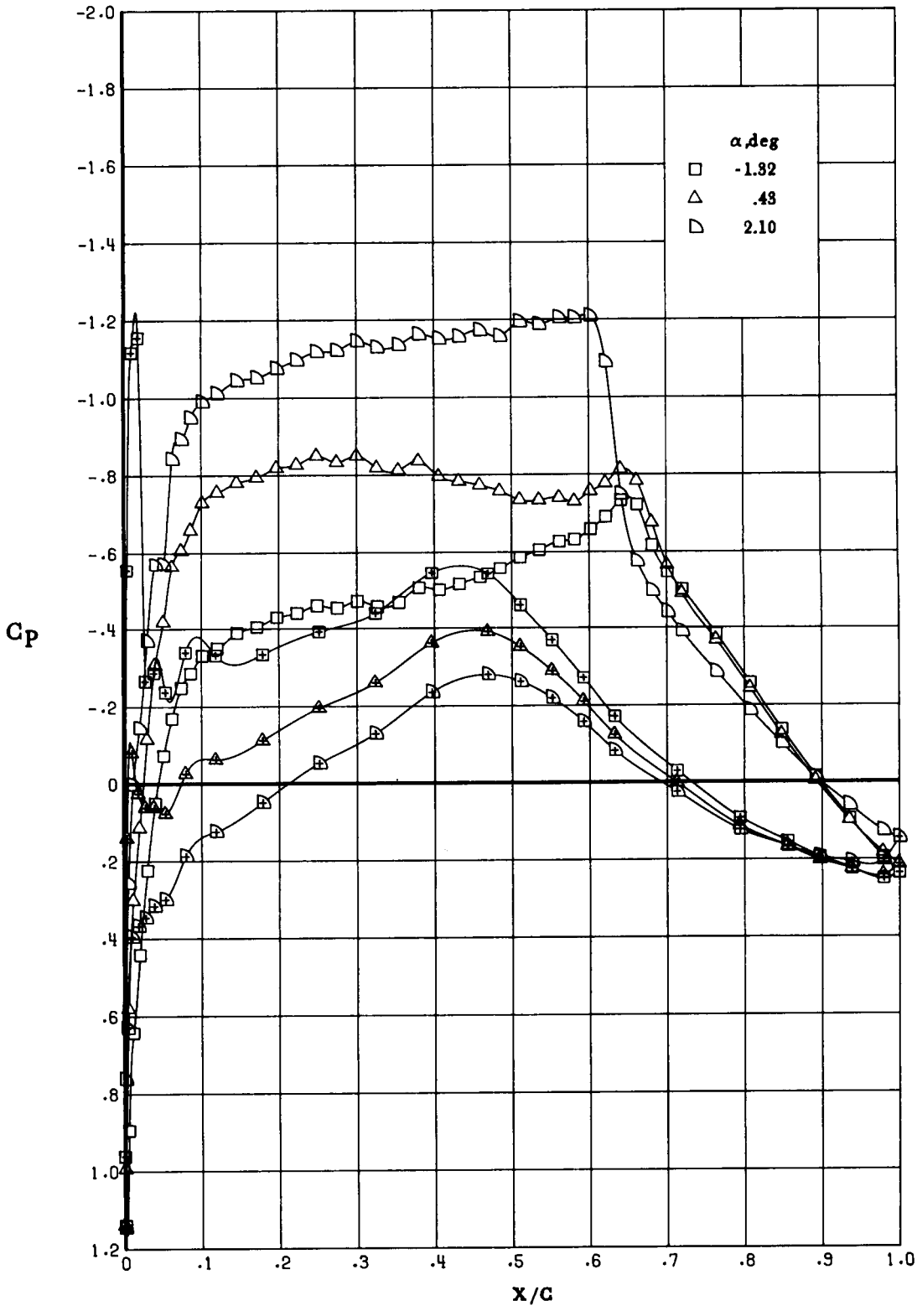

(d) Concluded.

Figure 17. Continued.

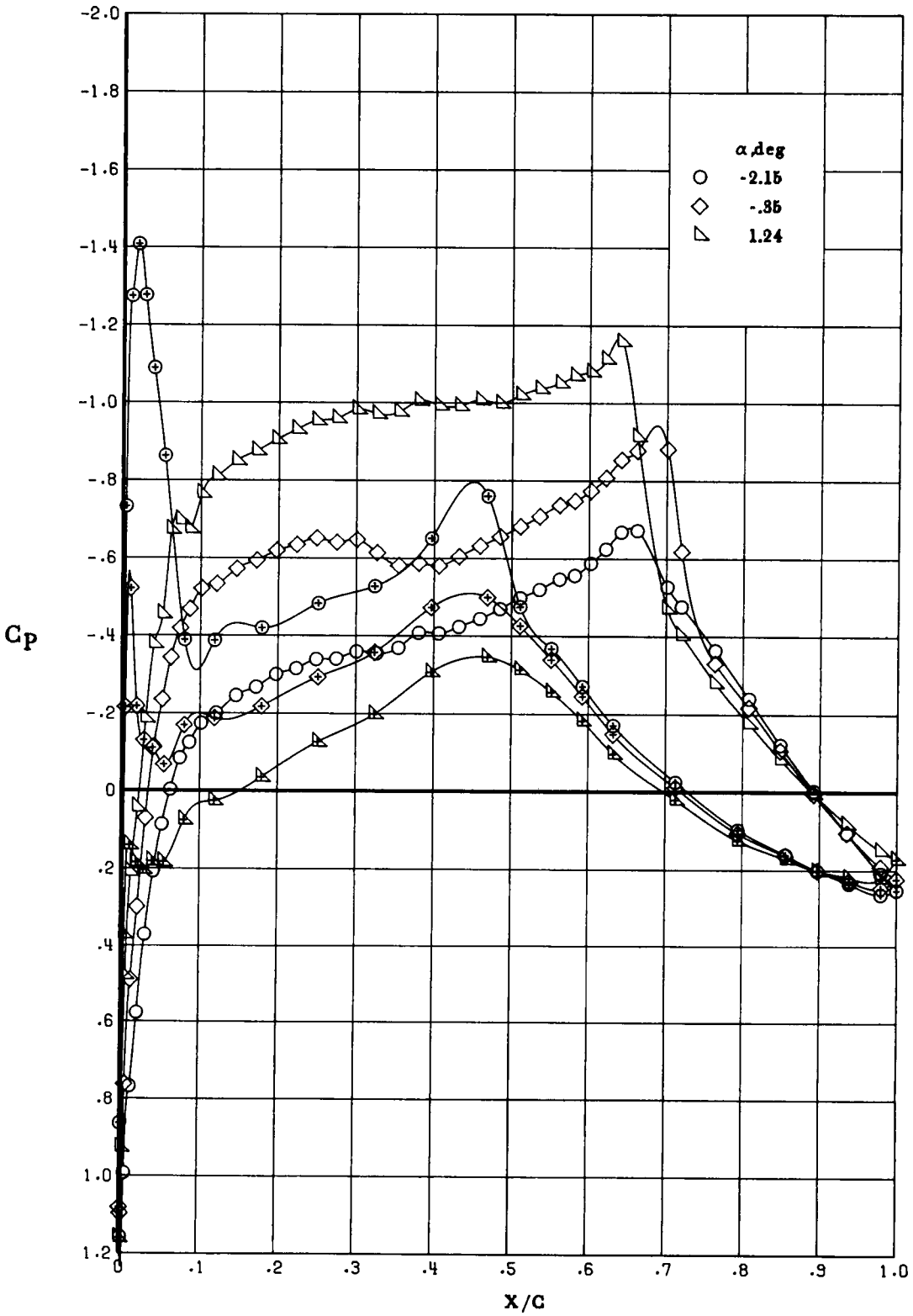

(e) $M_\infty = 0.78$.

Figure 17. Continued.

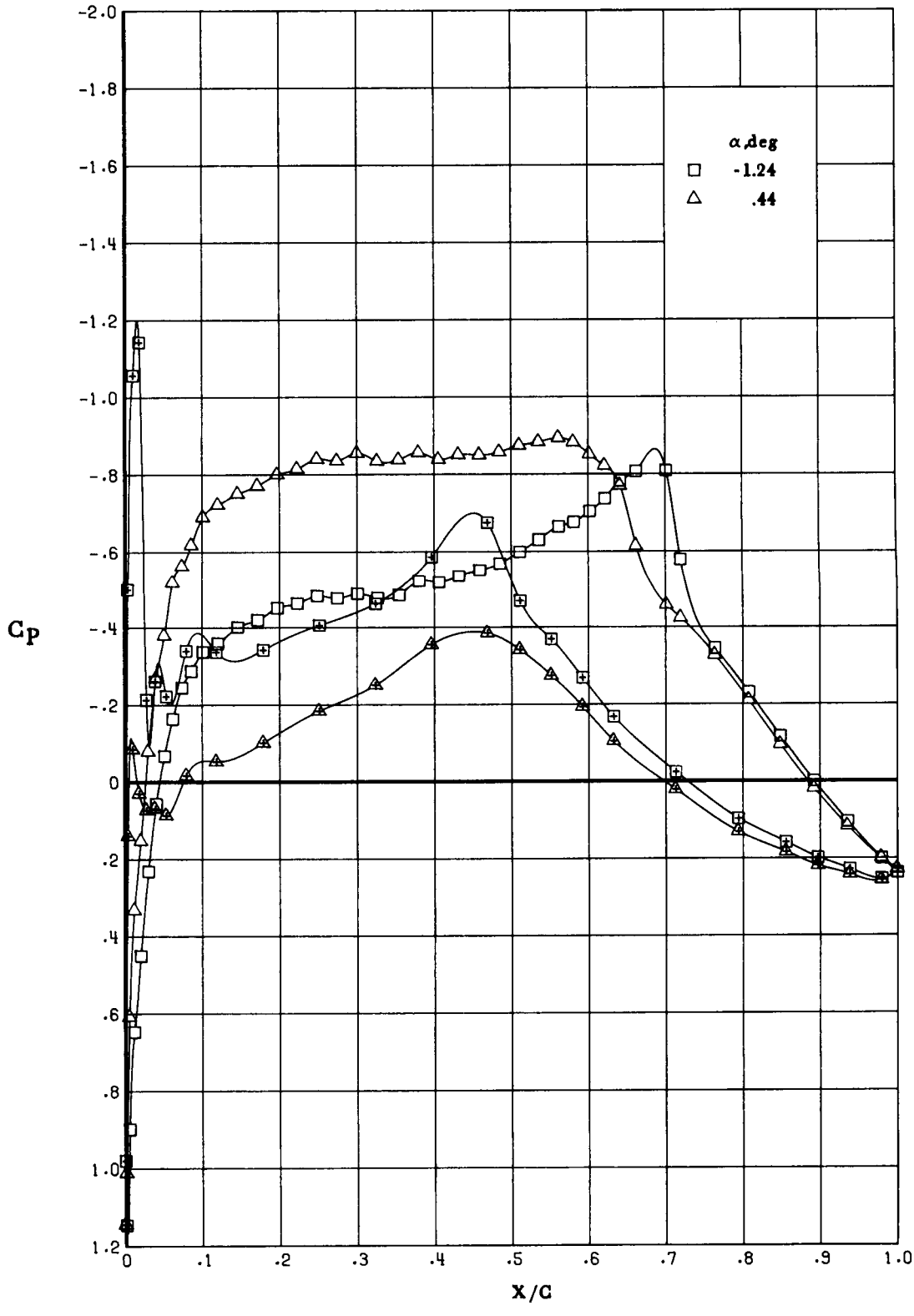

(e) Concluded.

Figure 17. Continued.

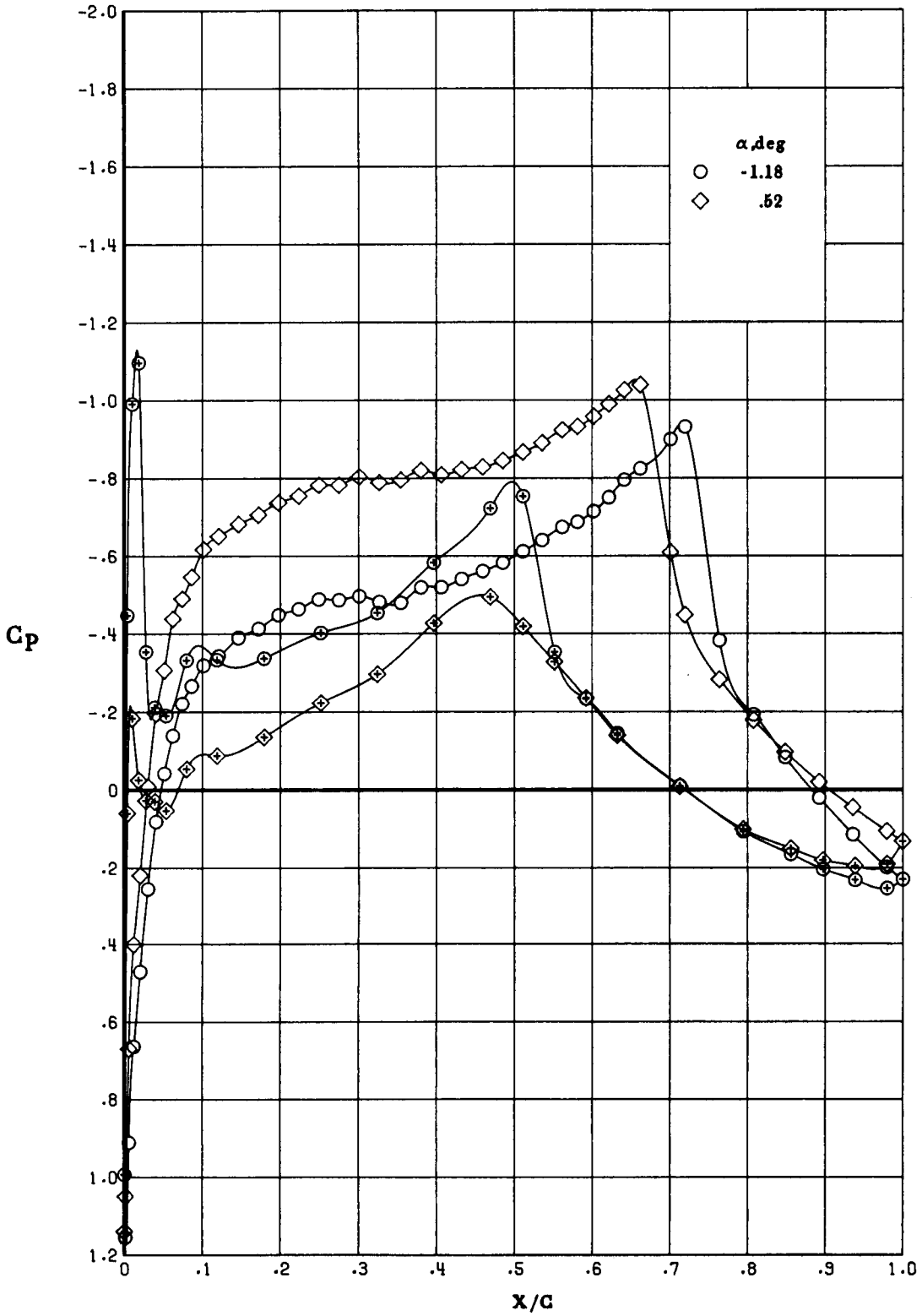

(f) $M_\infty = 0.80$.

Figure 17. Continued.

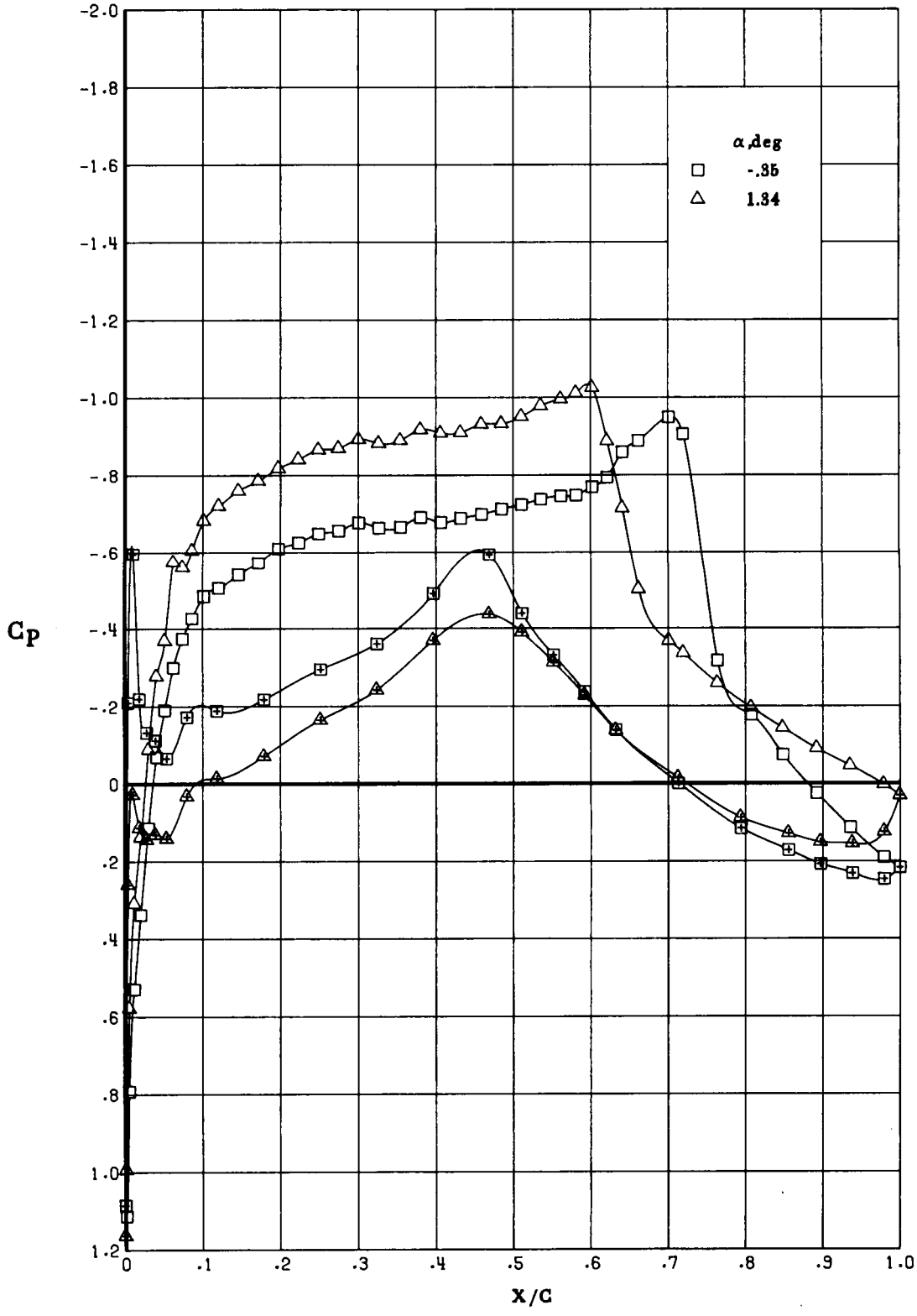

(f) Concluded.

Figure 17. Concluded.

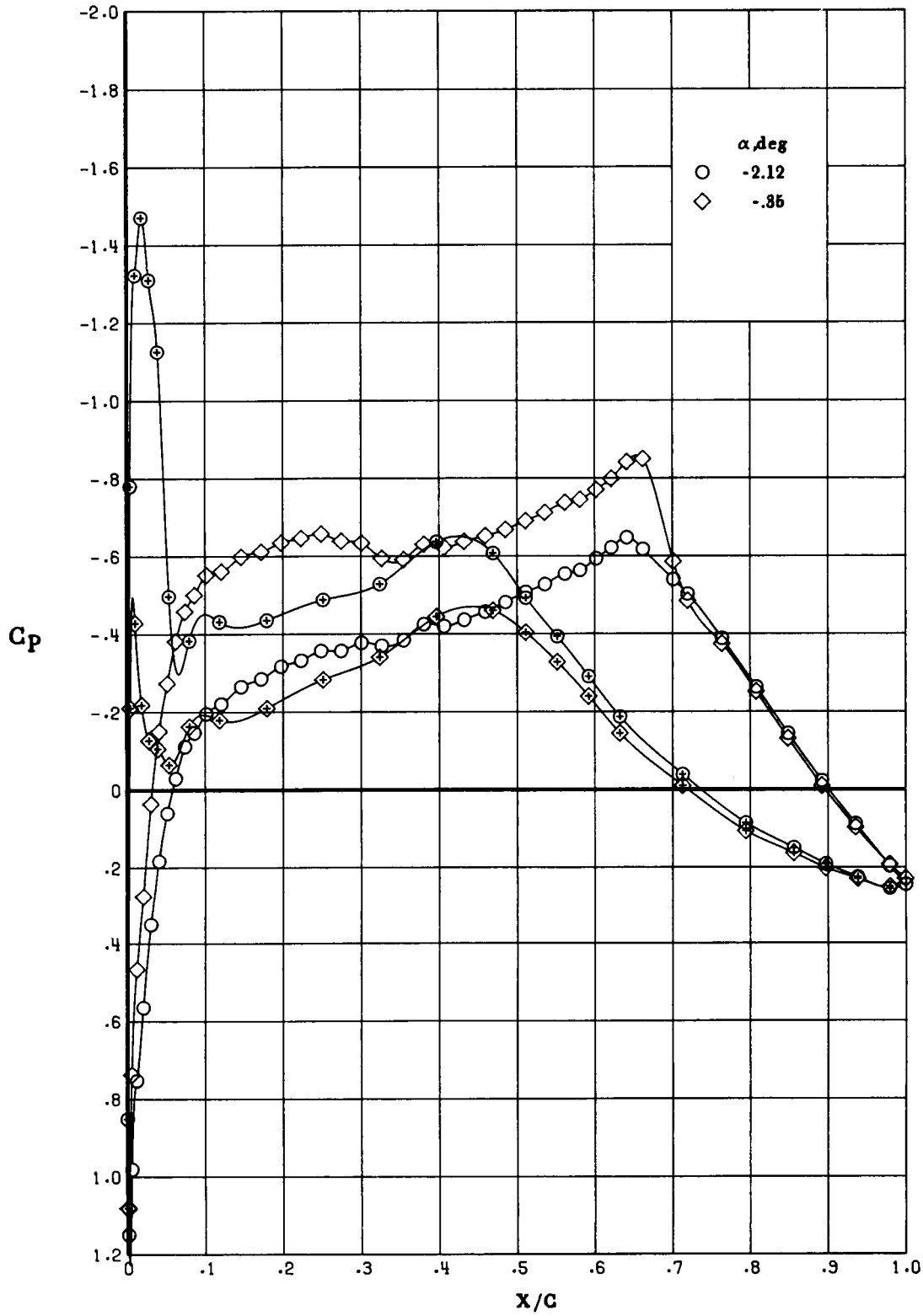

Figure 18. Effect of α on chordwise pressure distribution at $R_c = 40 \times 10^6$ and $M = 0.765$. Open symbols denote upper surface; "+" within symbol denotes lower surface.

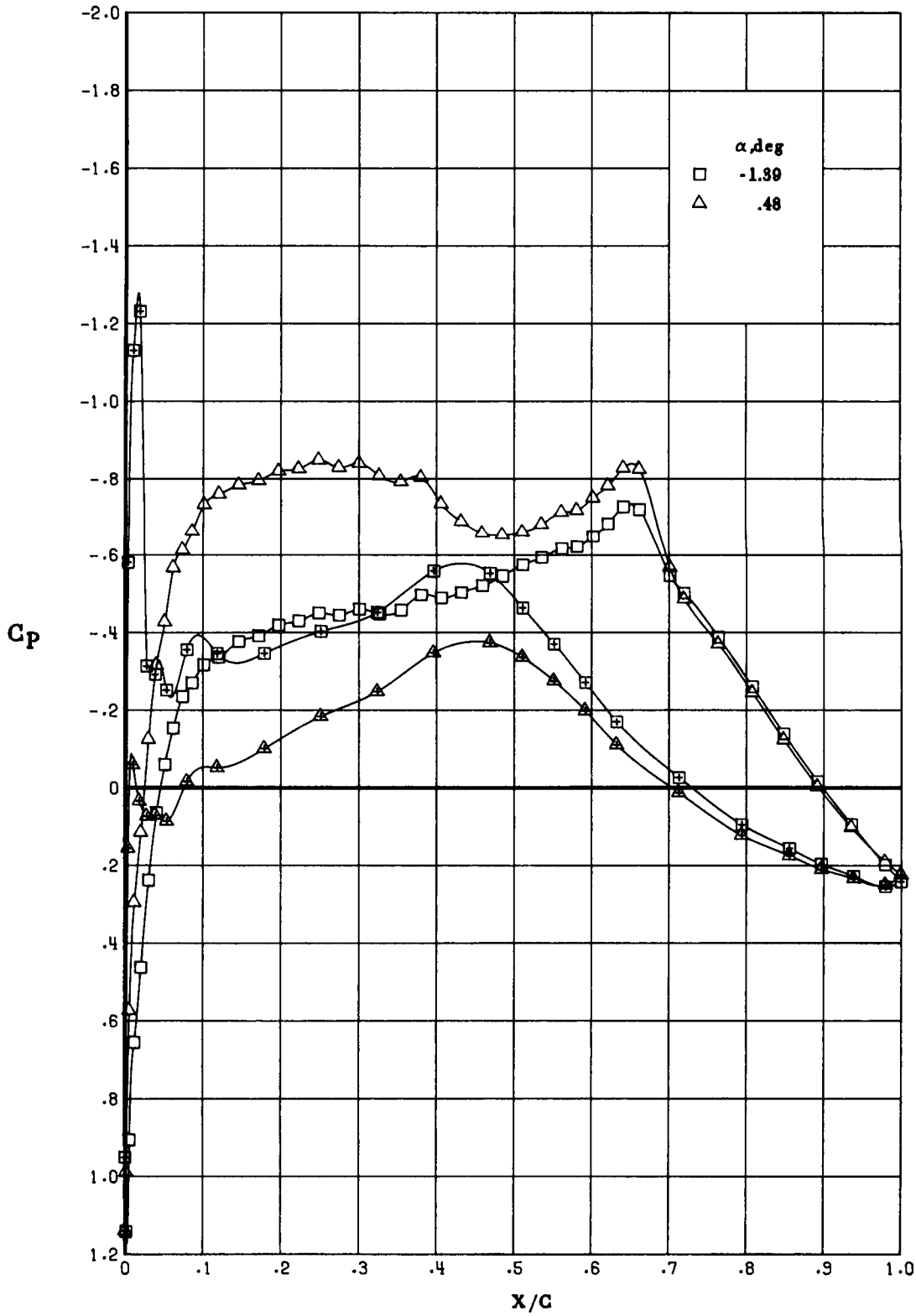

Figure 18. Concluded.

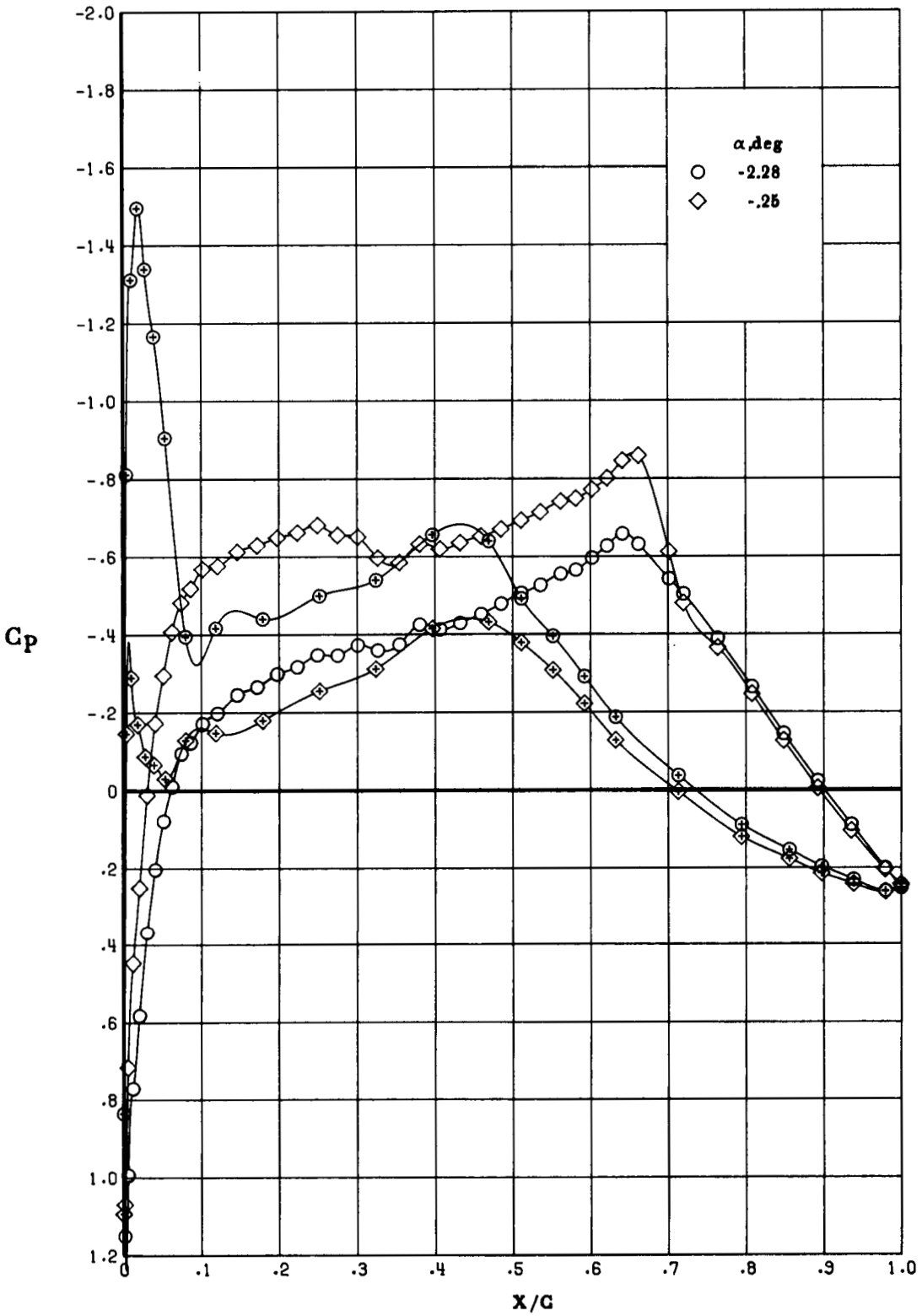

Figure 19. Effect of α on chordwise pressure distribution at $R_c = 70 \times 10^6$ and $M = 0.765$. Open symbols denote upper surface; "+" within symbol denotes lower surface.

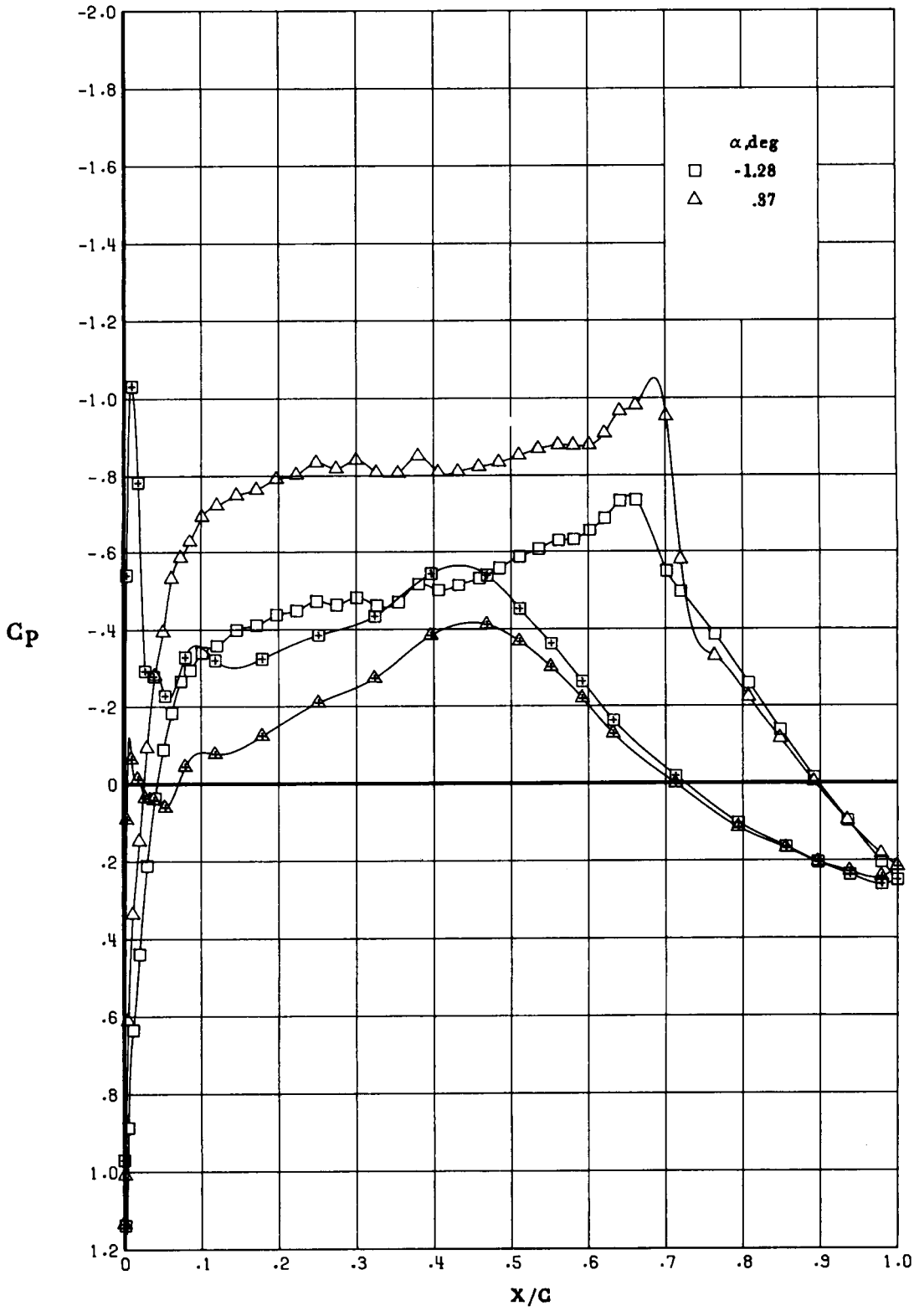

Figure 19. Concluded.

C-2

The run schedule for the tests in the 0.3-m TCT is presented in a "Supplement to NASA TM-4015." Also presented in the supplement are the tabulated airfoil pressure distributions, the integrated force-and-moment coefficients, and the wall boundary conditions.

Copies of this "Supplement to NASA TM-4015" will be furnished upon request. Requests for the supplement should be addressed to:

NASA Scientific and Technical Information Facility
P.O. Box 8757
Baltimore/Washington International Airport, Maryland 21240

Cut

- -

Date_____

Please forward "Supplement to NASA TM-4015" to

_____
Name of organization

_____
Street number

_____
City and State Zip code

Attention: _____
Mr.

_____
Title

NASA
National Aeronautics and Space Administration

Report Documentation Page

1. Report No.	2. Government Accession No.	3. Recipient's Catalog No.
NASA TM-4015		

4. Title and Subtitle	5. Report Date
Wall Interference Tests of a CAST 10-2/DOA 2 Airfoil in an Adaptive-Wall Test Section	December 1987
	6. Performing Organization Code
7. Author(s)	8. Performing Organization Report No.
Raymond E. Mineck	L-16334
9. Performing Organization Name and Address	10. Work Unit No.
NASA Langley Research Center Hampton, VA 23665-5225	505-61-01-02
	11. Contract or Grant No.
12. Sponsoring Agency Name and Address	13. Type of Report and Period Covered
National Aeronautics and Space Administration Washington, DC 20546-0001	Technical Memorandum
	14. Sponsoring Agency Code

15. Supplementary Notes

16. Abstract

A wind-tunnel investigation of a CAST 10-2/DOA 2 airfoil model has been conducted in the adaptive-wall test section of the Langley 0.3-Meter Transonic Cryogenic Tunnel (0.3-m TCT) and in the National Aeronautical Establishment High Reynolds Number Two-Dimensional Test Facility. The primary goal of the tests was to assess two different wall-interference correction techniques: adaptive test-section walls and classical analytical corrections. Tests were conducted over a Mach number range from 0.3 to 0.8 and over a chord Reynolds number range from 6×10^6 to 70×10^6. The airfoil aerodynamic characteristics from the tests in the 0.3-m TCT have been corrected for wall interference by the movement of the adaptive walls. No additional corrections for any residual interference have been applied to the data, to allow comparison with the classically corrected data from the same model in the conventional National Aeronautical Establishment facility. The data are presented graphically in this report as integrated force-and-moment coefficients and chordwise pressure distributions. These data, as well as spanwise pressure coefficient distributions, the spanwise drag coefficient distributions, and the test-section top and bottom wall pressure distributions and wall vertical displacements, are presented in tabular form in a supplement to this report.

17. Key Words (Suggested by Authors(s))	18. Distribution Statement
High Reynolds number tests Airfoil tests Wall interference	Unclassified—Unlimited Subject Category 02

19. Security Classif.(of this report)	20. Security Classif.(of this page)	21. No. of Pages	22. Price
Unclassified	Unclassified	98	A05

For sale by the National Technical Information Service, Springfield, Virginia 22161-2171